

QC921.5  
J446  
2010

THESIS

COLORADO STATE UNIVERSITY

FREEZING DRIZZLE PRODUCTION IN WARM FRONTAL OVERRUNNING  
CLOUD LAYERS: AN OBSERVATIONAL STUDY

April 02, 2010

WE HEREBY RECOMMEND THAT THE THESIS PREPARED UNDER OUR  
SUPERVISION BY FRANK McDONOUGH ENTITLED FREEZING DRIZZLE  
PRODUCTION IN WARM FRONTAL OVERRUNNING CLOUD LAYERS: AN  
OBSERVATIONAL STUDY, BE ACCEPTED AS FULFILLING IN PART  
REQUIREMENTS FOR THE DEGREE OF MASTER OF SCIENCE

Submitted by

Frank McDonough

Department of Atmospheric Science

Committee on Graduate work

  
Sonia M. Kreidenweis

  
Paul W. Miska, Jr.

In partial fulfillment of the requirements

For the Degree of Master of Science

Colorado State University

Fort Collins, Colorado

Spring 2010

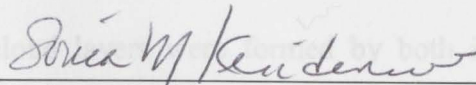
QC921.5  
.M446  
2010

COLORADO STATE UNIVERSITY

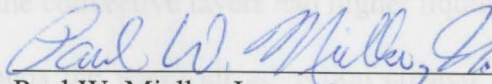
April 02, 2010

WE HEREBY RECOMMEND THAT THE THESIS PREPARED UNDER OUR SUPERVISION BY FRANK MCDONOUGH ENTITLED FREEZING DRIZZLE PRODUCTION IN WARM FRONTAL OVERRUNNING CLOUD LAYERS: AN OBSERVATIONAL STUDY BE ACCEPTED AS FULFILLING IN PART REQUIREMENTS FOR THE DEGREE OF MASTER OF SCIENCE.

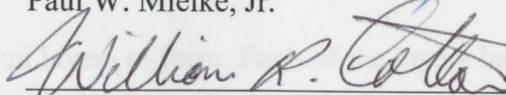
Committee on Graduate work



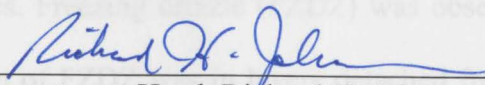
Sonia M. Kreidenweis



Paul W. Mielke, Jr.



Advisor: William R. Cotton



Department Head: Richard H. Johnson

condition. Isobaric mixing of clouds in the maritime case and was likely present at cloud top in both cases.

## ABSTRACT OF THESIS

### FREEZING DRIZZLE PRODUCTION IN WARM FRONTAL OVERRUNNING

#### CLOUD LAYERS: AN OBSERVATIONAL STUDY

Frank McDonough  
Atmospheric Science  
Colorado State University  
Fort Collins, CO 80523  
Spring 2010

National Weather Service operational and research aircraft data were used to analyze the large and small-scale structure of warm-frontal overrunning cloud layers forming freezing drizzle. Two detailed case studies, one from a maritime region (Juneau, AK), and one from a continental region (Green Bay, WI) are presented. The synoptic scale situation for both cases showed descending motion aloft, drying at the mid-levels and warming cloud top temperatures. The warming cloud top temperatures shut down the production of the ice phase and allowed supercooled liquid water to dominate the cloud microstructure. The cloud layers were formed by both isentropic lift and convective instability, although the convective layers had higher liquid water contents. In addition to helping form the clouds the warm air advection created thin warm layers aloft which allowed discrete cloud layers to form. Each of the layers had distinct thermodynamic and microphysical properties. Freezing drizzle (FZDZ) was observed in all the cloud layers but the initial formation of FZDZ was in layers detached from the boundary layer with low droplet concentrations. Radiational cooling at the highest cloud top was likely present in both cases and may have formed FZDZ, but its presence was not a necessary

condition. Isobaric mixing at cloud top was observed in the maritime case and was likely present at cloud top in both cases.

1.0	Introduction.....	1
2.0	Instrumentation.....	4
2.1	University of Wyoming King Air.....	Frank McDonough
2.2	NASA Glenn Icing Research Aircraft.....	Department of Atmospheric Science
3.0	Maritime Case: Juneau, Alaska.....	Colorado State University
3.1	Introduction.....	Fort Collins, CO 80523
3.2	Synoptic Scale.....	Spring 2010
3.2.1	Overview.....	10
3.2.2	Horizontal structure at the mandatory levels.....	11
3.3	Mesoscale Structure.....	16
3.3.1	Overview.....	16
3.3.2	Thermodynamic and kinematic structure.....	19
3.3.3	Liquid Water Content.....	24
3.3.4	Liquid water content at Juneau.....	25
3.3.5	Liquid water content at Sitka.....	27
3.4	Microscale structure of cloud layers.....	29
3.4.1	Particle size distribution of the layers at Juneau.....	30
3.4.2	Particle size distributions at Sitka.....	41
3.4.3	Vertical Distribution of CCN.....	49
3.5	Discussion.....	52
3.5.1	Conceptual view of the evolution of the cloud layers.....	52
3.5.2	Cloud top layer.....	52
3.5.3	King at JNU.....	61
4.0	Green Bay continental case.....	62
4.1	Introduction.....	62
4.1.1	Geography.....	63
4.2	Synoptic Situation.....	64
4.2.1	Evolution of the synoptic-scale vertical structure at KGRB.....	69
4.3	Mesoscale structure.....	71
4.3.1	Evolution of the layers.....	71
4.3.2	North-south cross section.....	75
4.3.3	East-west cross section.....	76
4.3.4	Thermal and LWC structure across Lake Michigan.....	78
4.4	Micro-scale structure of the cloud layers.....	79
4.5	Discussion.....	84
4.5.1	Layer 2.....	88
4.5.2	Lower Warm Front.....	91
4.5.3	Layer 3.....	92

## TABLE OF CONTENTS

5.0	Principal findings	96
5.1	Identification of weather features associated with SLD forming clouds	97
1.0	Introduction	1
2.0	Instrumentation	4
2.1	University of Wyoming King Air	4
2.2	NASA Glenn Icing Research Aircraft	5
3.0	Maritime Case Juneau, Alaska	7
3.1	Introduction	7
3.2	Synoptic Scale	10
3.2.1	Overview	10
3.2.2	Horizontal structure at the mandatory levels	11
3.3	Mesoscale Structure	16
3.3.1	Overview	16
3.3.2	Thermodynamic and kinematic structure	19
3.3.3	Liquid Water Content	24
3.3.4	Liquid water content at Juneau	25
3.3.5	Liquid water content at Sitka	27
3.4	Microscale structure of cloud layers	29
3.4.1	Particle size distribution of the layers at Juneau	30
3.4.2	Particle size distributions at Sitka	41
3.4.3	Vertical Distribution of CCN	49
3.5	Discussion	52
3.5.1	Conceptual view of the evolution of the cloud layers	52
3.5.2	Cloud top layer	52
3.5.3	Icing at JNU	61
4.0	Green Bay continental case	62
4.1	Introduction	62
4.1.1	Geography	63
4.2	Synoptic Situation	64
4.2.1	Evolution of the synoptic-scale vertical structure at KGRB	69
4.3	Mesoscale structure	71
4.3.1	Evolution of the layers	71
4.3.2	North-south cross section	75
4.3.3	East-west cross section	76
4.3.4	Thermal and LWC structure across Lake Michigan	78
4.4	Micro-scale structure of the cloud layers	79
4.5	Discussion	84
4.5.1	Layer 2	88
4.5.2	Lower Warm Front	91
4.5.3	Layer 3	92

4.5.4	Icing at KGRB .....	96
5.0	Principal findings .....	97
5.1	Identification of weather features associated with SLD forming clouds.....	97
5.2	Large drop formation .....	98
5.3	Implications for models .....	98
5.4	Icing .....	98
5.5	Future Work.....	100
6.0	References.....	101

dangerous supercooled large drop (SLD; drop sizes > 50  $\mu\text{m}$ ) icing conditions, which allows ice to form on unprotected surfaces of the aircraft (Sand et al 1984; Politovich 1989). Two commuter aircraft accidents that caused more than 100 fatalities have been directly linked to icing caused by SLD aloft (Marwitz et al 1997; NTSB 1996, 1998). Aircraft certified to operate in known icing conditions are not required to demonstrate performance in large drop icing conditions (FAA Appendix C).

Freezing drizzle is generally recognized to form through a predominantly liquid process where air is cooled to saturation and condensation causes cloud drops to form. If a few of these drops then grow to sizes exceeding 40  $\mu\text{m}$  in diameter, the size where collision and coalescence becomes appreciable (Koops and Yau 1989), freezing drizzle may form. This mechanism is known as the supercooled warm rain process (Ohtake 1963; Kajikawa et al 1988; Huffman and Norman 1989). A second mechanism which can lead to freezing drizzle formation is when snow flakes melt into drizzle sized drops as they fall into a layer of warmer air with temperatures greater than 0°C, then subsequently supercool within a surface based subfreezing layer.

## 1.0 Introduction

Freezing drizzle (FZDZ) continues to negatively impact transportation both at the surface and aloft. Freezing drizzle aloft can create a significant threat to aviation due to the dangerous supercooled large drop (SLD; drop sizes  $> 50 \mu\text{m}$ ) icing conditions, which allows ice to form on unprotected surfaces of the aircraft (Sand et. al 1984; Politovich 1989). Two commuter aircraft accidents that caused more than 100 fatalities have been directly linked to icing caused by SLD aloft (Marwitz et. al 1997; NTSB 1996, 1998). Aircraft certified to operate in known icing conditions are not required to demonstrate performance in large drop icing conditions (FAA Appendix C).

Freezing drizzle is generally recognized to form through a predominantly liquid process where air is cooled to saturation and condensation causes cloud drops to form. If a few of these drops then grow to sizes exceeding  $40 \mu\text{m}$  in diameter, the size where collision and coalescence becomes appreciable (Rogers and Yau 1989), freezing drizzle may form. This mechanism is known as the supercooled warm rain process (Ohtake 1963; Kajikawa et. al 1988; Huffman and Norman 1988). A second mechanism which can lead to freezing drizzle formation is when snow flakes melt into drizzle sized drops as they fall into a layer of warmer air with temperatures greater than  $0^{\circ}\text{C}$ , then subsequently supercool within a surface based subfreezing layer.

The cloud mechanisms which allow freezing drizzle to form may include, the presence of giant or ultra-giant aerosols serving as cloud condensation nuclei (CCN) and producing large drops (Johnson 1980); increased supersaturation caused by radiational cooling of drops at cloud top (Harrington et al. 2000, Rasmussen et. al. 2002), low CCN and low drop concentration clouds resulting in a lack of competition for the available vapor (Cooper , Rasmussen et. al. 1995, Ikeda et. al. 2005); and isobaric mixing at cloud top (Korolev and Isaac 2000).

A few case studies where SLD were present have been documented over different regions of North America. Rasmussen et al. (1995) documented a multi-layered freezing drizzle cloud over Colorado. Cober et al. (1996) documented a supercooled drizzle cloud over the Canadian Maritimes. Additional studies of SLD clouds, using in-situ research aircraft, were also conducted by Sand et al. (1984), Politovich (1989), Pobanz et. al. (1993), and Ikeda et al. (2005).

Bernstein et al. (2006), using research aircraft observations, suggested that supercooled liquid cloud layers with low drop concentrations were more likely to produce larger drop sizes and these types of clouds were often associated with warm air advection. Bernstein et al. (1997), using a large group of icing pilot reports, determined that the region ahead of a warm front was the most likely quadrant of a cyclone to produce icing clouds over the continental US.

This study will examine two freezing drizzle cases using research aircraft observations. The paper will document the large and small-scale structure of clouds forming FZDZ undergoing the warm rain process in an overrunning region. A continental and a maritime case are examined. The study documents the synoptic, meso, and micro-scale structure of atmosphere and clouds forming FZDZ. The study also compares the cloud structure against the various possible FZDZ formation mechanisms. Finally the potential icing threat from these clouds is discussed.

## 2.1 University of Wyoming King Air

The University of Wyoming King Air research aircraft is well instrumented for cloud physics research. Ashenden (1997) provides a detailed discussion on the aircraft instrumentation and post flight data processing. The aircraft measures ambient air temperature from the Minco stream reverse flow probe. The aircraft's compressional heating term was removed and the probe has an accuracy of 0.5°C. The dewpoint temperature probe is a Cambridge 137C3 that claims a 2.0°C accuracy at temperatures below freezing. Pressure is measured by a Rosemount 1501 with an accuracy of 0.5mb. A GPS system is used to identify the aircraft's altitude and location.

The cloud properties are measured with several of the Particle Measuring System's (PMS) instruments. The PMS Forward Scattering Spectrometer Probe (FSSP) obtains concentrations of particles using forward scattered light. The instrument provides concentrations of drops with diameters between the sizes of 0.5µm – 46.3µm with a bin

resolution of 3µm. Baumgardner (1993) suggests that a properly operating FSSP probe, in liquid water conditions, should have a maximum error of 20% in both size and concentration.

## 2.0 Instrumentation

The PMS one dimensional optical probe (200X) obtains particle size distributions. The case studies are initially analyzed standard National Weather Service data sets, including soundings, upper air charts, METARs, along with in-situ pilot reports of aircraft icing. The fine-scale structure of the atmosphere and clouds are completed using the King Air and both the 2D-C and 2D-P probes. In post-processing the 2D images were sorted by habit (ice crystal or liquid drop). They were then sized using the

### 2.1 University of Wyoming King Air

The University of Wyoming King Air research aircraft is well instrumented for cloud physics research. Ashenden (1997) provides a detailed discussion on the aircraft instrumentation and post flight data processing. The aircraft measures ambient air temperature from the Minco element reverse flow probe. The aircraft's compressional heating term was removed and the probe has an accuracy of 0.5°C. The dewpoint temperature probe is a Cambridge 137C3 that claims a 2.0°C accuracy at temperatures below freezing. Pressure is measured by a Rosemount 1501 with an accuracy of 0.5mb. A GPS system is used to identify the aircraft's altitude and location.

The cloud properties are measured with several of the Particle Measuring System's (PMS) instruments. The PMS Forward Scattering Spectrometer Probe (FSSP) obtains concentrations of particles using forward scattered light. The instrument provides concentrations of drops with diameters between the sizes of 0.5µm – 46.5µm with a bin

resolution of  $3\mu\text{m}$ . Baumgardner (1983) suggests that a properly operating FSSP probe, in liquid water conditions, should have a maximum error of 20% in both size and concentration.

The PMS one dimensional optical probe (200X) obtains particle size distributions between  $12.5$  and  $187.0\mu\text{m}$  with a  $12.5\mu\text{m}$  resolution. The two-dimensional optical array probes (OAP) provide concentrations of cloud particles, along with a shadow image of the particle. The King Air had both the 2D-C and 2D-P probes. In post-processing the 2D images were sorted by habit (ice crystal or liquid drop). They were then sized using the center-in method, with the resulting sized particle placed in one of the 20 bins depending on the particle's diameter. The University of Wyoming's 2D-C post processing allows for  $50\mu\text{m}$  resolution from  $50\mu\text{m} - 300\mu\text{m}$ ,  $100\mu\text{m}$  resolution to  $600\mu\text{m}$ , and  $200\mu\text{m}$  resolution above  $600\mu\text{m}$ . Cober et al (2001) suggests that using the OAP probes to measure small particles ( $<100\mu\text{m}$  in diameter) can introduce significant sizing errors due to depth-of-field uncertainties. The presence of supercooled liquid water was determined from the Rosemount 871FA icing detector. This icing detector goes through a heating cycle after a  $0.5\text{mm}$  accretion of supercooled liquid. This instrument does not measure frozen condensate and only increases its voltage when supercooled water is present (Cober et al. 2001).

## 2.2 NASA Glenn Icing Research Aircraft

The NASA Glenn Icing Research Aircraft is a modified DeHavilland 6 Twin Otter. The instrumentation on board and used in this study are: a Forward Scattering Spectrometry

Probe (FSSP) which measures particles in the size range 2 - 47  $\mu\text{m}$ ; a two-dimensional Optical Array Cloud Probe (OAP 2D-C Gray) which measures and records images of particles in the size range 7.5 - 968  $\mu\text{m}$ ; a CSIRO Liquid Water Content (LWC) probe; a Rosemount Outside Air Temperature (OAT) probe; and a Rosemount icing detector.

### 3.1 Introduction

The state of Alaska (Fig. 3.1) accounts for the highest number of aircraft icing accidents in the United States (Perry and Floyd 2004). In addition, many parts of Alaska are only accessible by air or sea, including the southeast coastal town and state capital of Juneau (Fig. 3.2). In order to help allow aircraft to safely operate in these cloudy regions an understanding of the large and small structure of clouds that produce icing conditions is necessary. Aircraft icing occurs when an aircraft encounters liquid water clouds at temperatures below freezing. The sub-freezing (supercooled) water drops can freeze to the airframe and affect the aircraft performance. Supercooled large drop (SLD) icing can be particularly hazardous (Bernstein and McDonough 2002). In-depth studies of the structure of SLD icing clouds over the southeastern Alaska Pacific coastal region have been minimal. Bernstein (2005a), using a special version of Current Icing Product (Bernstein et al. 2005b), suggested that icing conditions may be present more than 60% of the time over southeastern Alaska.

### 3.0 Maritime Case Juneau, Alaska

#### 3.1 Introduction

The state of Alaska (Fig. 3.1) accounts for the highest number of aircraft icing accidents in the United States (Petty and Floyd 2004). In addition, many parts of Alaska are only accessible by air or sea, including the southeast coastal town and state capitol of Juneau (Fig. 3.2). In order to help allow aircraft to safely operate in these cloudy regions an understanding of the large and small structure of clouds that produce icing conditions is necessary. Aircraft icing occurs when an aircraft encounters liquid water clouds at temperatures below freezing. The sub-freezing (supercooled) water drops can freeze to the airframe and affect the aircraft performance. Supercooled large drop (SLD) icing can be particularly hazardous (Bernstein and McDonough 2002). In-depth studies of the structure of SLD icing clouds over the southeastern Alaska Pacific coastal region have been minimal. Bernstein (2005a), using a special version of Current Icing Product (Bernstein et al. 2005b), suggested that icing conditions may be present more than 60% of the time over southeastern Alaska.

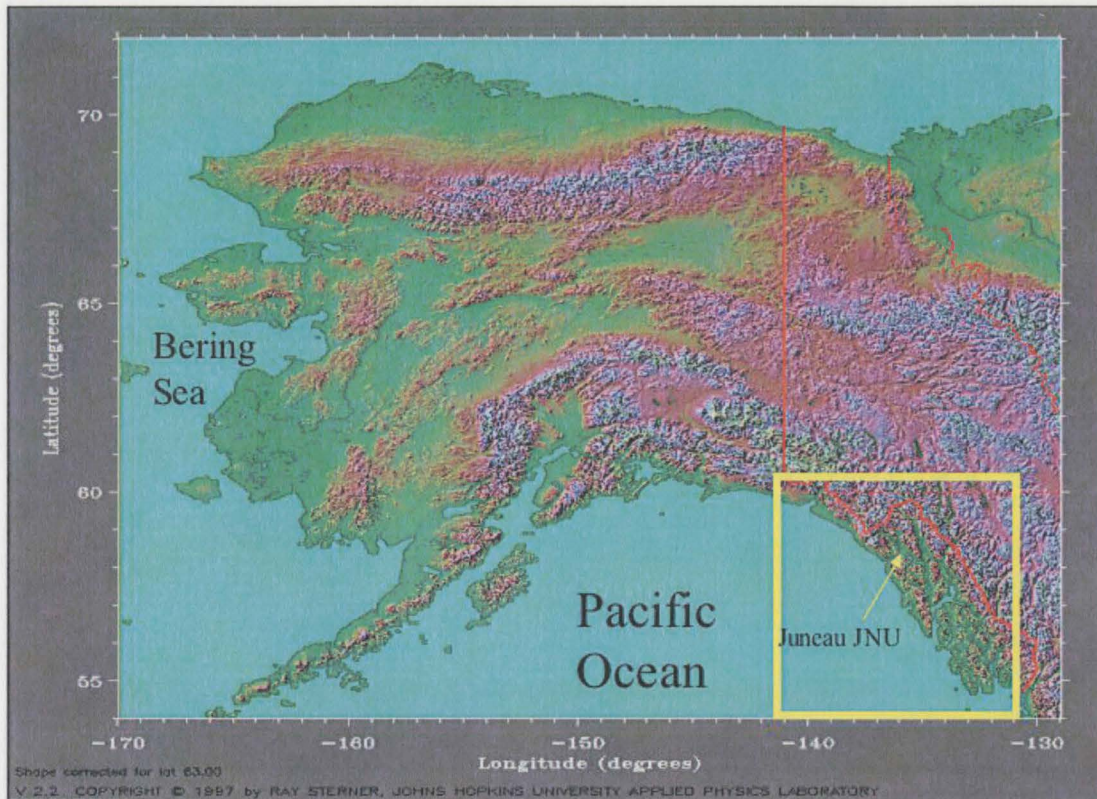


Figure 3.1 Relief map of the state of Alaska. Inset identifies the Juneau region.

The Juneau Wind Shear Warning Research project was conducted during the winter of 2000 in the Juneau region. As part of this field campaign, the University of Wyoming King Air research aircraft was used to sample the atmosphere. On the afternoon of 19 January 2000, during an extended freezing drizzle episode, a research flight was completed. The research flight sampled the entire depth of the cloud layers that formed SLD icing conditions and the freezing drizzle observed at the sea face. This chapter will document the synoptic and mesoscale atmospheric conditions that formed the cloud layers along with the microscale structure of the clouds that were present during the episode. Section 3.2 discusses the data available from the instrumentation on the King Air as well as their limitations. Section 3.3 provides a discussion on the large scale

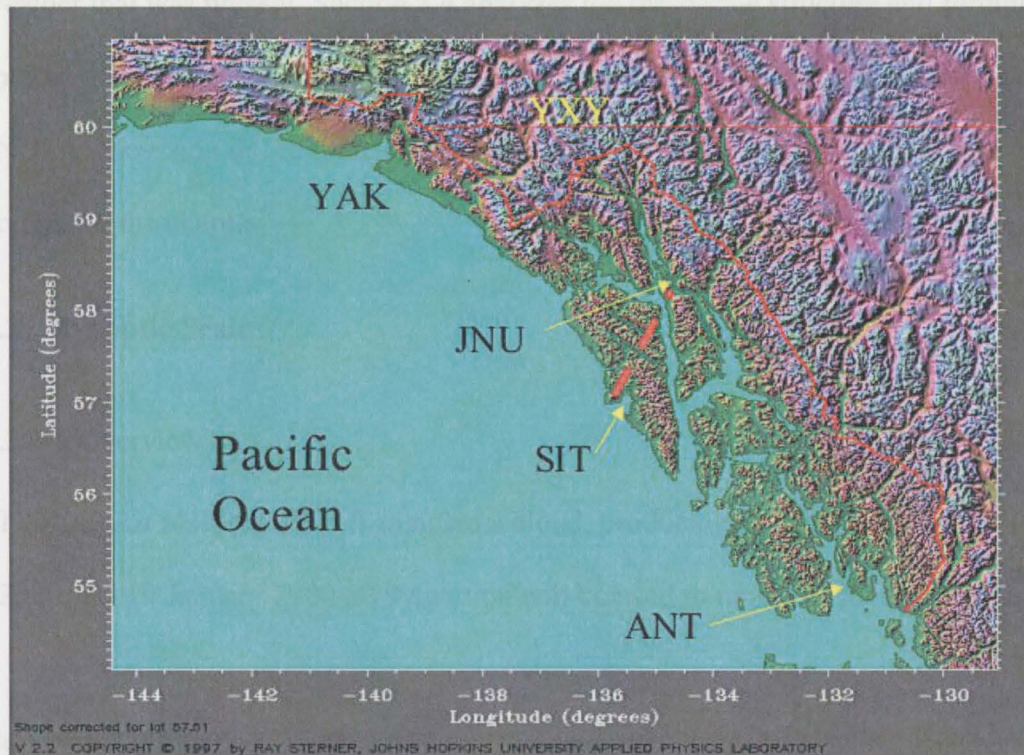


Figure 3.2. Relief map of the Juneau region with upper air sites and Sitka and Juneau

The Juneau Wind Shear Warning Research project was conducted during the winter of 2000 in the Juneau region. As part of this field campaign, the University of Wyoming King Air research aircraft was used to sample the atmosphere. On the afternoon of 19 January 2000, during an extended freezing drizzle episode, a research flight was completed. The research flight sampled the entire depth of the cloud layers that formed SLD icing conditions and the freezing drizzle observed at the surface. This chapter will document the synoptic and mesoscale atmospheric conditions that formed the cloud layers along with the microscale structure of the clouds that were present during the episode. Section 3.2 discusses the data available from the instrumentation on the King Air as well as their limitations. Section 3.3 provides a discussion on the large scale

weather that was present. Section 3.4 analyzes the mesoscale structure and forcing that formed the cloud. Section 3.5 documents the microscale structure of the cloud above JNU. A discussion of the freezing drizzle formation and icing conditions within the cloud completes the chapter.

## 3.2 Synoptic Scale

### 3.2.1 Overview

The King Air research aircraft sampled a cloud, producing freezing drizzle, at JNU at 2300 UTC 19 January 2000 (J19 notation will be used to represent month and day).

Between 2000 January 15- 2000 January 16 a synoptic scale short-wave and associated cyclone had crossed southeastern Alaska from northwest to southeast. In the wake of the short-wave a ridge and associated low-level anticyclone formed. This forced a cold surface high-pressure system, originating over the interior of Alaska and the Yukon, to move south and cover the islands and bays along the Pacific coast of southeastern Alaska. At Juneau, the surface pressure increased to 1029mb and the temperature cooled to  $-12^{\circ}\text{C}$  before precipitating clouds formed (Fig. 3.3). The precipitation began at 0800 UTC 2000 January 18 as snow (SN), and continued as SN and/or freezing drizzle (FZDZ) for 39 hours prior to the research flight time.

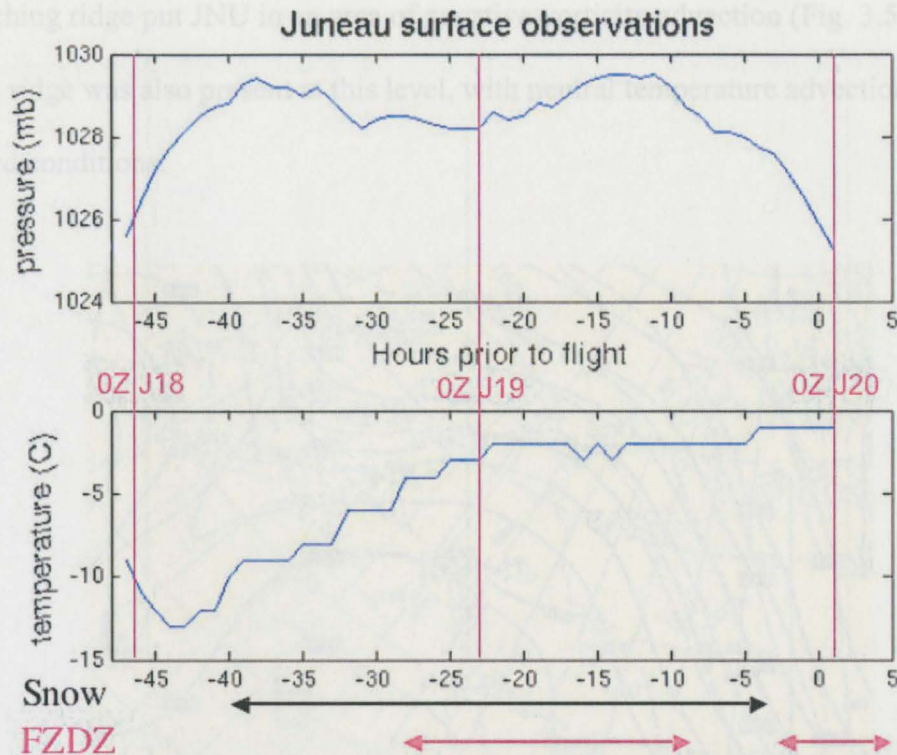


Figure 3.3. Time series of pressure, temperature, and precipitation type at the surface at Juneau region. The King Air flight occurred at hour 0 (2300 UTC 19 JAN 2000)

The synoptic situation at the research flight time is described below, using operational NWS observations and two research aircraft soundings. The soundings are from a King Air ascent over JNU at 2300 UTC on 2000 January 19 from the surface to 735mb, and a descent from 795mb through 980mb over Sitka, AK (SIT) at 2335 UTC 19 January 2000.

### 3.2.2 Horizontal structure at the mandatory levels

A 500mb ridge approached JNU from the west (Fig. 3.4). To the south of JNU, a cutoff low was moving north along the Pacific coast causing a wind shift from westerly to easterly. The anticyclonic shear plus the negative vorticity associated with the

approaching ridge put JNU in an area of negative vorticity advection (Fig. 3.5). A thermal ridge was also present at this level, with neutral temperature advection and sub-saturated conditions.

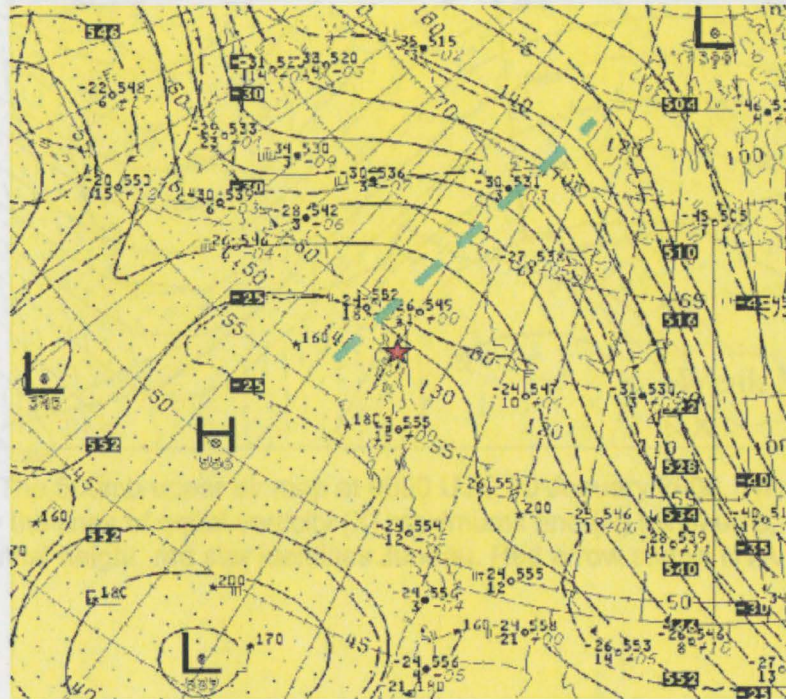


Figure 3.4. The 500mb upper air map at 0000 UTC 20 January 2000. The green dashed line identifies the ridge axis and red star identifies Juneau.

Plymouth State Weather Center

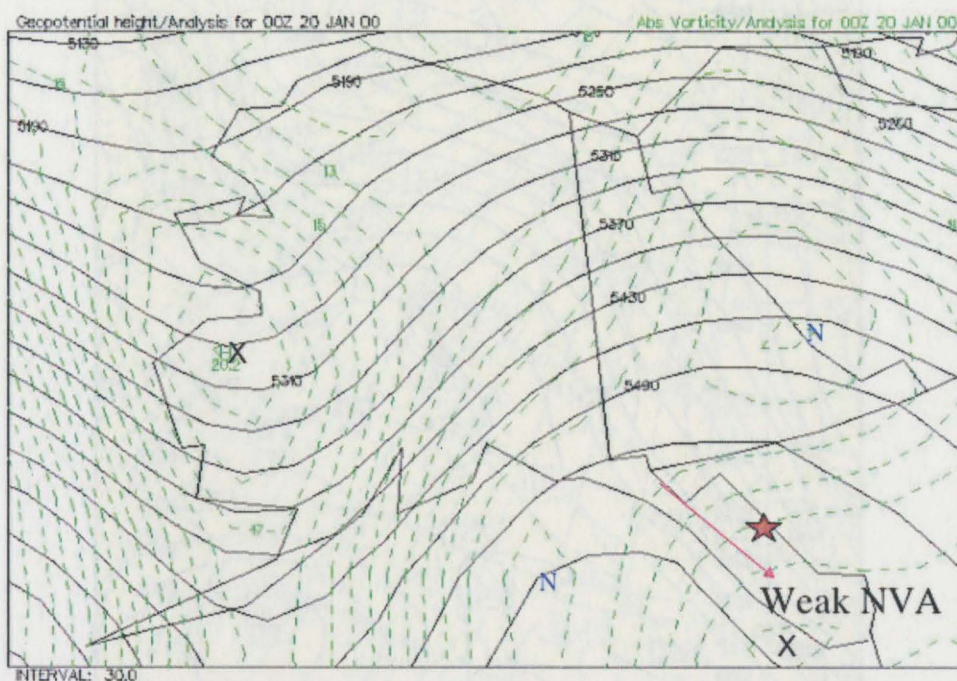


Figure 3.5. The 500mb upper air map at 0000 UTC 20 January 2000. The green dashed lines identify the lines of equal vorticity (X) maximums and (N) minimums, black lines are geopotential height, red star identifies Juneau. Red arrow shows NVA flow over JNU.

At 700mb an area of high geopotential height was centered beneath the upper-level ridge axis, west of JNU (Fig. 3.6). Also beneath the 500mb negative relative vorticity region was an area of warm air advection (WAA) associated with a subsidence inversion. The inversion layer descended through the 700mb level at JNU several hours before the research flight. This process resulted in a warming of the cloud top temperatures and the transition at the JNU surface from a mixture of SN and FZDZ to only FZDZ (see Fig 3.3). In the wake of the subsidence inversion, dry northwesterly flow moved over the region.

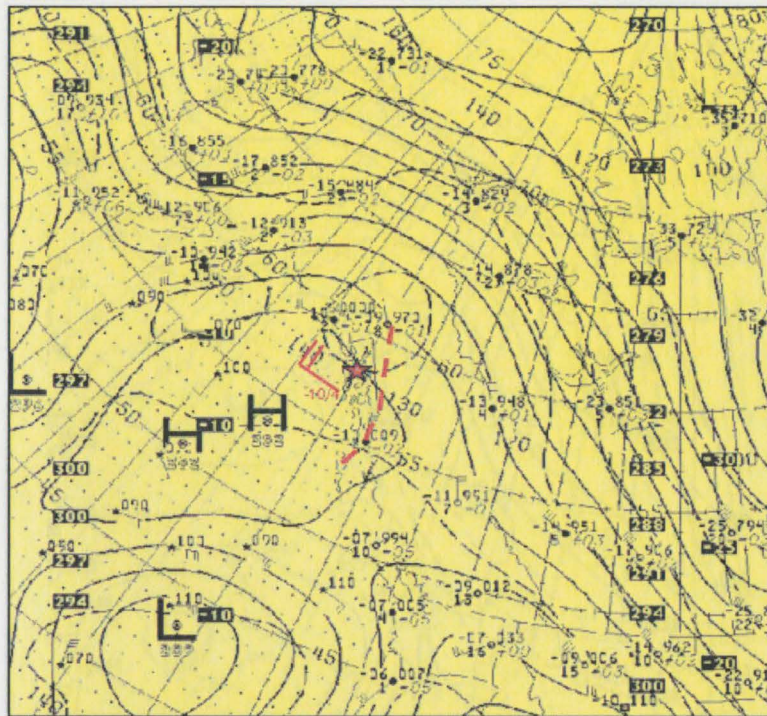


Figure 3.6. The 700mb upper air map at 0000 UTC 20 January 2000. The red dashed line identifies the upper level warm front, red text and wind from research aircraft and red star identifies Juneau.

After 1200 UTC on 2000 January 19 the surface high pressure at JNU began to slowly

At 850mb the center of the anticyclone was west of SIT, also beneath the upper-level ridge (Fig. 3.7). Westerly flow from the Pacific, around the north side of the high, established a moist WAA onshore flow toward the colder air in-place already in place at the surface over JNU and SIT.

of the coastline. The surface pressure decreased from northeast to southwest, establishing a weak cold air advection off-shore flow as the temperature increased from northeast to southwest.

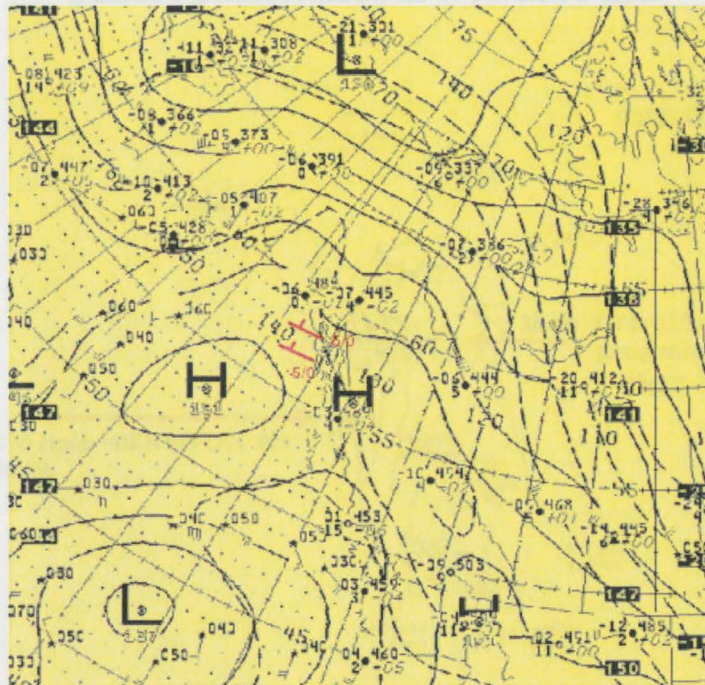


Figure 3.7. The 850mb upper air map at 0000 UTC 20 January 2000. The red text and winds a observed conditions at SIT and JNU from the research aircraft.

After 1200 UTC on 2000 January 19 the surface high pressure at JNU began to slowly weaken (see Fig. 3.3). By 0000 UTC J20 the highest surface pressure was north of JNU (Fig. 3.8). This was significantly east of the 850mb high center. The surface frontal boundary, delineating the cold air mass from the interior and warmer Pacific air mass, was likely present to the west of the coastline. The surface pressure decreased from northeast to southwest, establishing a weak cold air advection off-shore flow as the temperature increased from northeast to southwest.

## Surface observations at 1/19/2000 23Z

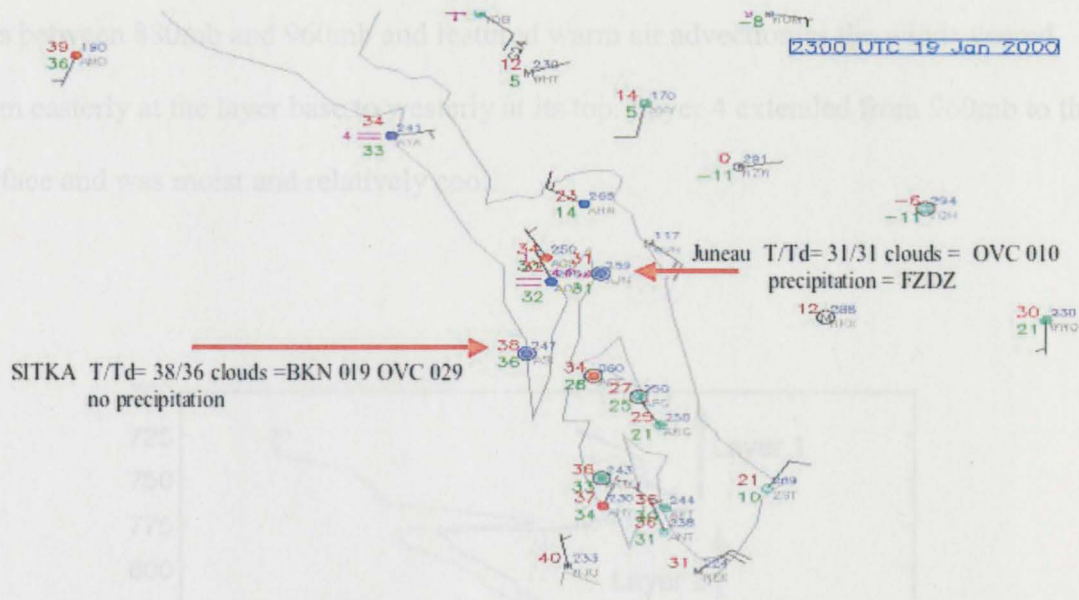


Figure 3.8. The surface map at 2300 UTC 19 January 2000. The highest pressures are north of Juneau. Off shore flow was present across the region.

### 3.3 Mesoscale Structure

#### 3.3.1 Overview

The atmosphere in the JNU and SIT region contained several stably stratified layers.

Cooler cloudy layers resided beneath the subsidence inversion with dryer, higher  $\theta_e$  air above the inversion (Fig. 3.9). Four primary layers were identified at JNU. Layer 1 was the mid-tropospheric (500 and 700mb) northwesterly flow dry layer which was just downstream of the ridge axis and was cloud free. Its base was the top of the strong

subsidence temperature inversion. Layer 2 was just beneath the subsidence inversion between 880mb and 775mb. It was quite moist and dominated by westerly flow. Layer 3 was between 880mb and 960mb and featured warm air advection as the winds veered from easterly at the layer base to westerly at its top. Layer 4 extended from 960mb to the surface and was moist and relatively cool.

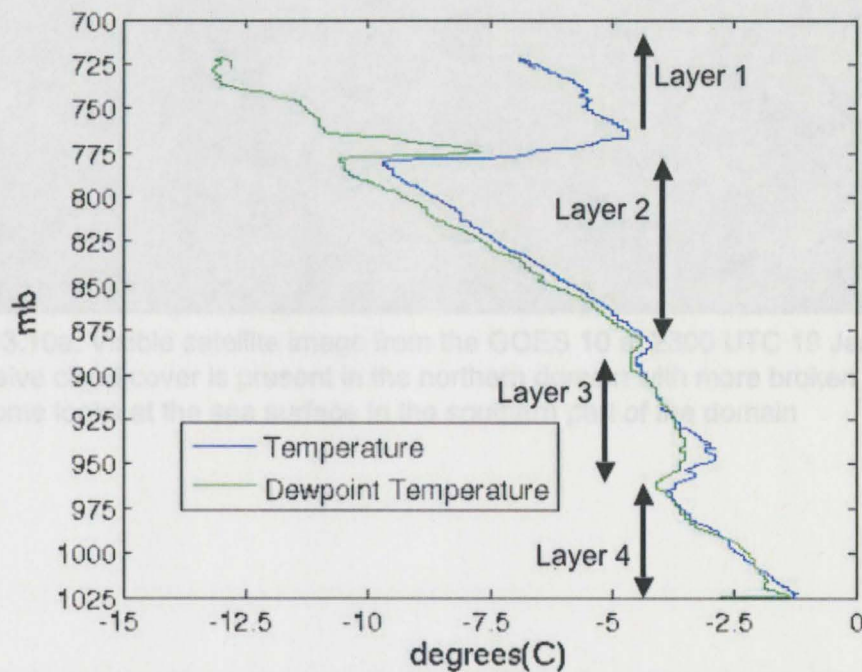


Figure 3.9. Sounding from the research aircraft at Juneau 2300 UTC 19 January 2000. The 4 synoptic layers are identified.

Overcast conditions covered the JNU and SIT area with more broken clouds to the south (Fig. 3.10a). The cloud top temperatures warmed slightly from northeast to southwest (Fig. 3.10b).

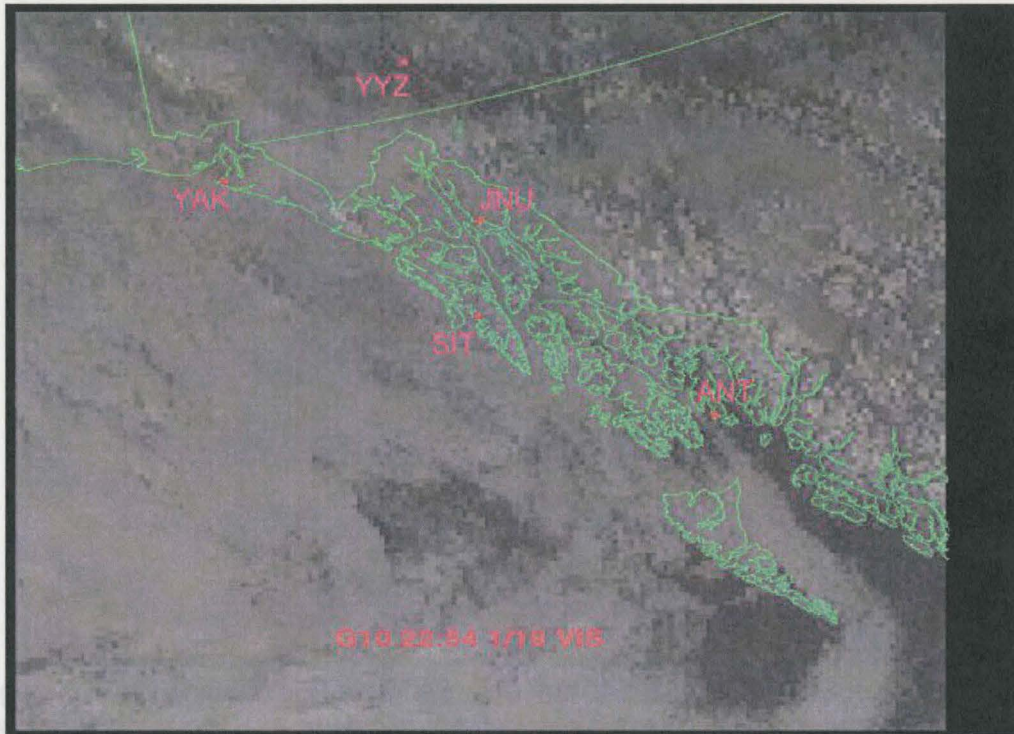


Figure 3.10a. Visible satellite image from the GOES 10 at 2300 UTC 19 January 2000. Extensive cloud cover is present in the northern domain with more broken cloud coverage and some looks at the sea surface in the southern part of the domain

### 3.3.2 Thermodynamic and kinematic structure

In this section the mesoscale structure of the layers are presented. The layers were differentiated based upon their thermodynamic, kinematic, and microphysical structure. Each layer was separated from the layers above and below by a capping inversion (i.e. a thin warm layer aloft).

The vertical profiles of temperature ( $T$ ), dew point temperature ( $T_d$ ), equivalent potential temperature ( $\theta_e$ ), relative humidity, winds, along with the defined layers from the

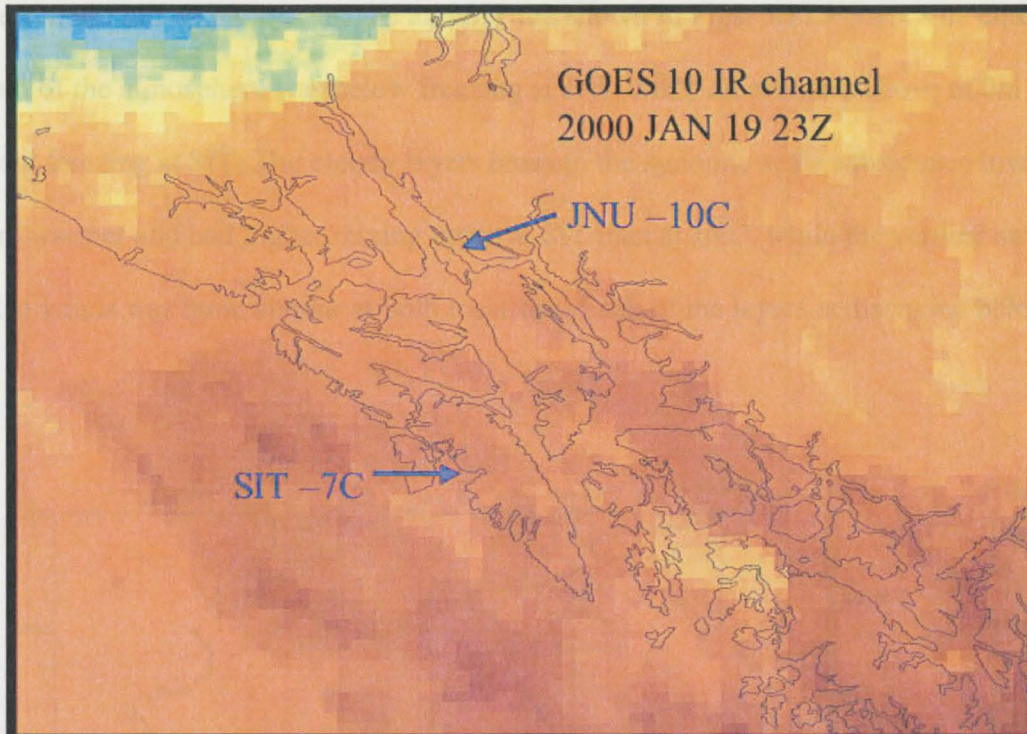


Figure 3.10b. Long-wave IR satellite image from the GOES 10 at 2300 UTC 19 Jan 2000. Extensive cloud cover is present in the northern domain with more broken cloud coverage and some looks at the sea surface in the southern part of the domain

### 3.3.2 Thermodynamic and kinematic structure

In this section the mesoscale structure of the layers are presented. The layers were differentiated based upon their thermodynamic, kinematic, and microphysical structure. Each layer was separated from the layers above and below by a capping inversion (i.e. a thin warm layer aloft).

The vertical profiles of temperature ( $T$ ), dew point temperature ( $T_d$ ), equivalent potential temperature ( $\theta_e$ ), relative humidity, winds, along with the defined layers from the

research aircraft soundings at JNU and SIT are shown in Figs. 3.11 – 3.13. The entire depth of the atmosphere was below freezing at JNU while all altitudes above 600m were below freezing at SIT. The cloudy layers beneath the synoptic scale subsidence inversion were warmer and had higher mixing ratios at SIT than at JNU, while the vertical structure of the winds was quite similar at both locations. Each of the layers is discussed below.

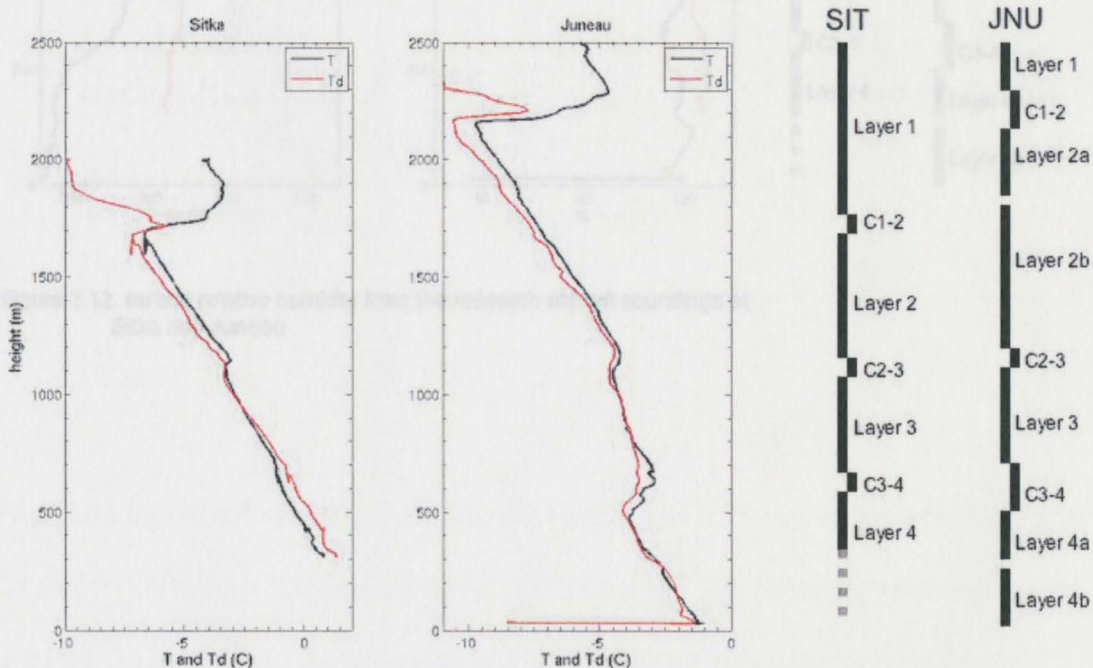


Figure 3.11. Research aircraft temperature, dew point temperature and layers from the Sitka and Juneau soundings.

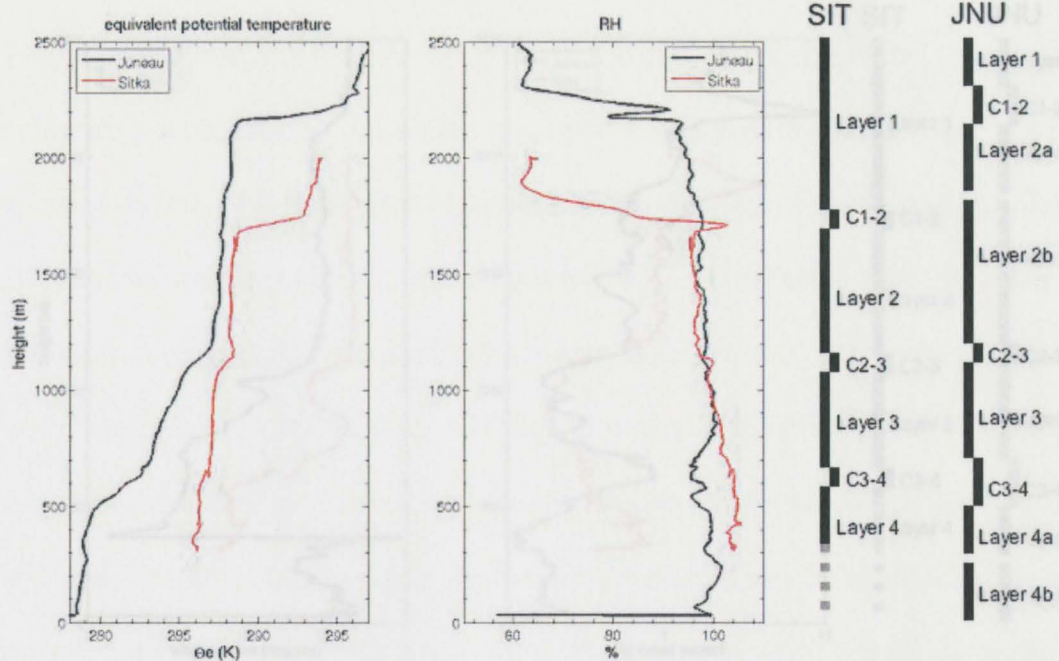


Figure 3.12.  $\theta_e$  and relative humidity from the research aircraft soundings at Sitka and Juneau

Dry air and light northwesterly flow characterized Layer 1, which included all altitudes above the inversion, at 2300m at JNU and 1730m at SIT. The boundary between Layer 1 and Layer 2 was the capping inversion (C1-2) formed by the strong synoptic scale subsidence. This thin (150m deep), very stable layer featured 5°C and 3.5°C inversions at JNU and SIT respectively. Of interest was the 450m slope of this boundary between SIT and JNU and the sharp increase in the dewpoint temperature within the inversion layer at both locations. A wind speed maximum along the base of the inversion advected the warmer and higher dew point temperature air toward Sitka and Juneau. A decrease in the Richardson's number was present suggesting that mixing was possible between the stable inversion and the layer below.

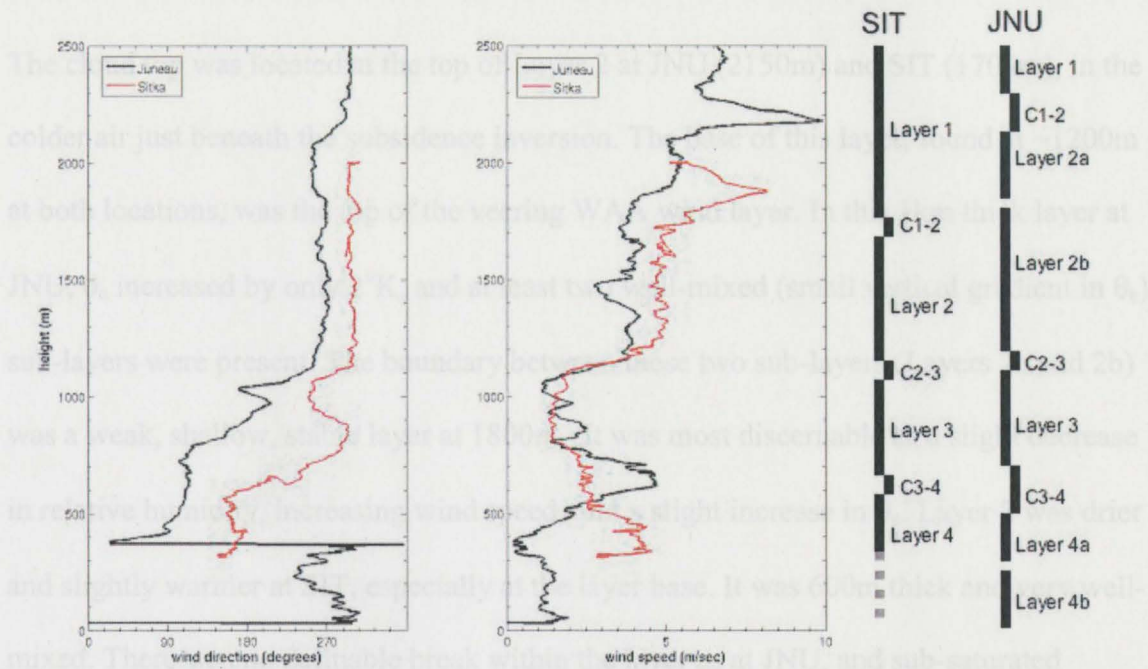


Figure 3.13. Wind speed and direction from the research aircraft soundings at Sitka and Juneau

Dry air and light northwesterly flow characterized Layer 1, which included all altitudes above the inversion, at 2300m at JNU and 1750m at SIT. The boundary between Layer 1 and Layer 2 was the capping inversion (C1-2) formed by the strong synoptic scale subsidence. This thin (150m deep), very stable layer featured 5°C and 3.5°C inversions at JNU and SIT respectively. Of interest was the 450m slope of this boundary between SIT and JNU and the sharp increase in the dewpoint temperature within the inversion layer at both locations. A wind speed maximum along the base of the inversion advected the warmer and higher dew point temperature air toward Sitka and Juneau. A decrease in the Richardson's number was present suggesting that mixing was possible between the stable inversion and the layer below.

The cloud top was located at the top of Layer 2 at JNU (2150m) and SIT (1700m), in the colder air just beneath the subsidence inversion. The base of this layer, found at ~1200m at both locations, was the top of the veering WAA wind layer. In this 1km thick layer at JNU,  $\theta_e$  increased by only 2°K, and at least two well-mixed (small vertical gradient in  $\theta_e$ ) sub-layers were present. The boundary between these two sub-layers (Layers 2a and 2b) was a weak, shallow, stable layer at 1800m. It was most discernable as a slight decrease in relative humidity, increasing wind speed, and a slight increase in  $\theta_e$ . Layer 2 was drier and slightly warmer at SIT, especially at the layer base. It was 600m thick and very well-mixed. There was no definable break within the layer as at JNU, and sub-saturated relative humidities were present through much of its depth.

The WAA layer, also the tilted region of the anticyclone, consisted of two capping inversions bounding the layer between. These are identified as three distinct mesoscale layers. The 100m thick inversion layer, at 1150m at both locations, denotes the boundary between Layer 2 and Layer 3 (C2-3). The wind veered sharply and the speed increased through this inversion.

Layer 3, between the capping inversions, was characterized by weak WAA from SIT towards JNU. At SIT the layer was relatively warm, had veering southerly to westerly flow, warmer  $\theta_e$ , and was very well-mixed. Downstream at JNU this layer was much more stable with colder air and southeasterly flow at its base veering to southerly at the

layer top. Both aircraft soundings showed the veering wind profile through most of the layer, although the winds backed slightly at the layer top.

An inversion (C3-4) was present near 600m separating Layer 3 and the surface based Layer 4. This feature was stronger at JNU due to the colder  $\theta_e$  air within the surface based layer.

The surface based layer (Layer 4) was the air below the C3-4 inversion. Only the upper 250m of this layer was sampled by the King Air at SIT, whereas the entire layer was sampled at JNU. The  $\theta_e$  in Layer 4 was cooler at JNU and two sub-layers appeared to be present. Weak veering winds and a slight warming was present in Layer 4a (300 – 500m), while weak winds backed through Layer 4b (sfc – 300m) suggesting that cold air advection was still occurring near the surface. It is doubtful that the air sampled at the base of the missed approach at SIT was the boundary layer, since the surface  $\theta_e$  based on the METAR was colder than the bottom of the missed approach.

### 3.3.3 Liquid Water Content

The liquid water content (LWC) within the cloud layers was estimated by integration of the concentrations from each of the bins of the FSSP (drop diameters smaller than 45 $\mu$ m) and 200X (drop diameters between 12.5 $\mu$ m and 187.5 $\mu$ m) and the assumption that the particles were spherical liquid water drops. As previously mentioned, uncertainties exist in the 200X estimates of LWC, because the smaller bins with the out of focus particles are included in the liquid water calculation. To address these uncertainties and to insure

the probes were measuring liquid water, not ice crystals, the LWC was also estimated from the Rosemount icing detector voltage (R-LWC). Recall that this instrument measures only subfreezing liquid in all drop sizes and is not affected by the presence of ice crystals. Examination of 2D probe imagery indicated a near total lack of ice crystals throughout both profiles, except Layer 4 at JNU. The King liquid water probe was not functioning on this flight.

### 3.3.4 Liquid water content at Juneau

Supercooled liquid water was present within all of the layers beneath the main subsidence inversion (C1-2) at Juneau. In addition there were also distinct LWC minima within some of the inversion layers (Fig. 3.14). The maxima within the layers and minima within the capping inversions showed the good agreement with the layers defined in the thermodynamic and kinematic discussion.

Layer 2a had its maximum LWC at its cloud top. The FSSP and Rosemount probes, which showed good agreement, measured LWCs exceeded  $0.1 \text{ g m}^{-3}$ . Only 100m below cloud top the LWC quickly decreased below  $0.03 \text{ g m}^{-3}$  and remained low through the rest of the layer. The 200X LWC was very low in this layer, increasing slightly at the layer base. This suggests Layer 2a was dominated by small cloud drops near the cloud top and transitioned to larger drops toward its base. The drop size distributions are presented in the next section.

Layer 2b had supercooled liquid water through much of its depth. At the layer top Rosemount LWC values were near  $0.07 \text{ g m}^{-3}$ , while the 200X reached  $0.1 \text{ g m}^{-3}$ . In

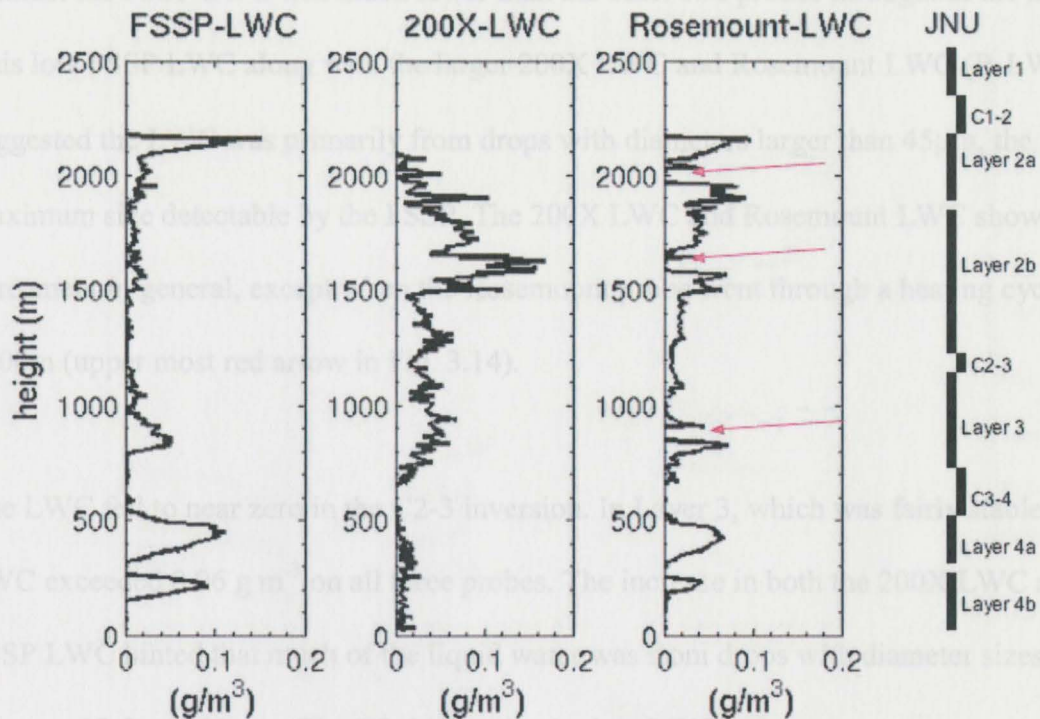


Figure 3.14. Liquid water content from the FSSP, 200X and Rosemount instruments from the research aircraft soundings at Juneau. Rosemount heating cycles (no data) are noted by the red arrows.

Layer 2a had its maximum LWC at the cloud top. The FSSP and Rosemount probes, which showed good agreement, measured LWCs exceeded  $0.1 \text{ g m}^{-3}$ . Only 100m below cloud top the LWC quickly decreased below  $0.03 \text{ g m}^{-3}$  and remained low through the rest of the layer. The 200X LWC was very low in this layer, increasing slightly at the layer base. This suggests Layer 2a was dominated by small cloud drops near the cloud top and transitioned to larger drops toward its base. The drop size distributions are presented in the next section.

Layer 2b had supercooled liquid water through much of its depth. At the layer top Rosemount LWC values were near  $0.07 \text{ g m}^{-3}$ , while the 200X reached  $0.1 \text{ g m}^{-3}$ . In

contrast the FSSP LWC was much lower than the other two probes throughout the layer. This low FSSP LWC along with the larger 200X LWC and Rosemount LWC (R-LWC) suggested the LWC was primarily from drops with diameters larger than  $45\mu\text{m}$ , the maximum size detectable by the FSSP. The 200X LWC and Rosemount LWC show good agreement in general, except when the Rosemount probe went through a heating cycle at 1600m (upper most red arrow in Fig. 3.14).

The LWC fell to near zero in the C2-3 inversion. In Layer 3, which was fairly stable, the LWC exceeded  $0.06\text{ g m}^{-3}$  on all three probes. The increase in both the 200X LWC and FSSP LWC hinted that much of the liquid water was from drops with diameter sizes between 12.5 and  $45\mu\text{m}$ . The C3-4 inversion had no LWC.

Supercooled liquid water was also detected in the two well-mixed layers within Layer 4, as measured by the FSSP-LWC and R-LWC. There were also increased numbers of ice crystals, as observed in the 2DC imagery. The lack of any additional 200X-LWC suggested that both Layer 4a and Layer 4b had most of their LWC in smaller drops.

### 3.3.5 Liquid water content at Sitka

Profiles of the FSSP, 200X, and Rosemount LWCs found over SIT, are shown in (Fig. 3.15). The top of Layer 2 had much lower LWC than at JNU, and did not have the thin liquid water layer at cloud top. The rest of Layer 2 and the inversion C2-3 also had minimal amounts of liquid water.

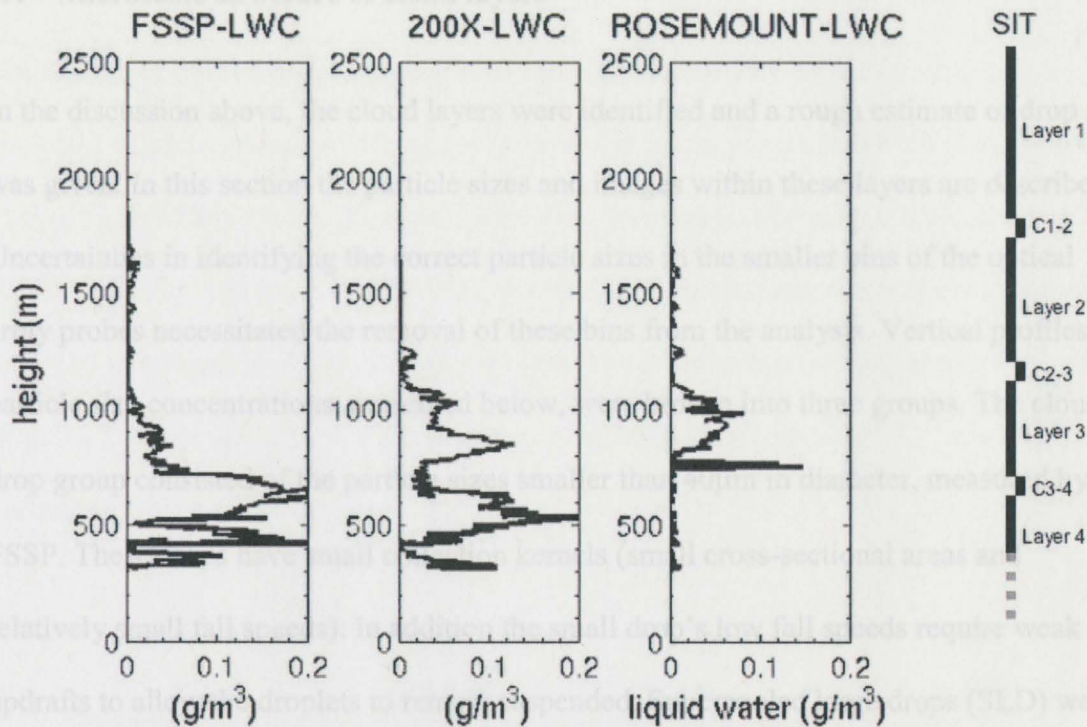


Figure 3.15. Liquid water content from the FSSP, 200X and Rosemount instruments from the research aircraft soundings at Sitka. The Rosemount icing probe only functions above 800m where the temperature is a few degrees below freezing.

In Layer 3, the Rosemount and 200-X probes each measured LWCs near  $0.1 \text{ g m}^{-3}$ , while the 2D-C images showed no ice crystals. The 200X LWC, more than double the FSSP LWC, suggested this layer had much of its liquid water in drops larger than  $45 \mu\text{m}$ . Near the base of Layer 3 the temperature approached  $0^\circ\text{C}$  ending the Rosemount probe's ability to accrete ice and estimate LWC.

At the top of the weak inversion layer C3-4 the FSSP LWC increased sharply to  $0.2 \text{ g m}^{-3}$ , indicating the presence of larger numbers of small drops. Layer 4 at SIT was poorly resolved by the aircraft but both the FSSP and 200X measured more than  $0.1 \text{ g m}^{-3}$  of LWC.

### 3.4 Microscale structure of cloud layers

In the discussion above, the cloud layers were identified and a rough estimate of drop size was given. In this section the particle sizes and images within these layers are described. Uncertainties in identifying the correct particle sizes in the smaller bins of the optical array probes necessitated the removal of these bins from the analysis. Vertical profiles of particle size concentrations, presented below, were broken into three groups. The cloud drop group consisted of the particle sizes smaller than  $40\mu\text{m}$  in diameter, measured by the FSSP. These drops have small collection kernels (small cross-sectional areas and relatively small fall speeds). In addition the small drop's low fall speeds require weak updrafts to allow the droplets to remain suspended. Supercooled large drops (SLD) were identified by the drop concentrations from the FSSP bins exceeding  $40\mu\text{m}$  and from the 200X bins exceeding  $75\mu\text{m}$  in diameter. SLD drops have larger collection kernels, large sedimentation rates, and can initiate precipitation via a collision coalescence process (Klett and Davis 1973). Using only 200X bins exceeding  $75\mu\text{m}$  reduces the counts of out of focus drops but creates a gap in the drop size spectrum between  $45 - 75\mu\text{m}$ . Supercooled drizzle, following Rasumssen et al. (2002) is defined in this paper as drops with diameters  $\geq 100\mu\text{m}$ , was identified from the 200X and 2DC probes. The differences between the 200X and 2DC drizzle concentrations may have been due to the probes' different sample volumes. Particle size distributions, at specific levels, are also presented below.

### 3.4.1 Particle size distribution of the layers at Juneau

The thin layer of liquid water, found near the highest cloud top (top of Layer 2a), consisted of cloud droplets with a concentration of  $50 \text{ cm}^{-3}$  and small SLD (Fig. 3.16a). Larger SLD, in lower concentrations, were first detected just beneath the cloud droplet dominated cloud top layer (Fig. 3.16b). A broad size distribution was already present only 150 m below cloud top, with many of the cloud drops approaching the SLD size (Fig. 3.17, bin counts). Low concentrations of supercooled drizzle,  $0.1 \text{ L}^{-1}$ , were also present.

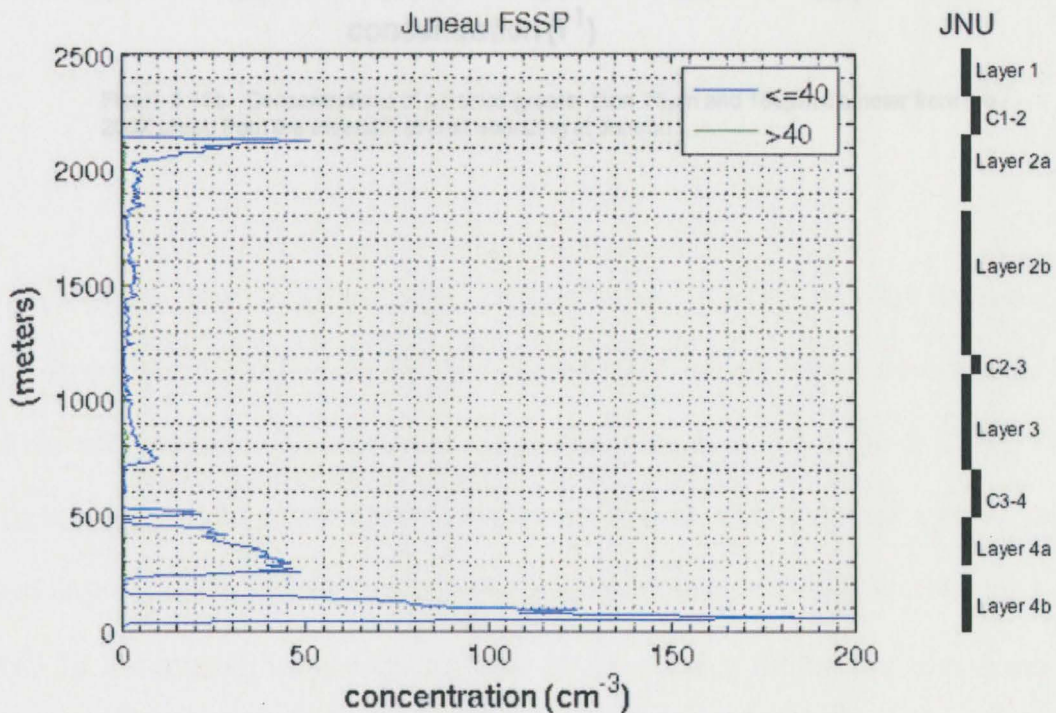


Figure 3.16a. Particle concentrations for cloud drops and small SLD from the FSSP from the research aircraft sounding at Juneau.

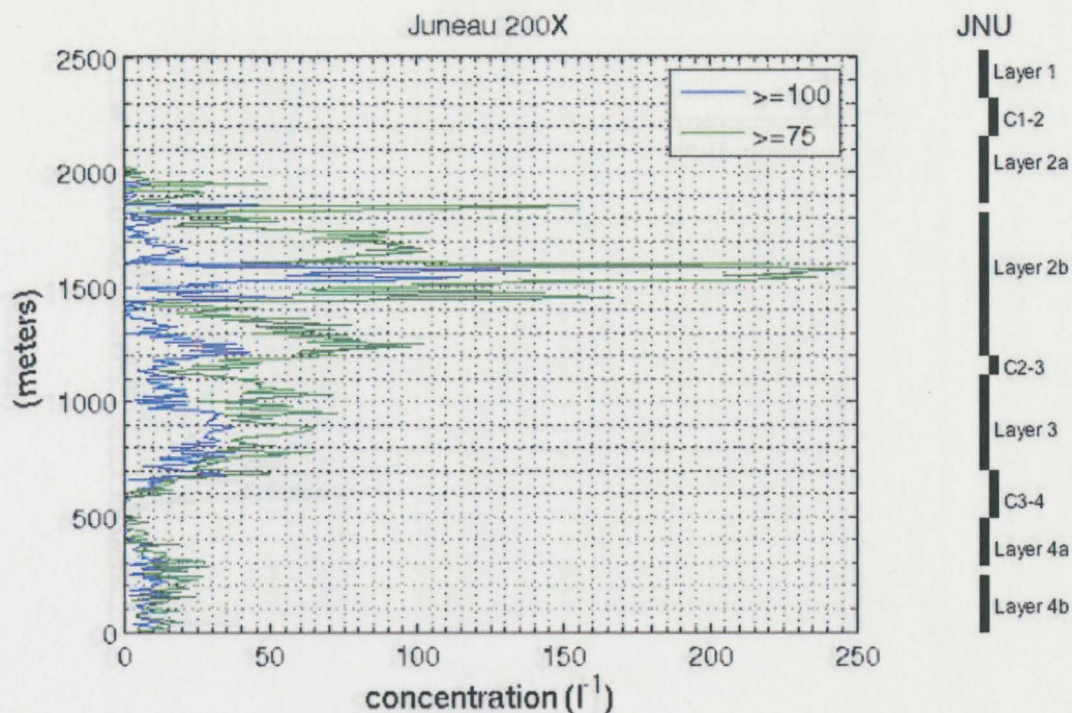


Figure 3.16b. Concentrations of particles greater than 75 $\mu\text{m}$  and 100 $\mu\text{m}$  diameter from the 200X probe from the research aircraft sounding at Juneau.

In Layer 2b the cloud drop concentrations were quite low ( $< 5 \text{ cm}^{-3}$ ) through the entire layer. In contrast the STD concentrations exceed  $100 \text{ L}^{-1}$  at several levels within the layer and supercooled drizzle also appeared in significant numbers (Fig. 3.16b & 3.16c). The particle size distribution near 1550m shows a wide range of sizes present with the small cloud drop concentrations more than an order of magnitude less than the cloud top layer (Fig. 3.18, bin counts). Many drops had diameters exceeding  $100\mu\text{m}$ , and some exceeded  $200\mu\text{m}$ . The particle images from the 2D-C were all spherical, suggesting liquid drops. They increased in size towards the layer base (Fig. 3.19).

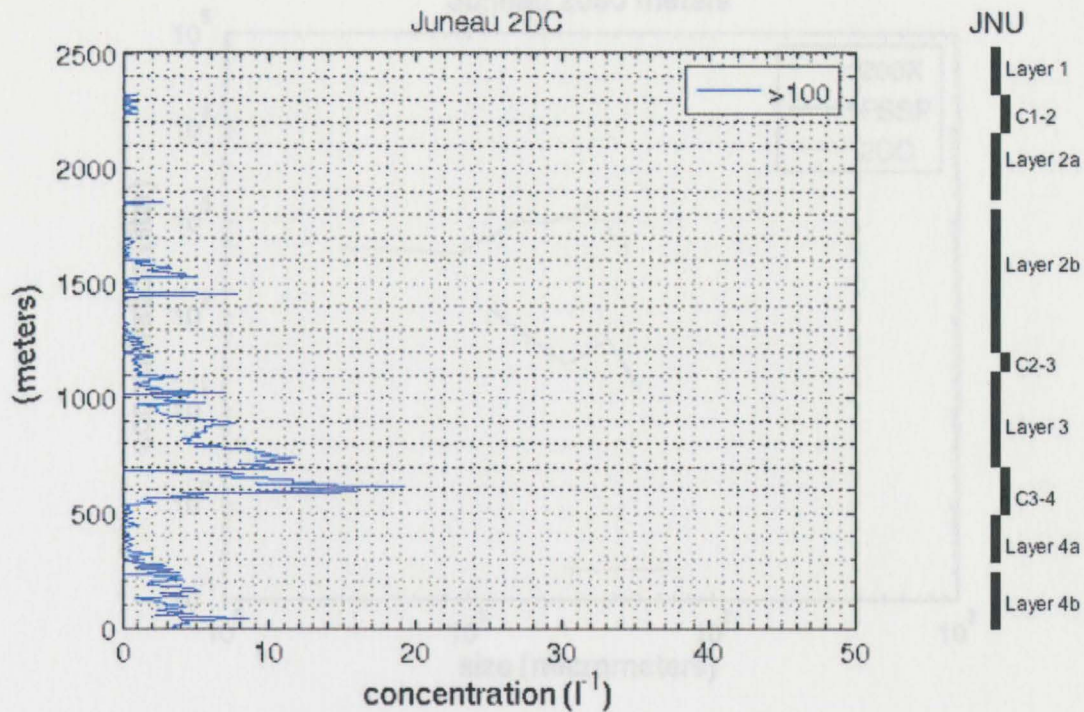


Figure 3.16c. Concentrations of particles larger than  $100\mu\text{m}$  diameter and from the 2DC from the research aircraft sounding at Juneau.

In Layer 2b the cloud drop concentration was quite low ( $< 5 \text{ cm}^{-3}$ ) through the entire layer. In contrast the SLD concentrations exceed  $100 \text{ L}^{-1}$  at several levels within the layer and supercooled drizzle also appeared in significant numbers (Fig 3.16b & 3.16c). The particle size distribution near 1550m shows a wide range of sizes present with the small cloud drop concentrations more than an order of magnitude less than the cloud top layer (Fig 3.18, bin counts). Many drops had diameters exceeding  $100\mu\text{m}$ , and some exceeded  $200\mu\text{m}$ . The particle images from the 2D-C were all spherical, suggesting liquid drops. They increased in size towards the layer base (Fig. 3.19).

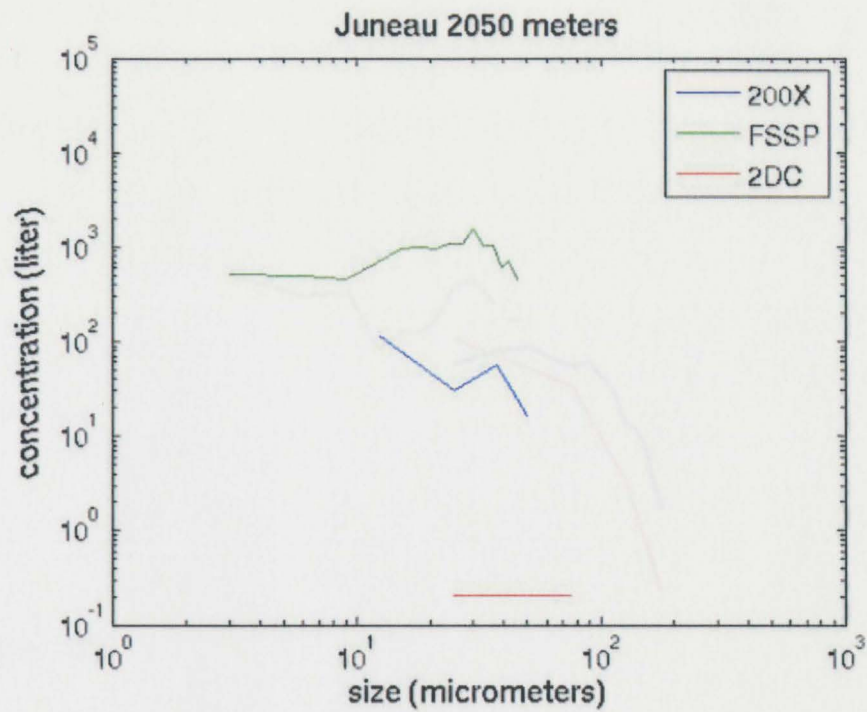


Figure 3.17. Concentrations of particles by size from the FSSP, 200X and 2DC from the research aircraft sounding at Juneau.

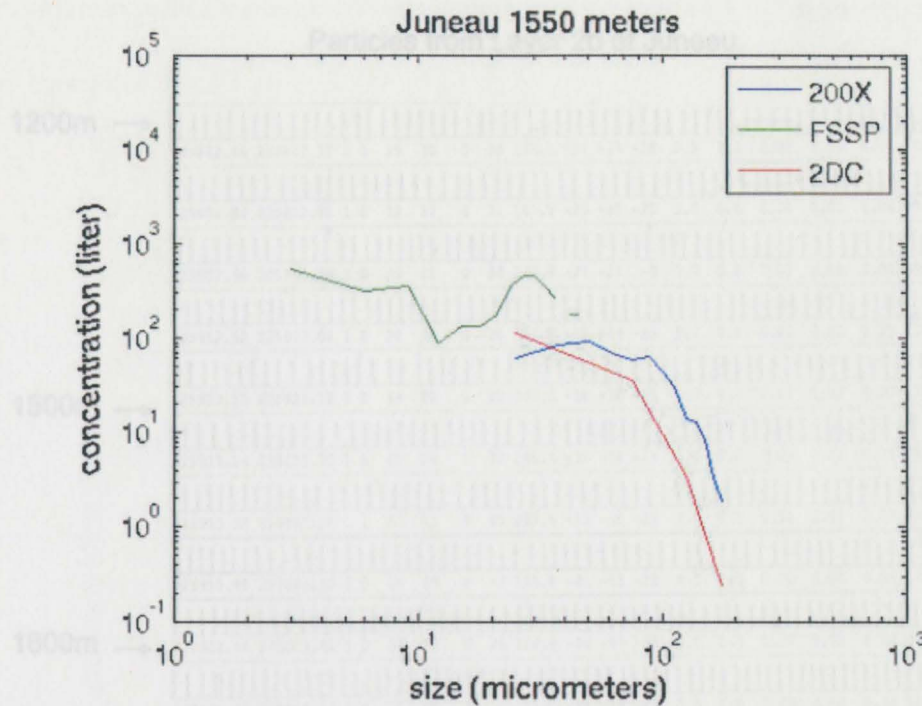


Figure 3.18. Concentrations of particles by size from the FSSP, 200X and 2DC from the research aircraft sounding at Juneau.

Particle concentrations decreased, with descending altitude, through the C2-3 inversion near 1150m. In the stable warm air subsaturated cloud layer below the inversion (Layer 3) the cloud drop concentration increased to  $10 \text{ cm}^{-3}$ . Just above this thin cloud drop layer (at 750m) the SLD and supercooled drizzle concentrations increased. As these drops fall through the cloud drop layer, the drizzle concentration appeared to increase. The size spectrum near 750 m shows a bimodal distribution with a small drop ( $< 10 \mu\text{m}$ ) and a SLD mode having a tail extending to 200  $\mu\text{m}$  drizzle (Fig. 3.20, bin counts). Particle images showed all spheres (Fig. 3.21). Within the strong subsaturated C3-4 inversion the cloud drop and SLD concentrations again decreased to near zero, whereas the drizzle

Particles from Layer 2b at Juneau

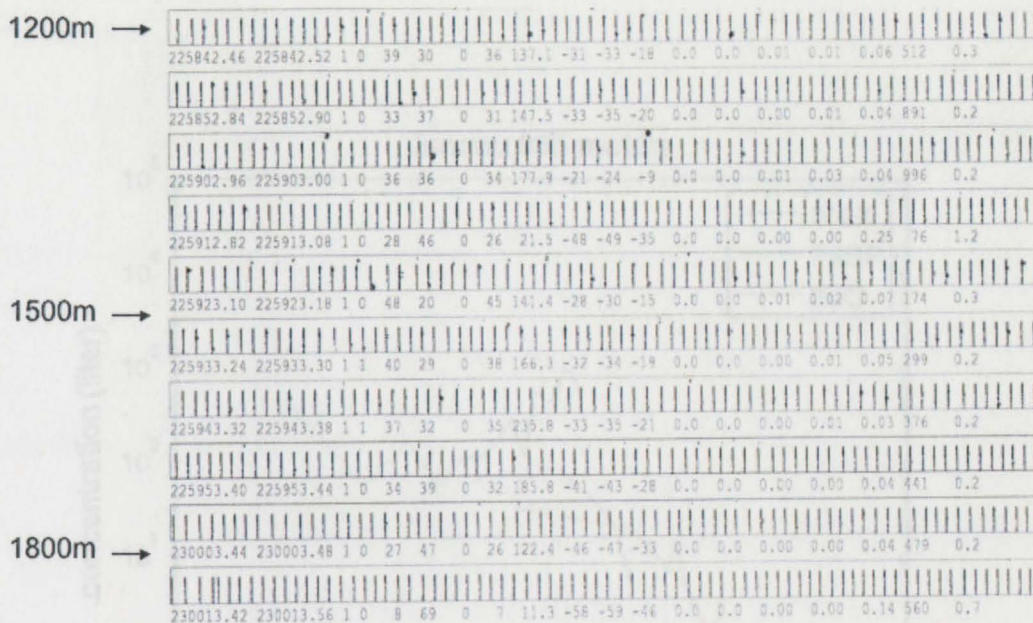


Fig 3.19. Particle images from the 2D-C with layer 2. Vertical bars | in plot span 960 $\mu$ m.

Particle concentrations decreased, with descending altitude, through the C2-3 inversion near 1150m. In the stable warm air advection cloud layer below the inversion (Layer 3) the cloud drop concentration increased to 10 cm<sup>-3</sup>. Just above this thin cloud drop layer (at 750m) the SLD and supercooled drizzle concentrations increased. As these drops fell through the cloud drop layer, the drizzle concentration appeared to increase. The size spectrum near 750 m shows a bimodal distribution with a small drop (< 10 $\mu$ m) and a SLD mode having a tail extending to 200  $\mu$ m drizzle (Fig. 3.20, bin counts). Particle images showed all spheres (Fig. 3.21). Within the strong subsaturated C3-4 inversion the cloud drop and SLD concentrations again decreased to near zero, whereas the drizzle

concentration initially increased then decreased to less than  $1 \text{ L}^{-1}$  toward the base of the C3-4 inversion (Figs 3.16 & 3.22).

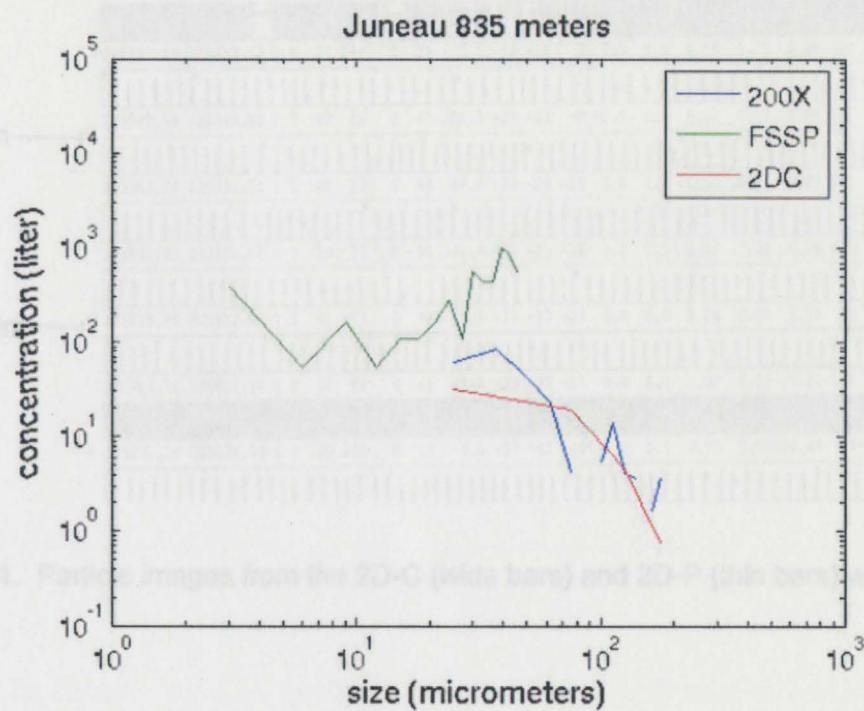


Figure 3.20. Concentrations of particles by size from the FSSP, 200X and 2DC from the research aircraft sounding at Juneau.

Particles from Layer 3 at Juneau

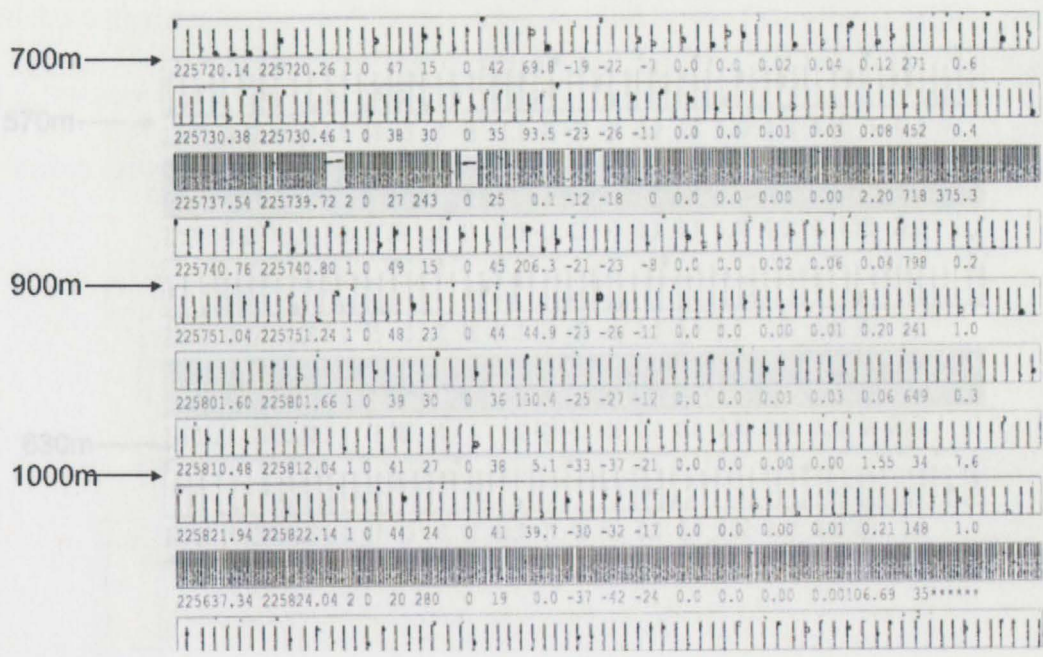


Fig 3.21. Particle images from the 2D-C (wide bars) and 2D-P (thin bars) within Layer 3.

In Layer 4a, beneath the C3-4 inversion, the cloud drop concentration quickly increased to  $45 \text{ cm}^{-3}$ . The ratio of SLD to the cloud drops was much smaller than in the layers above. SLD and drizzle concentrations increased towards the base of the layer. The size distribution at 270m (Fig. 3.23, bin counts), below the center of the layer, shows that two orders of magnitude more cloud drops were present than in the layers above. Even with the higher numbers of cloud drops a broad size spectrum was still present. SLD, in concentrations of  $10 \text{ L}^{-1}$  were present, with the largest drizzle diameters exceeding  $400 \mu\text{m}$ . The cloud drop concentration decreased to zero within the thin inversion separating Layers 4a and 4b. Layer 4b had significantly more cloud drops than any of the other layers approaching  $300 \text{ cm}^{-3}$ . The drizzle concentration continued to slowly increase with decreasing height. The particle size distribution through the 65m level of

Particles from the inversion B3-4 at Juneau

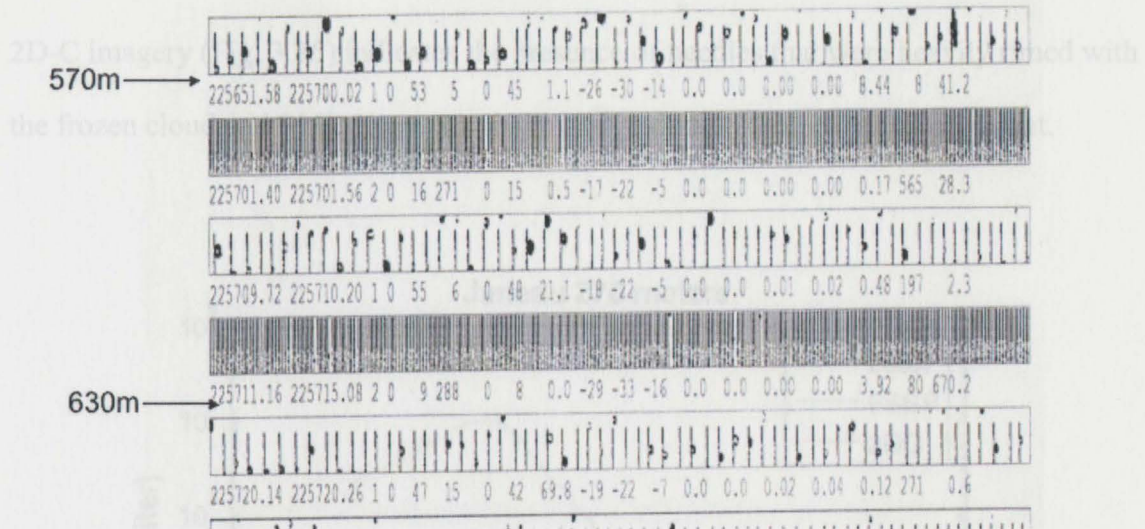


Fig 3.22. Particle images from the 2D-C (wide bars) and 2D-P (thin bars) within B3-4.

In Layer 4a, beneath the C3-4 inversion, the cloud drop concentration quickly increased to  $45 \text{ cm}^{-3}$ . The ratio of SLD to the cloud drops was much smaller than in the layers above. SLD and drizzle concentrations increased towards the base of the layer. The size distribution at 270m (Fig. 3.23, bin counts), below the center of the layer, shows that two orders of magnitude more cloud drops were present than in the layers above. Even with the higher numbers of cloud drops a broad size spectrum was still present. SLD, in concentrations of  $10 \text{ L}^{-1}$  were present, with the largest drizzle diameters exceeding  $400 \mu\text{m}$ . The cloud drop concentration decreased to zero within the thin inversion separating Layers 4a and 4b. Layer 4b had significantly more cloud drops than any of the other layers approaching  $300 \text{ cm}^{-3}$ . The drizzle concentration continued to slowly increase with decreasing height. The particle size distribution through the 65m level of

the layer shows the wide range of particle sizes and the large numbers of cloud drops. Particles with diameters up to  $800\mu\text{m}$  were identified by the 2DC (Fig. 3.24, bin counts). 2D-C imagery (Fig. 3.25) indicates the presence of needles that were heavily rimed with the frozen cloud and SLD drops. Some very large drizzle drops were also present.

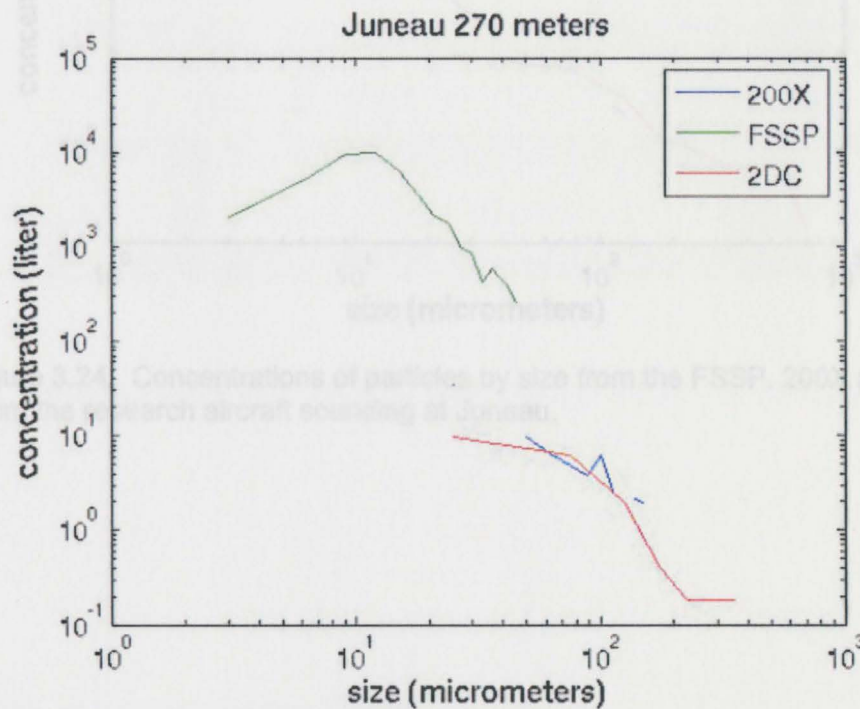


Figure 3.23. Concentrations of particles by size from the FSSP, 200X and 2DC from the research aircraft sounding at Juneau.

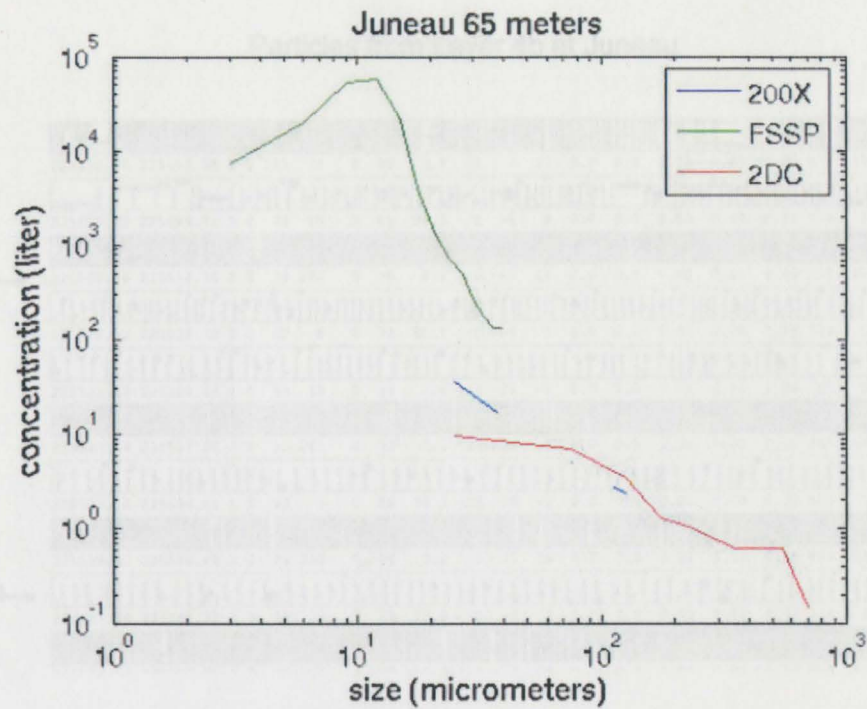


Figure 3.24. Concentrations of particles by size from the FSSP, 200X and 2DC from the research aircraft sounding at Juneau.

### 3.4.2 Particle size distributions at Sitka

Very low concentrations of cloud drops ( $1 \text{ cm}^{-3}$ ) and small SLD were in the low LWC cloud top layer at Sitka (Fig. 3.26a). Low to zero drop concentrations were observed throughout the rest of Layer 2 and through the inversion C2-3 (Fig. 3.26b and 3.26c). The size distribution at cloud top (Fig. 3.27), shows the low concentrations of cloud drops and SLD with the largest drops reaching  $\sim 50 \mu\text{m}$  in diameter.

Particles from Layer 4b at Juneau

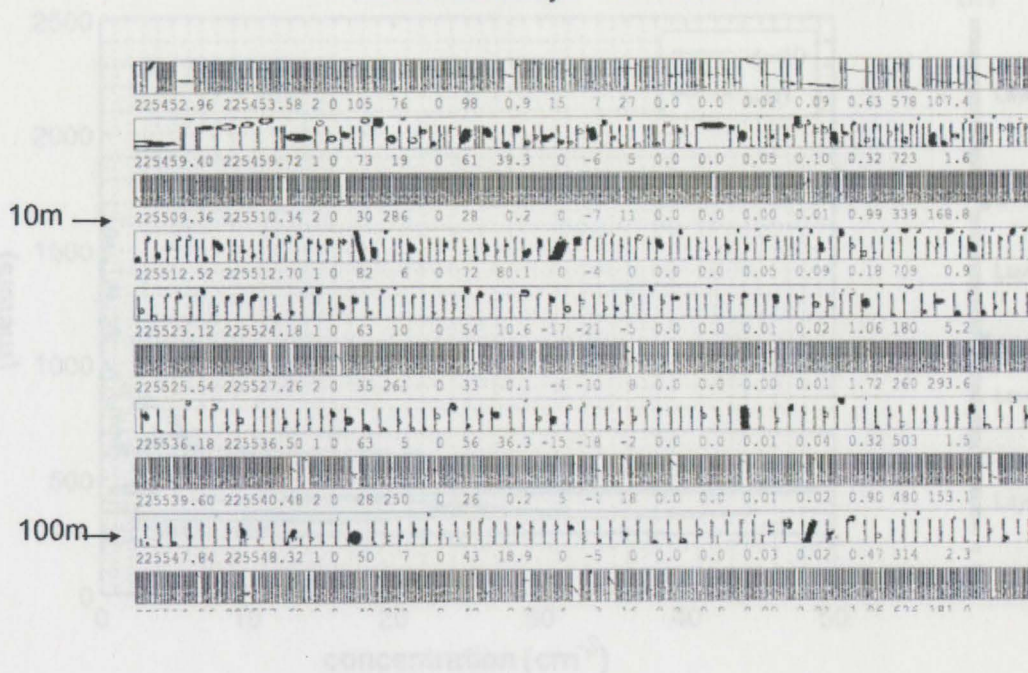


Fig 3.25. Particle images from the 2D-C (wide bars) and 2D-P (thin bars) within Layer 4b.

3.4.2 Particle size distributions at Sitka

Very low concentrations of cloud drops ( $1 \text{ cm}^{-3}$ ) and small SLD were in the low LWC cloud top layer at Sitka (Fig. 3.26a). Low to zero drop concentrations were observed throughout the rest of Layer 2 and through the inversion C2-3 (Fig. 3.26b and 3.26c). The size distribution at cloud top (Fig. 3.27), shows the low concentrations of cloud drops and SLD with the largest drops reaching  $\sim 50 \mu\text{m}$  in diameter.

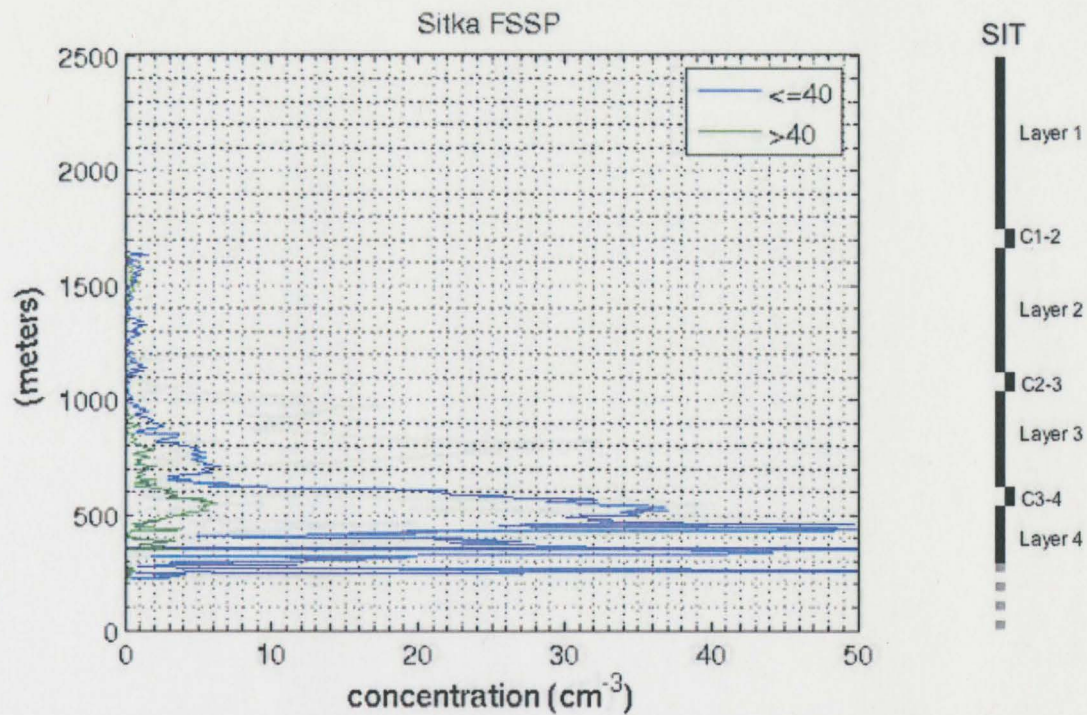


Figure 3.26a. Particle concentrations for cloud drops and small SLD from the FSSP from the research aircraft sounding at Juneau.

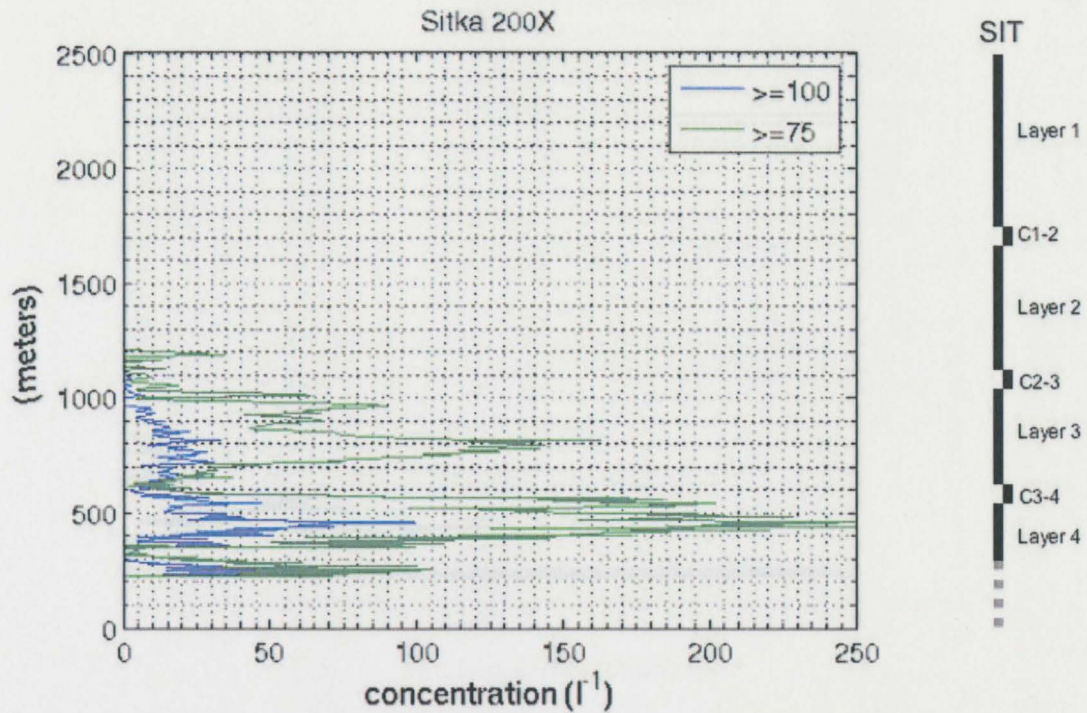


Figure 3.26b. Concentrations of particles greater than 75 $\mu\text{m}$  and 100 $\mu\text{m}$  diameter from the 200X probe from the research aircraft sounding at Juneau.

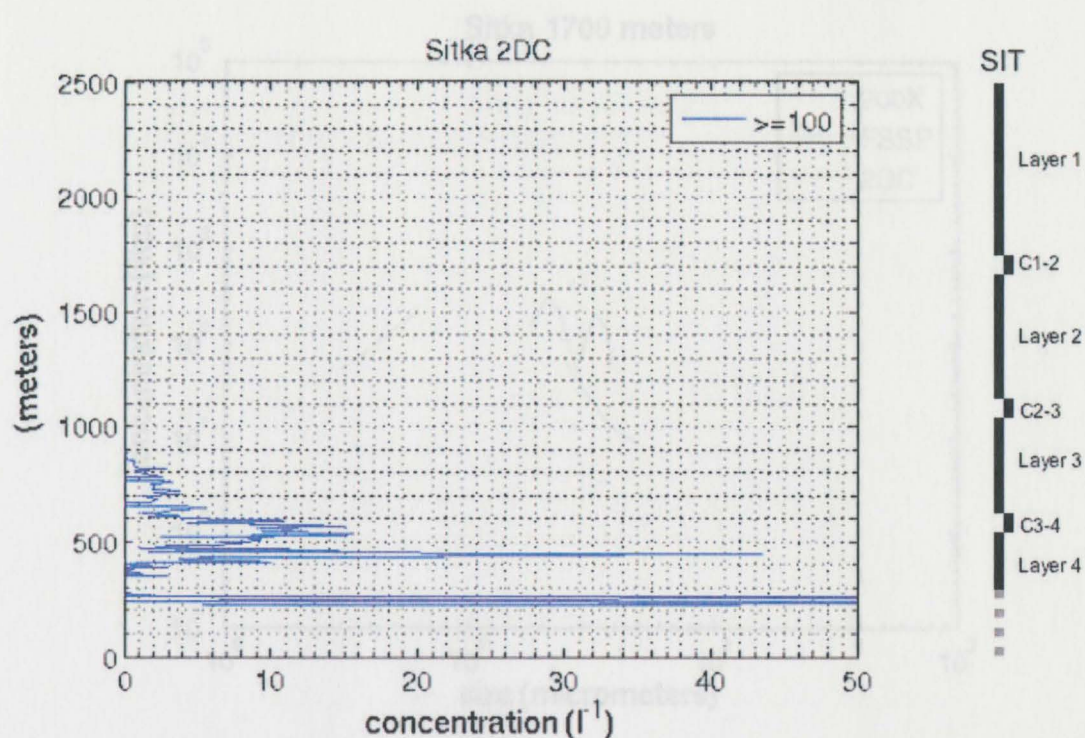


Figure 3.26c. Concentrations of particles larger than  $100\mu\text{m}$  diameter and from the 2DC from the research aircraft sounding at Juneau.

In Layer 3 the SLD concentrations increased significantly while the cloud drop concentrations remained remarkably low ( $< 10 \text{ cm}^{-3}$ ). Supercooled drizzle concentrations increased slowly, reaching a maximum of  $5 \text{ l}^{-1}$  near the layer base (Fig. 3.26c). The size distribution at the top of Layer 3 weakly hints at a bimodal distribution (Fig. 3.28). The tail of the distribution includes supercooled drizzle with diameters exceeding  $100\mu\text{m}$ . Two hundred meters below, the same broad particle size distribution was present with more drops in all size ranges (Fig. 3.29). The bimodal spectrum was still present and the concentration of supercooled drizzle increased. The largest drops captured approached  $200\mu\text{m}$  in diameter. The 2D-C particle images were all spheres suggesting an all-liquid cloud (Fig. 3.30).

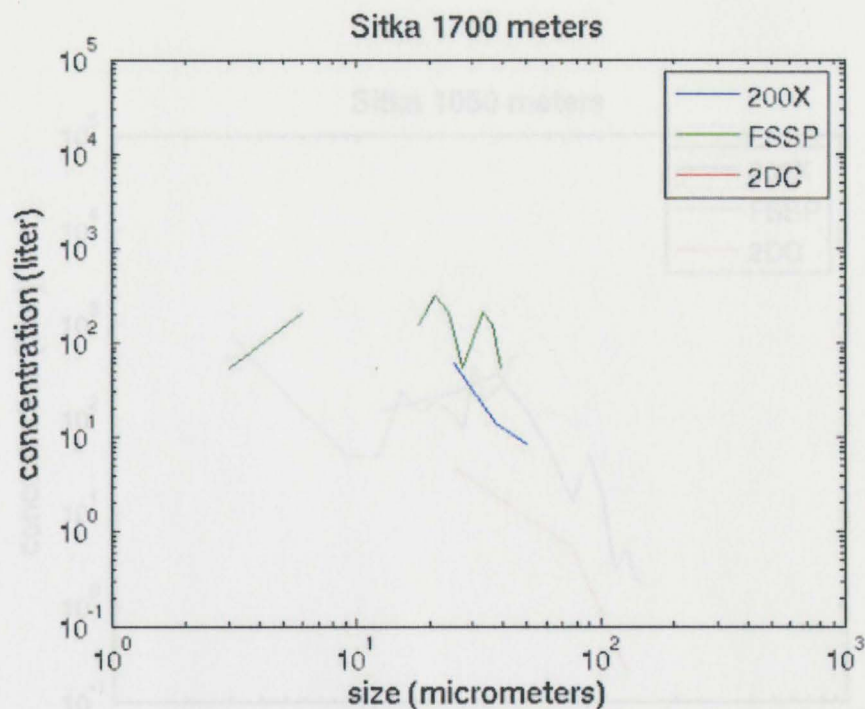


Figure 3.27. Concentrations of particles by size from the FSSP, 200X and 2DC from the research aircraft sounding at Sitka.

In Layer 3 the SLD concentrations increased significantly while the cloud drop concentrations remained remarkably low ( $< 10 \text{ cm}^{-3}$ ). Supercooled drizzle concentrations increased slowly, reaching a maximum of  $5 \text{ L}^{-1}$  near the layer base (Fig. 3.26c). The size distribution at the top of Layer 3 weakly hints at a bimodal distribution (Fig. 3.28). The tail of the distribution includes supercooled drizzle with diameters exceeding  $100 \mu\text{m}$ . Two hundred meters below, the same broad particle size distribution was present with more drops in all size ranges (Fig. 3.29). The bimodal spectrum was still present and the concentration of supercooled drizzle increased. The largest drops captured approached  $200 \mu\text{m}$  in diameter. The 2D-C particle images were all spheres suggesting an all-liquid cloud (Fig. 3.30).

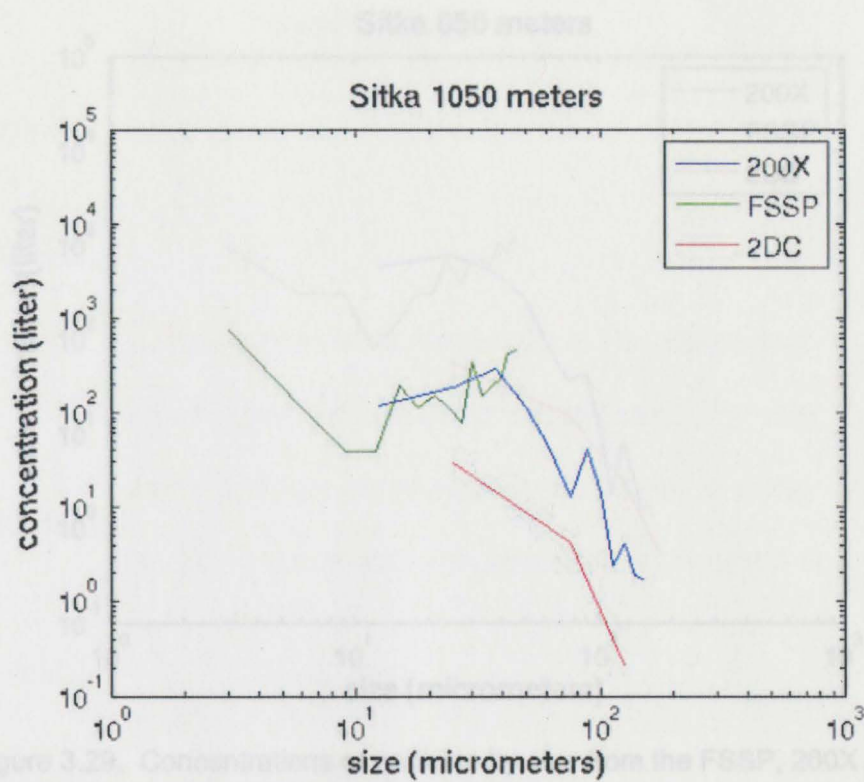


Figure 3.28. Concentrations of particles by size from the FSSP, 200X and 2DC from the research aircraft sounding at Sitka.

Figure 3.28. Concentrations of particles by size from the FSSP, 200X and 2DC from the research aircraft sounding at Sitka.

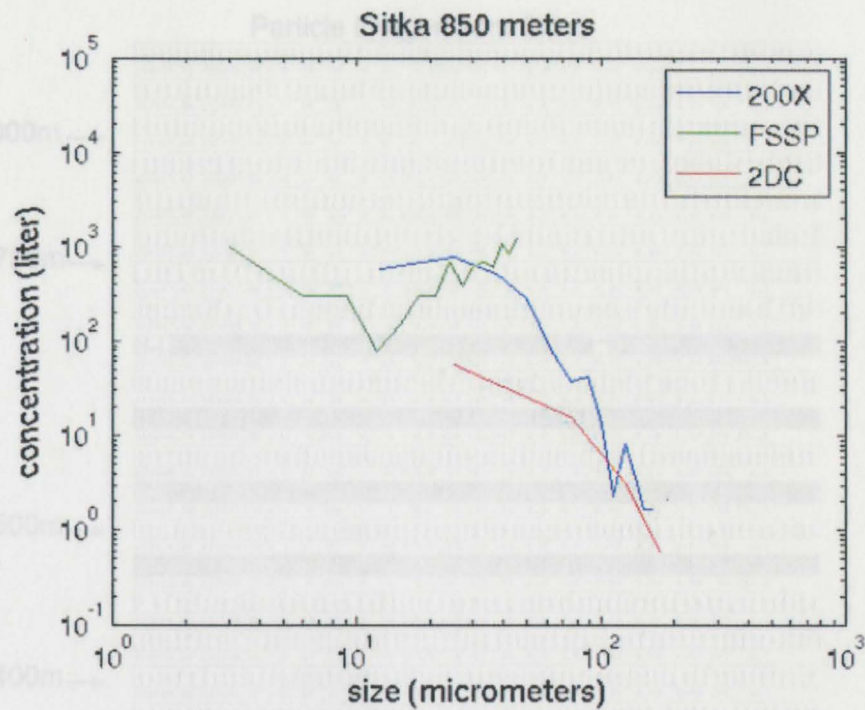


Figure 3.29. Concentrations of particles by size from the FSSP, 200X and 2DC from the research aircraft sounding at Sitka.

The cloud drop and SLD concentrations decreased slightly within the weak C3-4 inversion. They then increased in the top of Layer 4, with the cloud drop concentration increasing but still low ( $35 \text{ cm}^{-3}$ ). The SLD and freezing drizzle concentration also showed an increase at this level with the size distribution shown in (Fig. 3.31).

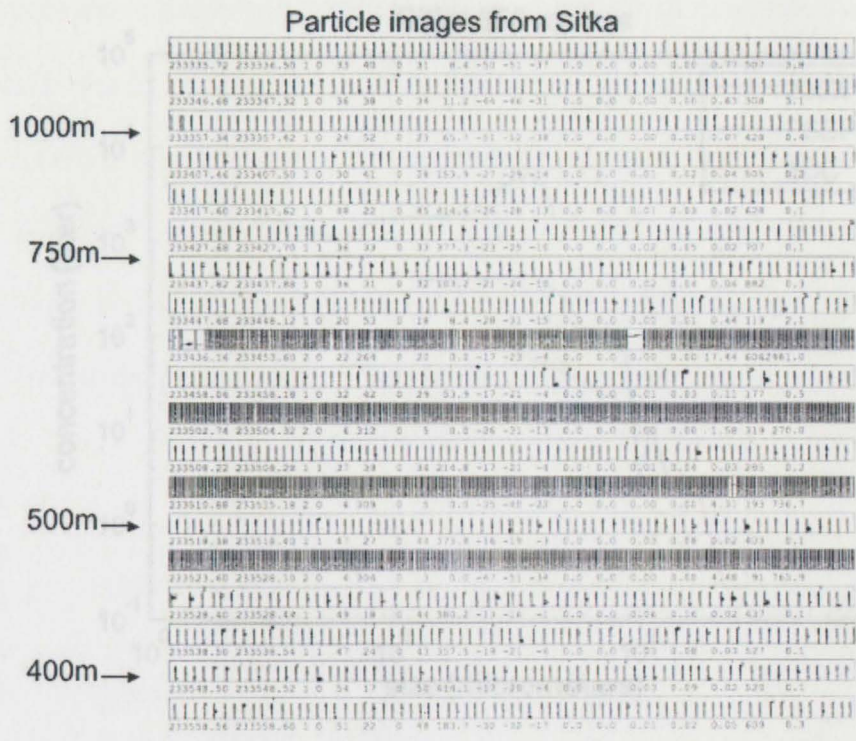


Figure 3.31. Concentrations of aerosols by size from the FSSP, 200X and ZDC  
 Fig 3.30. Particle images from the 2D-C (wide bars) and 2D-P (thin bars) at SIT.

The cloud drop and SLD concentrations decreased slightly within the weak C3-4 inversion. They then increased in the top of Layer 4, with the cloud drop concentration increasing but still low ( $35 \text{ cm}^{-3}$ ). The SLD and freezing drizzle concentration also showed an increase at this level with the size distribution shown in (Fig. 3.31).

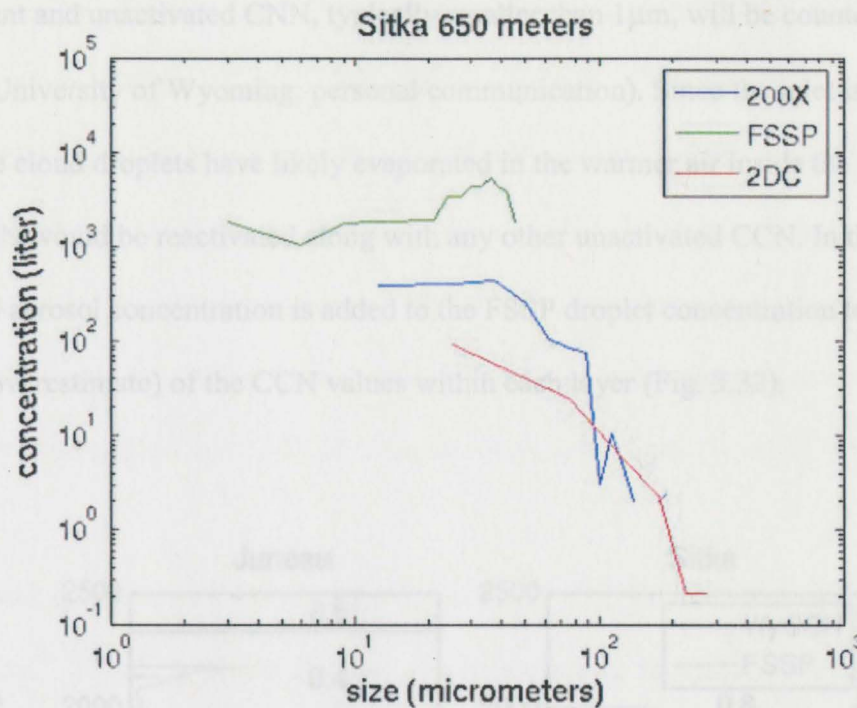


Figure 3.31. Concentrations of particles by size from the FSSP, 200X and 2DC from the research aircraft sounding at Sitka.

### 3.4.3 Vertical Distribution of CCN

The background aerosol population and its subsets, the cloud condensation nucleus (CCN) and ice nucleus (IN) population, are important in determining the microphysical character of clouds (Ludlam 1980, Levin and Cotton 2009). The thermal gradient diffusion chamber flown on the King Air (WyCCN), provided CCN concentrations through the JNU sounding depth. The instrument counted the number of activated CCN present in the airmass at different supersaturations, the IN concentrations were not available in this data set. Within the cloud layers the saturated air is drawn into the aircraft where it begins to warm to the cabin temperature. This air is then drawn into the

instrument and unactivated CCN, typically smaller than  $1\mu\text{m}$ , will be counted (Jefferson Snider, University of Wyoming; personal communication). Since the inlet is inside the cabin the cloud droplets have likely evaporated in the warmer air inside the cabin and their CCN would be reactivated along with any other unactivated CCN. In this paper the WyCCN aerosol concentration is added to the FSSP droplet concentration to get an upper bound (overestimate) of the CCN values within each layer (Fig. 3.32).

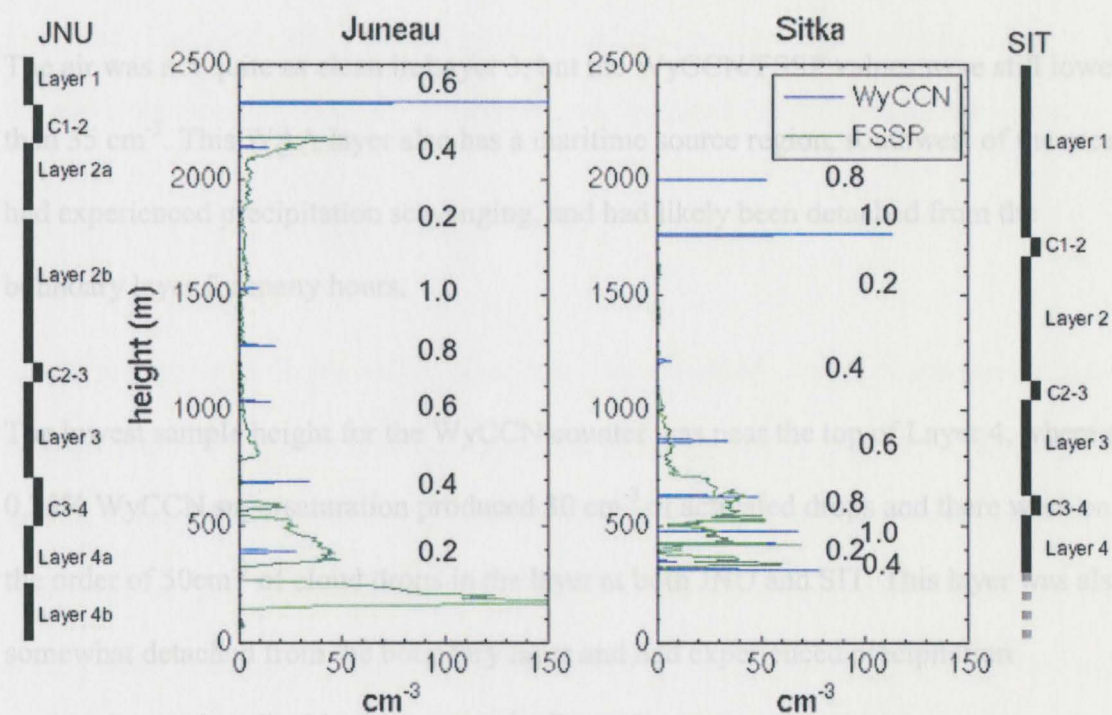


Fig 3.32. Thermal gradient diffusion chamber CCN and FSSP drop concentrations for the Juneau and Sitka soundings. Black numbers indicate WyCCN supersaturation setting in percent.

The WyCCN/FSSP concentrations in Layer 1, above the capping inversion, were much larger than those found in most of the cloud layers. Recall that Layer 1 was under large scale descending motion and the source region was the upper troposphere northwest of

the region. The air within Layer 2 was remarkably clean, with the WyCCN/FSSP concentrations less than  $10 \text{ cm}^{-3}$ . This was for a large WyCCN supersaturation value of 1.0%, which was probably greater than the cloud's supersaturation. Layer 2 was comprised of very clean Pacific Ocean source air, which had likely been detached from the boundary layer for an extended period due to the inversions below. It also had continuous precipitation fall through it for 39 hrs prior to the research aircraft flight. All of these would tend to reduce CCN concentrations in the layer (Ludlam 1980).

The air was not quite as clean in Layer 3, but the WyCCN/FSSP values were still lower than  $35 \text{ cm}^{-3}$ . This WAA layer also has a maritime source region, southwest of the area, had experienced precipitation scavenging, and had likely been detached from the boundary layer for many hours.

The lowest sample height for the WyCCN counter was near the top of Layer 4, where a 0.25% WyCCN supersaturation produced  $30 \text{ cm}^{-3}$  of activated drops and there were on the order of  $50 \text{ cm}^{-3}$  of cloud drops in the layer at both JNU and SIT. This layer was also somewhat detached from the boundary layer and had experienced precipitation scavenging as described in the mesoscale discussion.

Although the boundary layer, Layer 4b, was not sampled by the WyCCN counter, the FSSP indicated  $300 \text{ cm}^{-3}$  cloud drop concentrations, indicating that the boundary layer had by far the highest concentration of CCN. The source region for this layer was the frozen interior of Alaska and the Yukon. CCN from this region, along with any CCN added by

the inside passage bays and inlets, as well as CCN from the city of Juneau all may have contributed to the  $300 \text{ cm}^{-3}$  drop concentration.

### 3.5 Discussion

#### 3.5.1 Conceptual view of the evolution of the cloud layers

The large and small-scale structure of the atmospheric layers was presented above. In this section a conceptual view of the evolution of the cloud layers and their microstructure is presented. The interaction between synoptic and mesoscale vertical motions along with the available moisture and CCN concentrations produced the different cloud layers.

#### 3.5.2 Cloud top layer

The hypothesized evolution of the cloud top was particularly complex and interesting. As noted above, LWC greater than  $0.15 \text{ g m}^{-3}$ , along with a fairly broad size distribution was present at the JNU cloud top, whereas, very low LWC and a similarly broad spectrum was present at SIT. The cloud top layer's LWC evolution is thought to be primarily from mechanical (isentropic) lifting, perhaps enhanced by isobaric mixing and/or radiational cooling. The observed broad drop size spectrum, in particular, may have been a result of the isobaric mixing and radiational cooling, as well the background CCN concentration.

Recall that the cloud top and base of the synoptic scale inversion C1-2 was 500m higher at JNU than upstream at SIT. The 10 m/s westerly flow along C1-2 suggested that the air along the  $295^\circ\text{K } \theta_e$  surface was indeed rising. If we infer that the slope of the inversion is

at least ~500m over the 200km distance from SIT-JNU, then mechanical lifting of the layer of air along and just beneath the inversion suggests a  $25\text{cm s}^{-1}$  upward vertical velocity. In addition the maximum drop sizes were  $\sim 100\mu\text{m}$  and they were falling out of the layer base. A  $100\mu\text{m}$  drop has a fall speed of  $\sim 27\text{cm s}^{-1}$  (Rogers and Yau, 1989), thus the vertical velocity was likely less than this. A parcel model could also be constructed from the observations to confirm this vertical velocity estimate. The slope of the C1-2 inversion upstream of SIT was likely much shallower than between SIT and JNU, with weaker vertical motion. The low LWC at SIT, along with the IR satellite (Fig. 3.10b) showing similar cloud top temperatures near there and to the west, supports this idea.

In addition to the layer lift associated with the rising  $295\theta_e$  surface at Juneau, the speed shear within the strong inversion at cloud top produced Richardson numbers below 0.3, which suggested that mixing was possible between the warmer and higher dew point temperature air within the inversion and the colder cloudy air just below it. This mixing idea is supported by the higher drop concentrations measured in the cloud top layer, which suggest that air richer in CCN has mixed down into the cloud from the inversion layer just above cloud top (see Fig. 3.32). The higher CCN concentration within C1-2 may be a result of the evaporation of drops as they exit the cloud top and the subsequent release of their CCN, as well as a down-mixing of the mid-tropospheric Layer 1 air, which had not experienced precipitation scavenging. In addition to the higher CCN concentrations, the isobaric dilution of subsaturated, higher dew point temperature air from above, with colder saturated cloudy air, can lead to enhanced supersaturations as the parcels mix (Korolev and Issac 2000). We infer higher dew point temperature air just

above the cloud top mixed into the colder cloud layer. The T/Td profiles at both SIT and JNU (Fig. 3.11) show an increase in Td within C1-2 at the wind speed maxima. This feature is observed in a few of the cases observed but not discussed by Pobanz et al. (1993). The increase in Td was observed in both the ascent and descent soundings so wetting of the dew point probe is unlikely and the feature appears to be a real feature. The maximum Td is several degrees warmer than the cloud top temperature. Korolev and Issac (2000) further suggest that these higher supersaturations may eventually, after numerous mixing events, result in larger drops. At SIT the shear was weak and somewhat detached from the C1-2. This resulting higher Richardson number would therefore suggest decreased mixing and lower supersaturations and help explain the lower LWC at SIT as compared to JNU.

Evidence was presented in the microscale structure discussion that SLD and perhaps even small drizzle ( $\geq 100\mu\text{m}$ ) were present in the cloud top layer at Juneau. The role of giant and ultra-giant CCN in the production of the SLD was not available from this data set. Radiational cooling of the drops at and near cloud top has been offered as an explanation for the observation of larger drops at cloud top (Rasmussen et. al. 2002). At night radiational cooling occurs as the drops near cloud top emit long-wave radiation to space. Hartman and Harrington's (2005a) modeling study indicates that the heat losses occur primarily in the top 50m of the cloud top layer. Radiational cooling of the drop surface decreases the saturation vapor pressure and increases the supersaturation at the drop surface. The drop heat losses and potential increased growth occur primarily in the drops with diameters larger than  $20\mu\text{m}$  and having a longer residence time in the cloud

top layer. The modeling study of Hartman and Harrington (2005b) showed that the addition of weak short-wave solar radiation to the model cloud minimally changed the impacts of the long-wave IR losses to space.

In mid-January, Juneau and Sitka's high latitude ( $56^{\circ}\text{N}$ ) provides more than 16h of darkness. The cloud top was exposed directly to space, allowing for optimal long-wave radiational losses. By the 2300 UTC flight time the sun was above the horizon and had already passed through its maximum solar angle ( $77^{\circ}$ ). This solar angle likely provided very low amounts of short-wave radiation to the cloud and allowed the long-wave radiational losses to continue to dominate. The thin depth of the cloud top layer (Fig. 3.14) suggested that many of the drops would have spent a significant amount of time within 50 m of cloud top and experienced significant long wave IR radiational losses to space.

The mesoscale forcing, cloud top mixing, and LWC were greater at Juneau than Sitka, but both had similar CCN concentrations (see Fig. 3.32) and both had SLD present (Fig. 3.17 and Fig. 3.27). This may suggest that radiational cooling was the primary producer of the SLD in the cloud top layer. These observations are in agreement with modeling work presented in Rasmussen et al. 2002.

Although the temperature was near  $-10^{\circ}\text{C}$ , the ice phase was absent at the cloud tops. This was likely due to the relatively warm cloud temperatures (Fletcher 1964, Meyers et

al. 1993) where IN are not often active, and also the depletion of IN due to the earlier snow. In addition source if IN are probably low in this region at this time of year.

*NARR reanalysis was too coarse to correctly identify these thin layers and was not used.*

Layer 2, beneath the Sitka cloud top, had essentially no LWC. This was likely due to the warmer and drier air within Layer 2, upstream of SIT moving into the region. It is doubtful that this layer was formed by down mixing of lower dew point temperature air from Layer 1 since the CCN concentrations are so low (see Fig. 3.32). At Juneau a supercooled liquid water cloud with significant concentrations of SLD formed within Layer 2b. This cloud layer was formed by shallow convection driven by discrete layers of warm advection of moist air. As this warm moist air moved beneath cooler  $\theta_e$  air above, the layer became unstable. Weak convective updrafts rose until they hit a cap. The consistent layer-deep WNW wind direction (see Fig. 3.13) and relatively constant  $\theta_e$  (see Fig. 3.12) support this hypothesis. There likely were two levels within Layer 2b at JNU where weak WAA was occurring. The base of the layer had significant WAA. Above this (near 1400m), the wind speed decreased weakening the WAA, the wind speed increased at 1500m, again strengthening the WAA. This wind speed change appeared to form a cap and a break in the cloud layer. An additional convective layer formed above 1500m. It had more LWC and was capped at its top by the weak inversion separating Layers 2a and 2b.

*the clean air mass was likely responsible for the large drops.*

Recall that precipitation (snow and freezing drizzle) was present in the region for 39 hr prior to the research flight. This precipitation fell through this layer and greatly reduced the available CCN and probably IN (not measured) by precipitation scavenging. This

layer was likely detached from the boundary layer for several days, which would further reduce the aerosol concentration by aggregation. The back trajectory model using the NARR reanalysis was too coarse to correctly identify these thin layers and was not used. Settling, along with the precipitation scavenging would probably reduce the giant or ultra giant CCN concentration over time. Therefore the very low drop numbers seen in Layer 2b (less than  $5 \text{ cm}^{-3}$ ) with the LWC greater than  $0.1 \text{ g m}^{-3}$  suggest a lack of CNN and the associated decreased competition for the available condensate. The analysis suggests the optimum production of freezing drizzle in thin cloud layers is due to clean, low CCN, air. The lack of a source (the sea surface) and the presence of sinks (precipitation) for giant and ultra giant CNN hints that these are not responsible for the SLD.

Layer 3 also produced new freezing drizzle drops at both SIT and JNU. At SIT the WAA had progressed to the point where the layer was well mixed and convective updrafts were producing the cloud from the layer base to the C2-3 cap. This layer also had experienced hours of precipitation scavenging and had been detached from the boundary layer for an extended period, resulting in low numbers of CCN and IN, similar to Layer 2b at JNU. The result was LWC exceeding  $0.1 \text{ g m}^{-3}$  with only  $5 \text{ cm}^{-3}$  of cloud drops and significant concentrations of SLD and FZDZ (see Fig's 3.28 and 3.29). In this layer the clean air mass was likely responsible for the large drops.

At JNU Layer 3 was stable with veering winds, and convection was absent. The LWC in this layer was formed though mechanical lifting, as warm moist air was lifted along the top of the deepening cold boundary layer as it moved east. The cloud drop concentration

remained very low ( $< 10\text{cm}^{-3}$ ) while the SLD and freezing drizzle concentrations were significant. The LWC remained between 0.05 and  $0.1\text{ g m}^{-3}$ . The vertical motion in the weak flow was likely weak since the frontal slope was not steep. As the cloud drops formed and quickly grew to SLD sizes, the weak vertical motion could no longer suspend the larger drops so they fell towards the surface keeping the LWC low. Larger freezing drizzle seeders from Layer 2b were also present as seen in the largest sizes shown in Fig. 3.20.

Layer 4a at Juneau had cloud drop concentrations up to  $40\text{ cm}^{-3}$ . Except for the cloud top layer, this was a much larger drop concentration than the layers above. There may have been some new SLD formed in this layer but the vast majority of new drops were small. The forcing is difficult to determine but the best guess is a thin layer of WAA at 250m, the layer base, which destabilized the layer above. The wind speed decreases from light at 250m to near zero just above (Fig. 3.13) and the instability can be seen in the  $\theta_e$  profile (Fig 3.12). Although SLD may not have formed in this layer the higher numbers of small drops helped increase the sizes of the drizzle which had fallen into the layer from above. In addition this layer is in the warm end of the secondary ice production temperature range (Hallet and Mossop 1974). As small supercooled drops freeze to any frozen drops, ice splinters are formed. These splinters will quickly grow to ice phase needles with sizes  $> 100\text{ }\mu\text{m}$  in the favorable ice supersaturation environment. No ice was observed in this layer but ice crystals were observed in the layer below. The sample time in this layer was low. The cloud drop concentration ( $40\text{ cm}^{-3}$ ), less than the Hallet and Mossop model suggested though.

Layer 4b was the surface based boundary layer. The warmer sea water ( $3^{\circ}\text{C}$ ) beneath the colder boundary layer air provided the instability which formed this cloud layer. The  $\theta_e$  gradient between the moist air just above the water surface and Layer 4b's base was  $13^{\circ}\text{C}$ . This drove convective upward vertical motion in the boundary layer. The cap at the top of the layer was the thin inversion beneath Layer 4a. The boundary layer cloud had much larger numbers of CCN and resulting larger numbers ( $>200\text{cm}^{-3}$ ) of small cloud drop drops. This layer did not add new SLD sized drops but served to rapidly increase the maximum sizes of the drizzle seeding from above to beyond  $600\mu\text{m}$ . More needles and graupel, which presumably initially formed from rime splintering in the layer above (Layer 4b's coldest temperature is only  $-3^{\circ}\text{C}$ ), are also seen in the 2d imagery.

A summary of the JNU case is study is presented in Fig. 3.33.

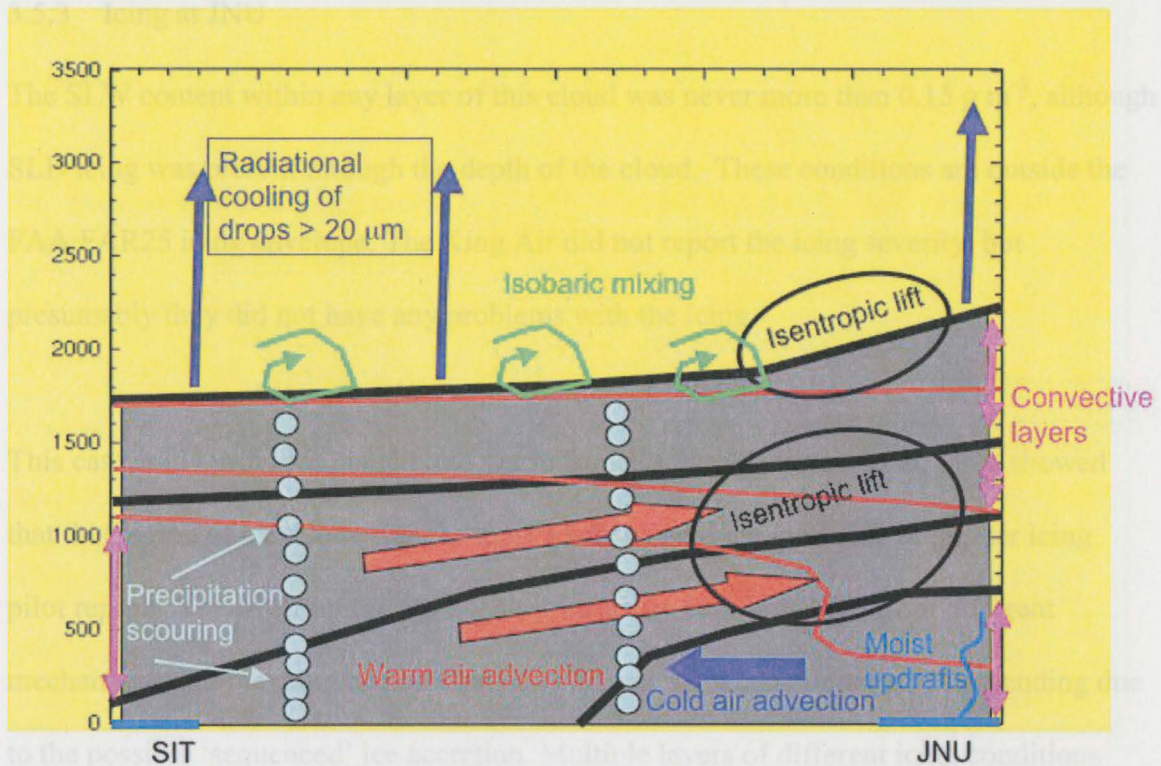


Fig. 3.33. The conceptual model of the cloud at JNU is presented. The black lines identify the  $\theta_e$  inversions, the red lines identify the isotherms, and the gray shaded region identifies the cloud layers. Radiational cooling (blue), isobaric mixing (green), and isentropic lift (black circles) all may have played a role in the FZDZ production at cloud top. Warm air advection of very clean Pacific air also produced FZDZ due to isentropic lifting, which led to shallow convective layers (magenta) beneath the cloud top layer. The boundary layer cloud at JNU was driven by moist updrafts from the open water into the cold air above the surface. Precipitation helped remove CCN from the cloud layers, which reduced the drop concentrations.

### 3.5.3 Icing at JNU

The SLW content within any layer of this cloud was never more than  $0.15 \text{ g m}^{-3}$ , although SLD icing was present through the depth of the cloud. These conditions are outside the FAA FAR25 icing envelope. The King Air did not report the icing severity, but presumably they did not have any problems with the icing.

This case study provides insight into warm frontal icing. Bernstein et al. 1998 showed that this region of a cyclone was the most likely to produce moderate or greater icing pilot reports. The overrunning atmospheric structure can form SLD from different mechanisms and the icing can be especially dangerous when climbing or descending due to the possible 'sequenced' ice accretion. Multiple layers of different icing conditions (i.e. temperature and drop size distribution) will be encountered and the result is each ice accretion shape is built on top of the previous accretion. This complex ice shape can result in unexpected aircraft behavior much different than conditions seen in icing wind tunnel tests. The boundary layer can have high liquid water contents from small drop production and also have a wide variety of SLD sizes, which have seeded from layers above. This dangerous surface layer is also where the aircraft operates at velocities close to stall speed. In addition the aircraft is flown at higher angles of attack, which can cause ice to accrete on unprotected surfaces. A safe zone within the frontal structure appears to be within the frontal inversions. All of the inversions had lower LWC except when the veering wind profile was present (Layer 3 at Juneau). Pilot knowledge of the heights of stable isothermal layers within the vertical structure can provide a last ditch escape seam from a dangerous icing layer.

## 4.0 Green Bay continental case

### 4.1 Introduction

On January 26, 1998 the NASA Glenn Twin Otter research aircraft sampled cloud layers near Green Bay, WI. These clouds contained supercooled large drop (SLD: drop diameters  $> 40 \mu\text{m}$ ) icing conditions and produced freezing drizzle (drop diameters  $> 100 \mu\text{m}$ ) at the surface. The icing conditions were reported as moderate to severe by the experienced NASA flight crew. The supercooled liquid water content (LWC) exceeded  $0.4 \text{ g m}^{-3}$  and the SLD accreted well aft of the deicing equipment (Fig. 4.1). This chapter will document the synoptic, mesoscale, and microscale structure and evolution of the cloud layers that produced these SLD icing conditions.

#### 4.1.1 Geography

Green Bay, WI is located at the southwest end of a shallow narrow bay (Green Bay) along the west shore of Lake Michigan (Fig. 4.2). The bay was frozen on 26 January 1998 while the region of Lake Michigan east of Green Bay was ice-free with a temperature of  $+4^{\circ}\text{C}$  <http://coastwatch.slerf.nasa.gov/glscg/morica/slscg1998.jp>

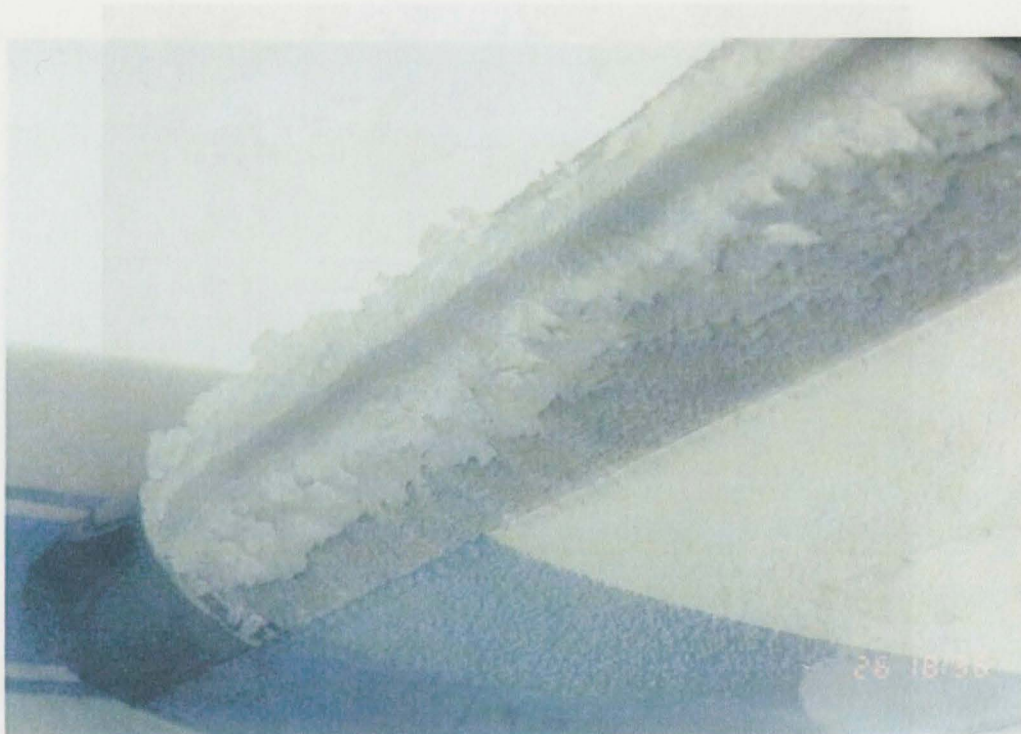


Figure 4.1. Supercooled large drop ice accretion on the wing of the NASA Glenn Twin Otter research aircraft. Jan 26, 1998 over Green Bay, WI. The icing conditions were reported as moderate to severe and ice accreted well aft of the black deicing boots.

#### 4.1.1 Geography

Green Bay, WI is located at the southwest end of a shallow narrow bay (Green Bay) along the west shore of Lake Michigan (Fig. 4.2). The bay was frozen on 26 January 1998 while the region of Lake Michigan east of Green Bay was ice-free with a temperature of  $+4^{\circ}\text{C}$  <http://coastwatch.glerl.noaa.gov/glsea/movies/glsea1998.flc>.

On Jan 26, 1998, just prior to 1940 UTC, the GOES 5 imager indicated the widespread, optically thick clouds covered the northern Lake Michigan area (Fig. 4.3). These clouds had cloud top temperatures ranging between  $-10^{\circ}\text{C}$  and  $-15^{\circ}\text{C}$  (Fig. 4.4). In this section the synoptic scale features that produced the clouds are discussed using observations from the National Weather Service.



Figure 4.2. Western Great Lakes area. KGRB is identified by the red star. Dashed lines identify the cross section locations.

## 4.2 Synoptic Situation

On Jan 26, 1998, just prior to 1900 UTC, the GOES 8 imager indicated that widespread, optically thick clouds covered the northern Lake Michigan area (Fig. 4.3). These clouds had cloud top temperatures ranging between  $-10^{\circ}\text{C}$  and  $-15^{\circ}\text{C}$  (Fig. 4.4). In this section the synoptic scale features that produced the clouds are discussed using observations from the National Weather Service.

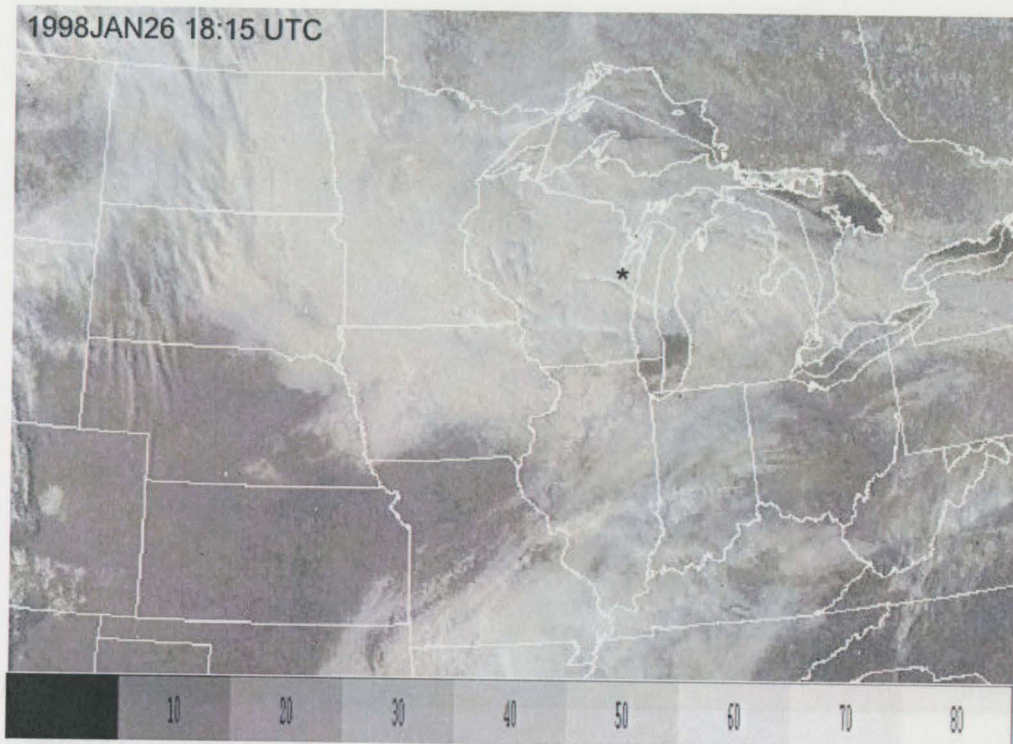


Figure 4.3. GOES-8 0.67 $\mu$ m visible image at 1998 JAN 26 18:15 UTC. KGRB is identified by the black star. Optically thick clouds cover the northern 2/3rds of Lake Michigan and all of Wisconsin.

At 1200 UTC Jan 26 1998 a 960mb trough approached the Green Bay (KGRB) area from the west. Within the trough a relative vorticity maximum was located southwest of KGRB and a relative vorticity minimum was to the northwest (Fig. 4.5). These features had created the structure observed in the lower levels of the atmosphere that were important to the formation and structure of the cloud layers sampled by the research aircraft.

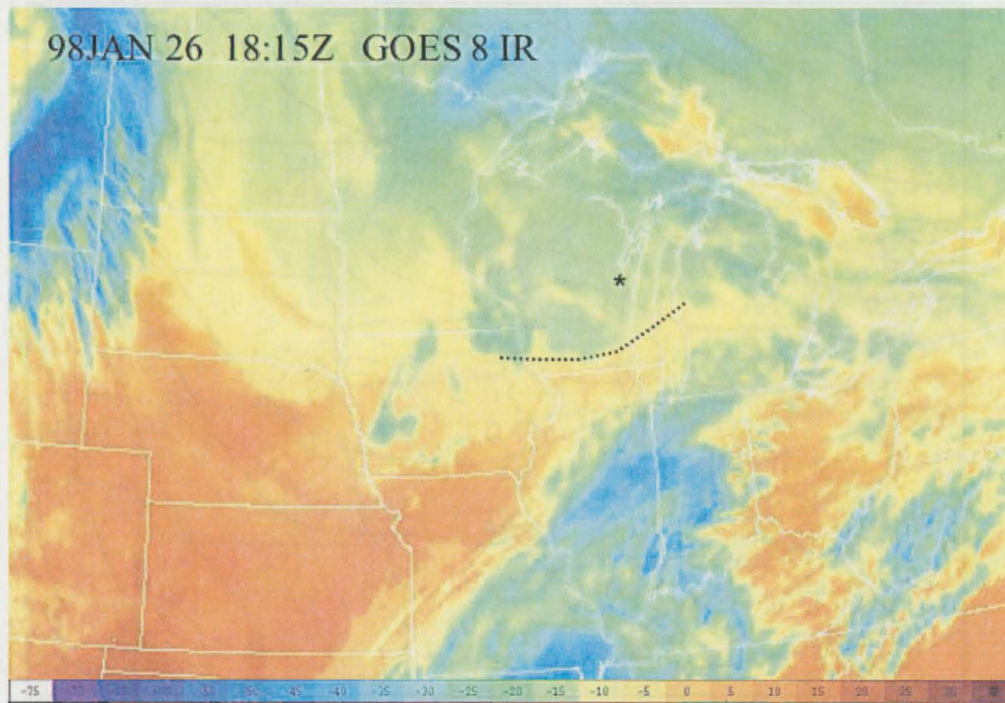


Figure 4.4. GOES-8 long-wave IR ( $10.7\mu\text{m}$ ) image at 1998 JAN 26 18:15 UTC. KGRB is identified by the black star. Widespread clouds with cloud top temperatures of  $-15^{\circ}\text{C}$  cover the most of Wisconsin and the northern 2/3rds of Lake Michigan. The black dashed line identifies the stationary front at the surface.

At 1200 UTC Jan 26 1998 a 500mb trough approached the Green Bay (KGRB) area from the west. Within the trough a relative vorticity maximum was located southwest of KGRB and a relative vorticity minimum was to the northwest (Fig. 4.5). These features had created the structure observed in the lower levels of the atmosphere that were important to the formation and structure of the cloud layers sampled by the research aircraft.

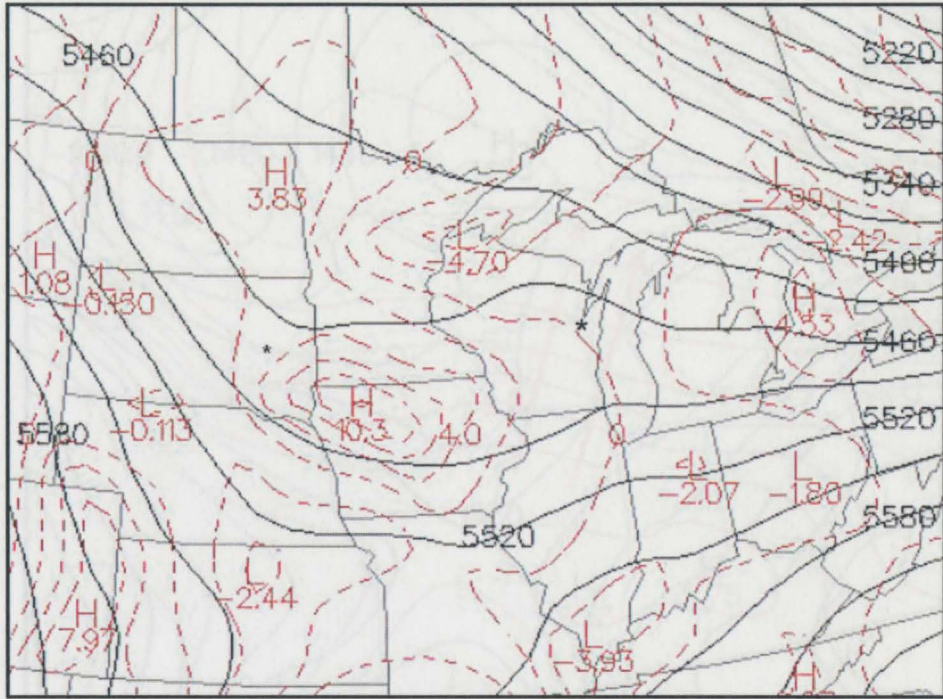


Figure 4.5. The 500mb geopotential height (black contours) and relative vorticity (dashed red lines), 1998 JAN 26 1200 UTC. Black star identifies KGRB.

At the same time, at 850mb, a negatively tilted trough was west of KGRB, across ND, MN, and IA (Fig. 6). This feature was associated with the trough and positive vorticity anomaly present at 500mb. The area of high geopotential heights north of KGRB was associated with the 500mb negative vorticity anomaly. This trough-ridge pattern established a southerly geostrophic flow, which set up warm air advection (WAA) towards KGRB.

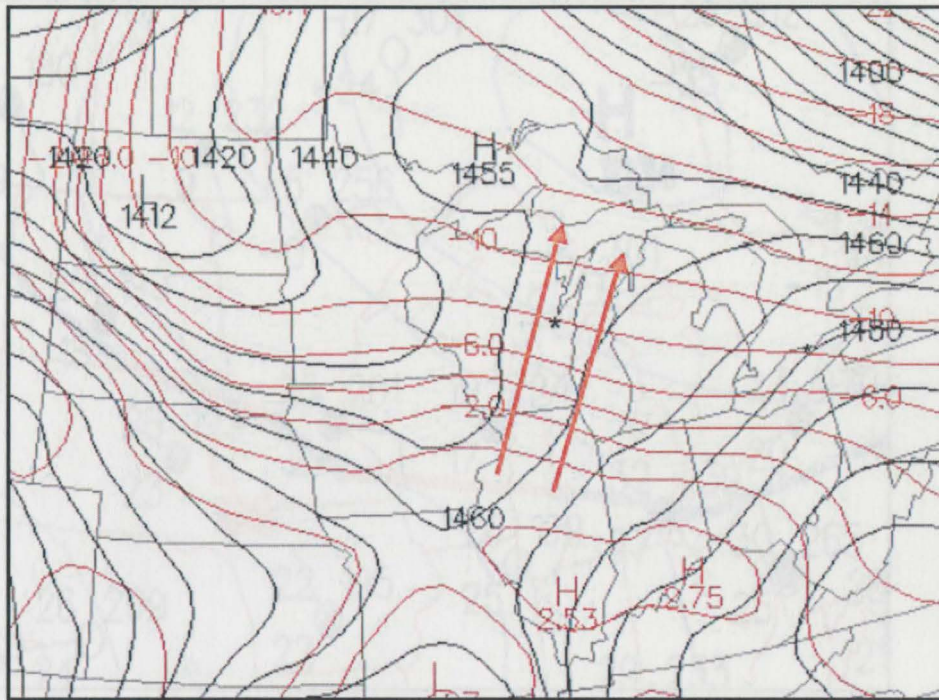


Figure 4.6. The 850mb geopotential height (black contours) and temperature ( $^{\circ}\text{C}$ ) (red lines), 1998 JAN 26 1200 UTC. Black star identifies KGRB. Warm air advection shown by red arrows is occurring at KGRB.

The surface pressure map at 1200 UTC Jan 26 (Fig 4.7) showed that a cold Arctic high pressure was centered northeast of KGRB. The southern boundary of the cold air mass area was located north of the WI-IL border but well south of KGRB. Northeasterly flow, overcast conditions, and scattered areas of precipitation (snow and freezing drizzle) were reported at stations north of the surface front.

$-FZRA$  at KGRB) at the surface were present throughout the period. The cloud top temperatures were colder than  $-20^{\circ}\text{C}$  between 0000 and 1200 UTC JAN 26 then warmed to  $-13^{\circ}\text{C}$  by 0000 UTC JAN 27.

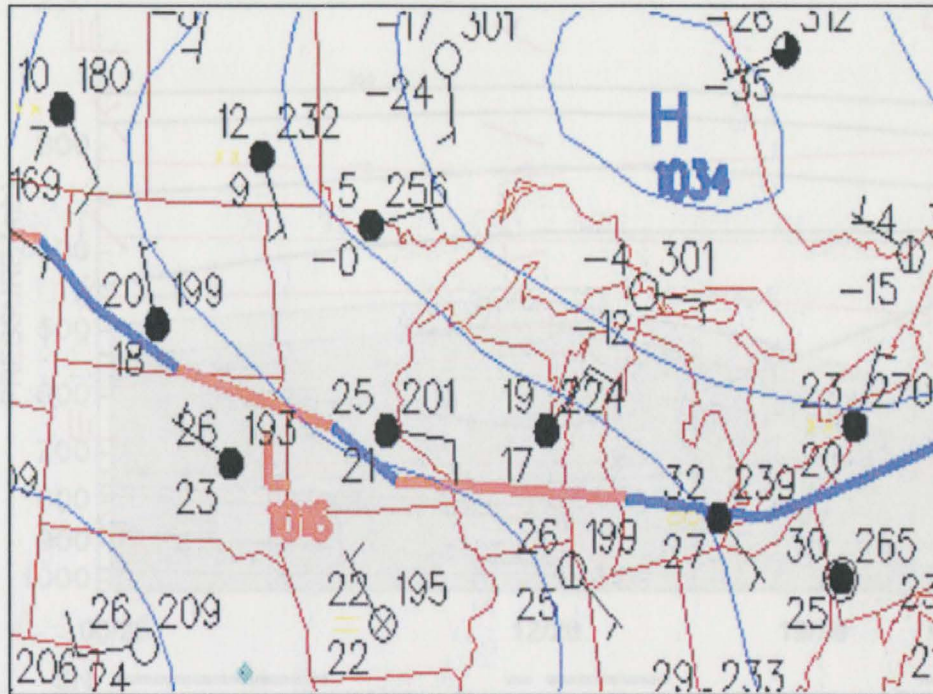


Figure 4.7. The surface map 1998 JAN 26 1200 UTC. A stationary front was south of KGRB, with a 1034mb arctic high pressure area to the north. Cold air advection was present at KGRB.

#### 4.2.1 Evolution of the synoptic-scale vertical structure at KGRB

The evolution of the thermodynamic structure at KGRB between 0000 UTC JAN 26 and 0000 UTC JAN 27 is shown in Fig. 4.8. Cloud layers producing intermittent light snow (-SN) and freezing drizzle (likely misreported as -FZRA at KGRB) at the surface were present throughout the period. The cloud top temperatures were colder than  $-20^{\circ}\text{C}$  between 0000 and 1200 UTC JAN 26 then warmed to  $-13^{\circ}\text{C}$  by 0000 UTC JAN 27.

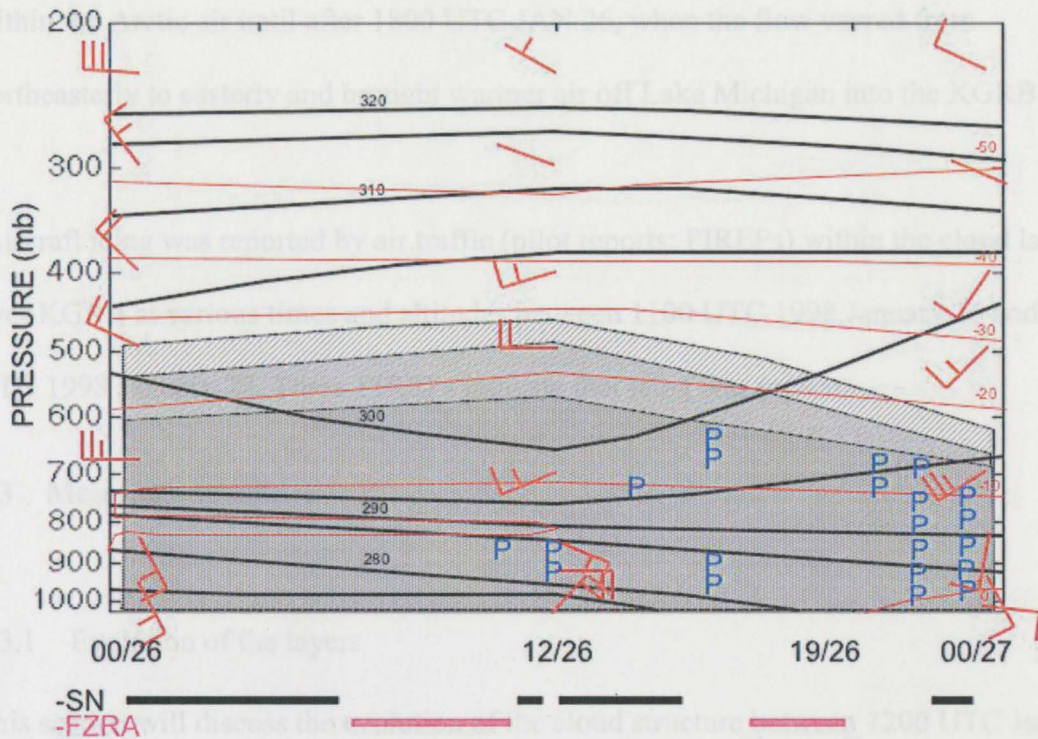


Figure 4.8. Time/pressure cross-section at KGRB from 1998 JAN 26 0000 UTC – 1998 JAN 27 0000 UTC. Black lines  $\theta_e$  ( $^{\circ}\text{K}$ ), red lines temperature  $^{\circ}\text{C}$ , winds (barb  $5 \text{ ms}^{-1}$ ), blue 'P' indicates positive icing pilot report at time and altitude. Relative humidity > 70% (hatched), > 80% (stippled), > 90% (gray). The surface precipitation type shown along bottom of graph.

The flow at the upper levels (200-300mb) was quite light, suggesting that the dynamics from the jet stream were not a factor in the cloud formation. At the mid-levels (550-700mb), the trough approached KGRB. A layer of warmer  $\theta_e$  air moved across KGRB at ~700mb ahead of the trough on 1200 UTC Jan 26. The warm advection (see the  $300^{\circ}\text{K}$  surface in Fig. 4.8) helped destabilize the layer and likely caused the cloud top height to increase to 550mb. After this time cooler  $\theta_e$  air moved in and the layer above dried significantly. The low-levels, below 700mb and above the boundary layer (970mb), remained very moist and slowly warmed as the WAA flow became firmly established. The WAA was best observed by the veering wind profile and lowering of the 290-275 $^{\circ}\text{K}$   $\theta_e$  surfaces. The boundary layer (surface – 970mb) remained shallow and very cool

within the Arctic air until after 1800 UTC JAN 26, when the flow veered from northeasterly to easterly and brought warmer air off Lake Michigan into the KGRB area.

Aircraft icing was reported by air traffic (pilot reports; PIREPs) within the cloud layers over KGRB at various times and altitudes between 1100 UTC 1998 January 26 and 0000 UTC 1998 January 27. These PIREPs indicate that icing was present.

### **4.3 Mesoscale structure**

#### **4.3.1 Evolution of the layers**

This section will discuss the evolution of the cloud structure between 1200 UTC Jan 26 and 0000 UTC Jan 27 including the flight time.

Four distinct cloud layers were present at KGRB on 1200 UTC Jan 26 (Fig. 4.9). By 0000 UTC Jan 27 the upper layer had dissipated while the lower cloud layers remained (Fig. 4.10). AT 1200 UTC Layer 0 was located between 3550m (650mb) and 5470m (500mb). The cloud top temperature observed by the GOES-8 10.7  $\mu\text{m}$  imager matched the  $-26^{\circ}\text{C}$  cloud top temperature from the sounding. Layer 0 appeared to be primarily ice saturated and sub-saturated with respect to water as indicated by the temperature (T) and dew point temperature (Td) differences. After 1200 UTC cooler and drier air moved in from the west and the layer dissipated.

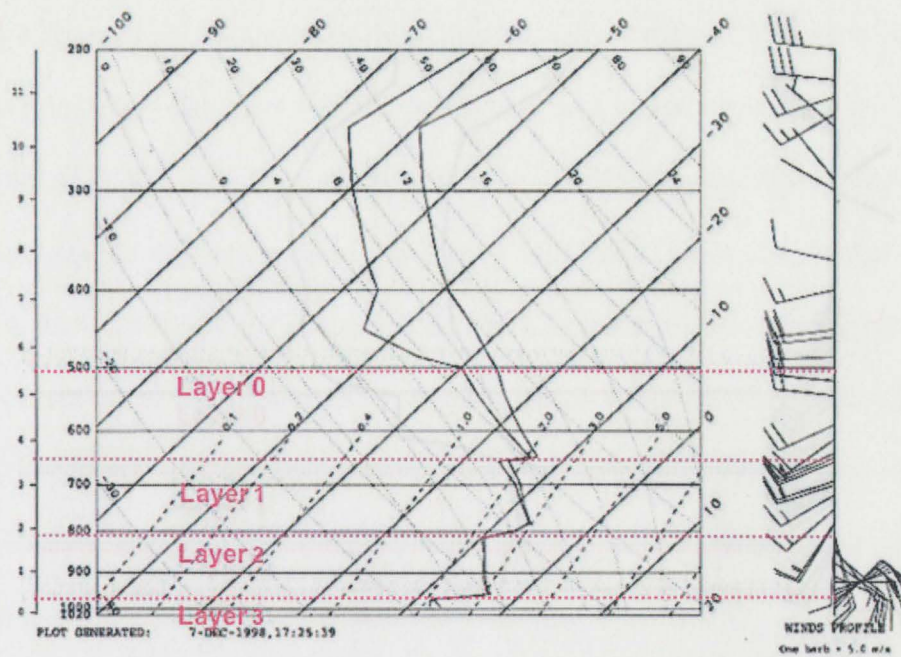


Figure 4.9. The NWS sounding from KGRB, 1998 JAN 26 1200 UTC. Four cloudy layers, Layers 0-3, are identified in red.

At 1200 UTC Layer 1 was located between 2000m (800mb) and 3450m (655mb). The layer had a moist adiabatic lapse rate and was isolated from Layers 0 and 2 by temperature inversions. The T/Td spread suggested that the ice phase was dominant at the -15°C cloud layer top. By 0000 UTC Jan 27 the inversion separating Layers 0 and 1 had lowered to 3250m (670mb) and the layer top had warmed slightly. Strong WAA (4°C over 12 hrs) at the bottom of Layer 1 had lowered its base by 500m. The smaller T/Td spreads and icing PIREPs at 0000 UTC Jan 27 suggest that Layer 1 contained supercooled liquid water.

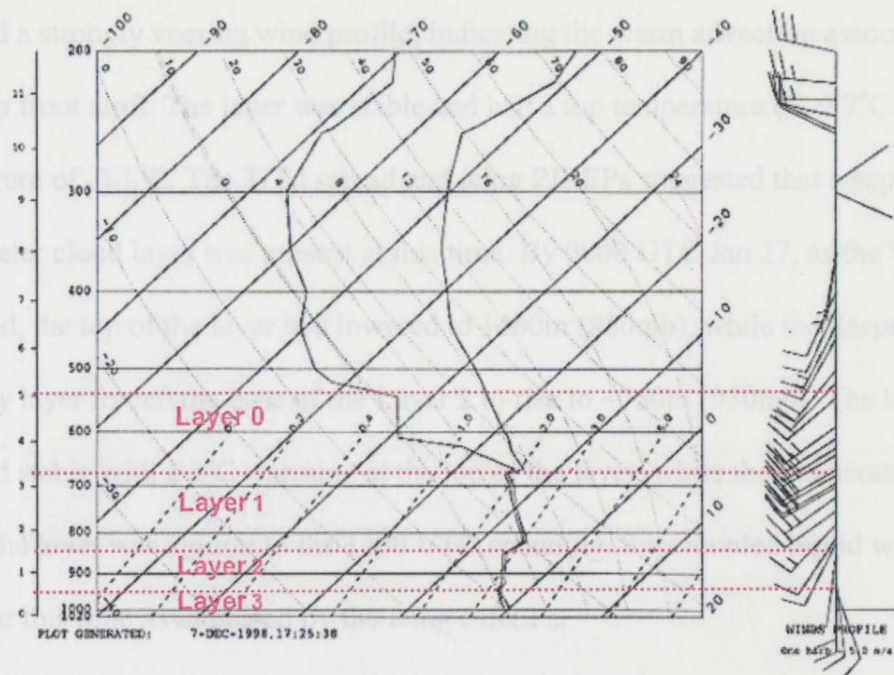


Figure 4.10. The NWS sounding from KGRB, 1998 JAN 27 0000 UTC. Four layers, Layers 0-3, are identified in red.

At 1200 UTC the boundary layer, Layer 3, was quite cold and rather shallow. This layer was also cloudy with a top at 400m (970mb) and a temperature of  $-8.5^{\circ}\text{C}$ . The base was at 189m (989mb). At 1200 UTC Layer 1 was located between 2000m (800mb) and 3450m (655mb). The layer had a moist adiabatic lapse rate and was isolated from Layers 0 and 2 by temperature inversions. The T/Td spread suggested that the ice phase was dominant at the  $-15^{\circ}\text{C}$  cloud layer top. By 0000 UTC Jan 27 the inversion separating Layers 0 and 1 had lowered to 3250m (670mb) and the layer top had warmed slightly. Strong WAA ( $4^{\circ}\text{C}$  over 12 hrs) at the bottom of Layer 1 had lowered its base by 500m. The smaller T/Td spreads and icing PIREPs at 0000 UTC Jan 27 suggest that Layer 1 contained supercooled liquid water.

Layer 2, at 1200 UTC, was located between 500m (970mb) and 1700m (820mb). This layer had a strongly veering wind profile, indicating the warm advection associated with the warm front aloft. The layer was stable and had a top temperature of  $-9.7^{\circ}\text{C}$  and a base temperature of  $-3.1^{\circ}\text{C}$ . The T/Td spread and icing PIREPs suggested that a supercooled liquid water cloud layer was present at this time. By 0000 UTC Jan 27, as the WAA continued, the top of the layer had lowered to 1460m (850mb), while the deepening boundary layer forced the base of the Layer 2 to rise to  $\sim 750\text{m}$  (930mb). The lapse rate remained stable with a  $3^{\circ}\text{C}$  warming at the top of the layer, while the temperature at the base of the layer was similar to the 1200 UTC sounding. Supercooled liquid was also present at this time as indicated by the icing PIREPs.

At 1200 UTC the boundary layer, Layer 3, was quite cold and rather shallow. This layer was also cloudy with a top at 400m (970mb) and a temperature of  $-8.5^{\circ}\text{C}$ . The base was the surface with a temperature of  $-7^{\circ}\text{C}$  and pressure of 1022mb. The KGRB surface observation reported light snow and a ceiling of  $\sim 350\text{m}$ . The flow within the layer was from the northeast across the frozen Green Bay. By 0000 UTC Jan 27 the flow had become easterly. This advected Arctic air, which had been warmed by the fluxes off the open Lake Michigan ( $+4^{\circ}\text{C}$ ), towards KGRB. In response to this, the top of the boundary layer rose to 650m (940mb) and warmed to  $-3.0^{\circ}\text{C}$ , while the surface temperature warmed to  $0^{\circ}\text{C}$ . The surface observation at 0000 UTC indicted a ceiling of 300m with light snow and the pressure had decreased slightly to 1021mb.

### 4.3.2 North-south cross section

The best available depiction of the warm frontal structure was between Davenport, IA (KDVN) and KGRB at 1200 UTC (see Fig. 4.2 for location). The soundings at KDVN and KGRB, along with GOES-8 imagery, icing PIREPs, and surface observations were used to construct the cross section (Fig. 4.11).

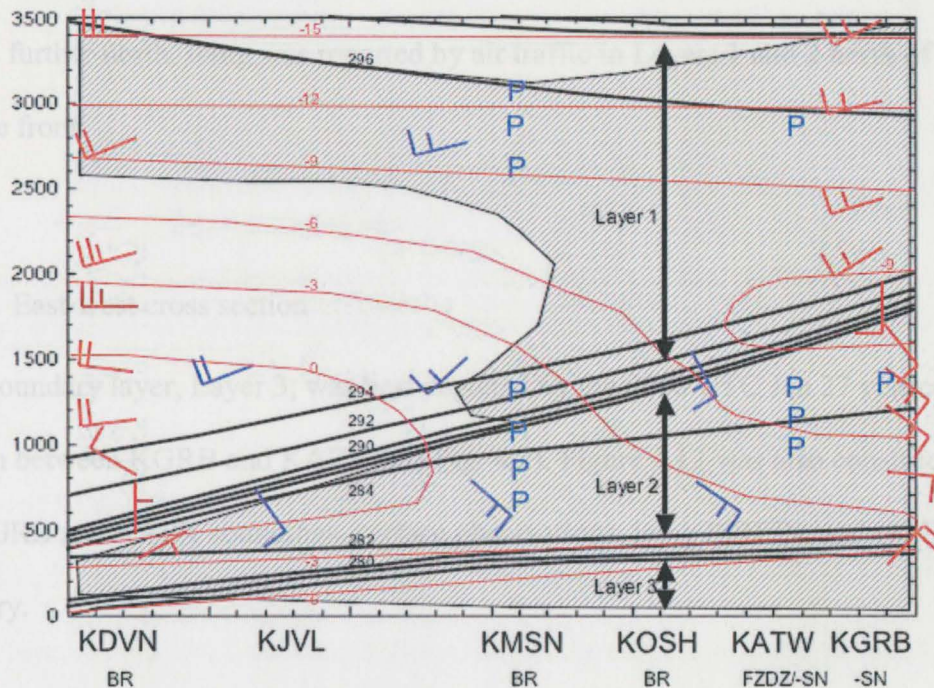


Figure 4.11. North-south cross-section KDVN - KGRB on 1998 JAN 26 at 1200 UTC (see Fig 2). Black lines  $\theta_e$  ( $^{\circ}$ K), red lines temperature  $^{\circ}$ C, winds (barb  $5 \text{ m s}^{-1}$ ) - red (observed), - blue (geostrophic), blue 'P' indicates positive icing pilot report at location and altitude. Hatched area; relative humidity > 90%. The surface stations and 1200 UTC surface observations at bottom of figure. Layers 1 - 3 are identified by the double black arrow lines.

The two  $\theta_e$  inversions (warm fronts) bounding the layers were associated with the levels of maximum warm advection. These two warm fronts bounded the well-mixed layers above and below and sloped upward from just north of KDVN towards KGRB. The upper warm front, between 1800-2000m at KGRB, featured a 1500m slope from KDVN

to KGRB, a strongly veering wind profile, and a very moist  $8^{\circ}\text{K}$   $\theta_e$  inversion. The lower warm front rose  $\sim 350\text{m}$  between KDVN and KGRB. It also featured a veering wind profile and a very moist  $6^{\circ}\text{K}$   $\theta_e$  inversion. The cold, cloudy, well-mixed Arctic boundary layer, beneath the lower warm front, was present within the northeasterly flow regime. This layer was deeper to the north and was indistinguishable from the nocturnal inversion at KDVN. Surface observations showed fog with no precipitation along and just north of the surface front, which transitioned to light snow and freezing drizzle in the deeper clouds further north. Icing was reported by air traffic in Layers 1 and 2 north of the surface front.

#### 4.3.3 East-west cross section

The boundary layer, Layer 3, was best depicted by the 0000 UTC Jan 27 vertical cross-section between KGRB and KAPX (see Fig. 4.2). Figure 4.12 was also constructed using the KGRB and KAPX soundings, surface observations, icing PIREPs, and GOES 8 imagery.

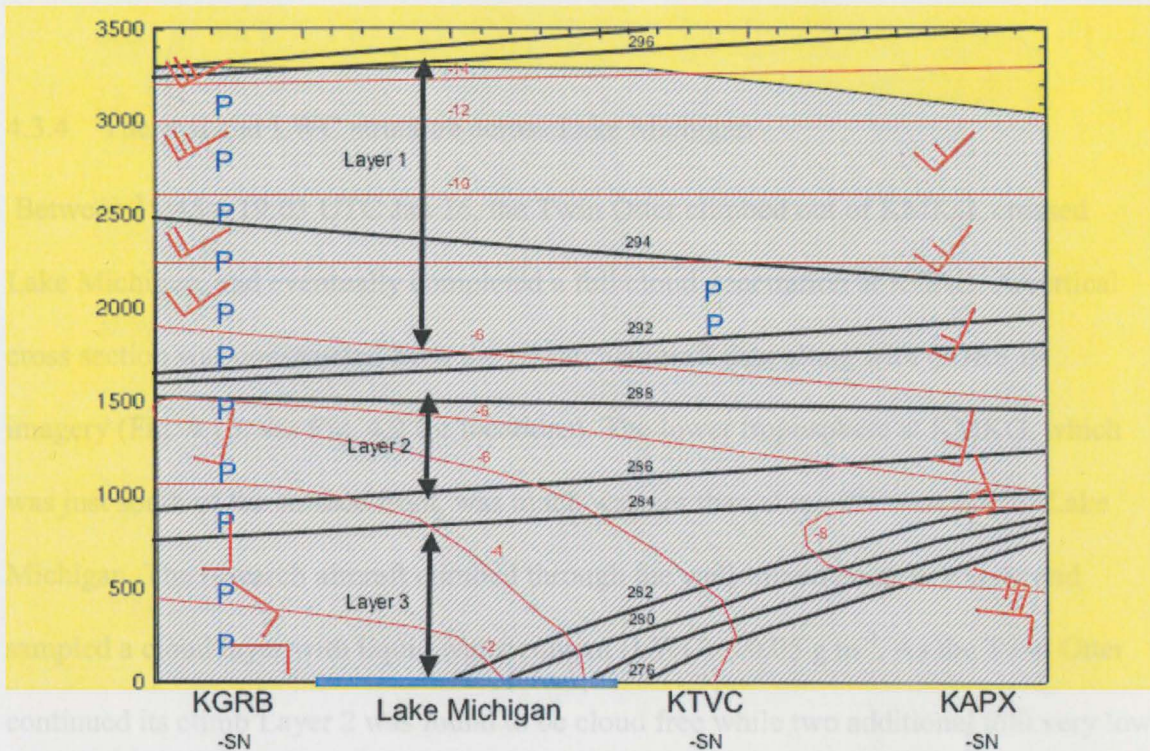


Figure 4.12. West-east cross-section KGRB - KAPX on 1998 JAN 27 at 0000 UTC (see Fig 2). Black lines  $\theta_e$  ( $^{\circ}\text{K}$ ), red lines temperature  $^{\circ}\text{C}$ , red winds (barb  $5 \text{ m s}^{-1}$ ), blue 'P' indicates positive icing pilot report at location and altitude. Hatched area relative humidity  $> 90\%$ . The surface stations and 0000 UTC observations at bottom of figure. Layers 1 - 3 are identified by the double black arrow lines.

The wind field in Layer 1 indicated the approaching trough, with southwesterly flow at KGRB and southerly flow at KAPX. Icing was reported on both sides of Lake Michigan in this layer. The warm frontal layer (Layer 2), tilting slightly upwards towards the east, was also clearly observed in the southerly flow. The thermal structure of the boundary layer (Layer 3), with its easterly flow, changed dramatically between the east and west sides of Lake Michigan. As the cold air crossed the lake it gained additional heat and moisture from fluxes off the warm lake surface as seen by the sharp increase in  $\theta_e$ . This warmer low-level air was unstable with respect to the very cold arctic airmass, forming a Lake Effect cloud between the surface and the base of the elevated lower warm front. Within this layer, along the west side of Lake Michigan, icing was reported.

#### 4.3.4 Thermal and LWC structure across Lake Michigan

Between 15:45 – 19:03 UTC Jan 26, the Twin Otter climbed out of KMKG, crossed Lake Michigan, and eventually completed a full cloud penetration at KGRB. A vertical cross section was constructed from the research aircraft data along with GOES IR imagery (Fig. 4.13; see Fig. 4.2 for locations). The lower troposphere at KMKG, which was just south of the surface front, was much warmer than along the west side of Lake Michigan. The research aircraft climbed through the well-mixed boundary layer and sampled a cloud layer with liquid water content (LWC)  $< 0.05 \text{ g m}^{-3}$ . As the Twin Otter continued its climb Layer 2 was found to be cloud free while two additional thin very low LWC layers were found within what appeared to be Layer 1. The research aircraft then crossed Lake Michigan dropping through a thin cloud layer with LWC  $> 0.2 \text{ g m}^{-3}$ . The Twin Otter penetrated Layer 2 along the west shore of the lake near KMTW where the LWC increased to more than  $0.24 \text{ g m}^{-3}$  and the temperature cooled. Once over KMTW, a missed approach was completed where the aircraft dropped into Layer 3. The boundary layer contained LWC exceeding  $0.34 \text{ g m}^{-3}$ . The Twin Otter then proceeded to KGRB, refueled, and sampled the entire cloud depth from the surface to the highest cloud top. The next section will analyze the microscale structure of the three cloud layers found at KGRB.

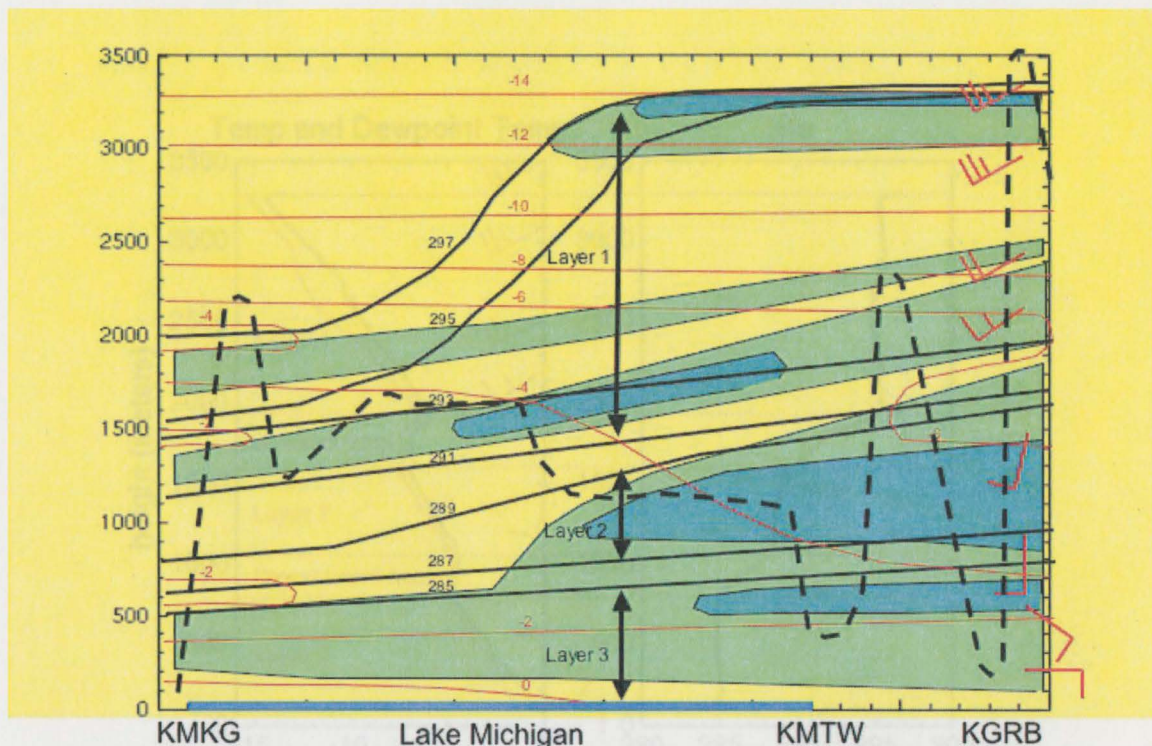


Figure 4.13. Research aircraft east-west cross-section, KMKG - KGRB, between 1998 JAN 26 1500 - 1900 UTC (see Fig 2). Black lines  $\theta_e$  ( $^{\circ}\text{K}$ ), red lines temperature ( $^{\circ}\text{C}$ ), red winds (kts) (0000 UTC JAN 27 1998 KGRB sounding). Green shading indicates King probe liquid water contents  $> 0.01 \text{ gm}^{-3}$ , blue-green liquid water contents  $> 0.2 \text{ gm}^{-3}$ . Heavy black dashed line shows the research aircraft flight track and the Layers 1 - 3 are identified by the double black arrow lines

#### 4.4 Micro-scale structure of the cloud layers

The Twin Otter took off from KGRB at 1850 UTC and climbed from the surface through at least three distinct cloud layers reaching clear air above 3250m at 1930 UTC. FZDZ was observed at the surface and the sun was clearly visible above the flat tops of the highest cloud layer (on-board meteorologist flight notes). The temperature and dew point temperature,  $\theta_e$ , King liquid water content (LWC), FSSP concentration, FSSP mass weighted median volume diameter (MVD), and 2DC Gray concentration for particles  $> 100 \mu\text{m}$  from this ascent are presented in Fig. 4.14 a-f.

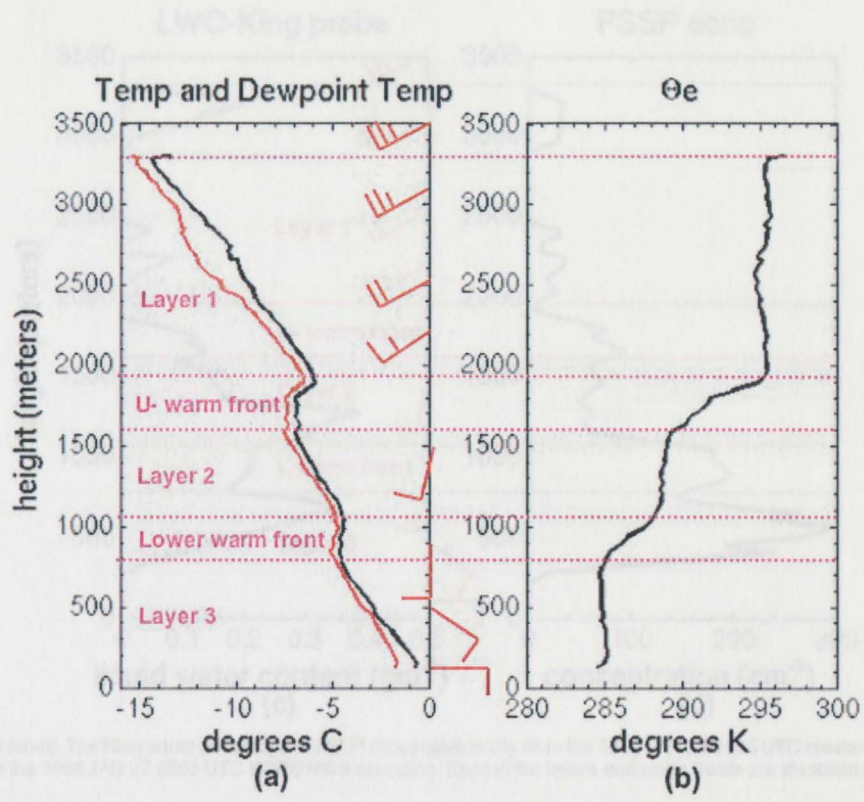


Figure 4.14. The temperature and dew point temperature (a) and  $\theta_e$  (b) from the 1998 JAN 26 1900 UTC research aircraft sounding. Winds from the 1998 JAN 27 0000 UTC KGRB NWS sounding. Each of the layers and warm fronts are identified in violet-red.

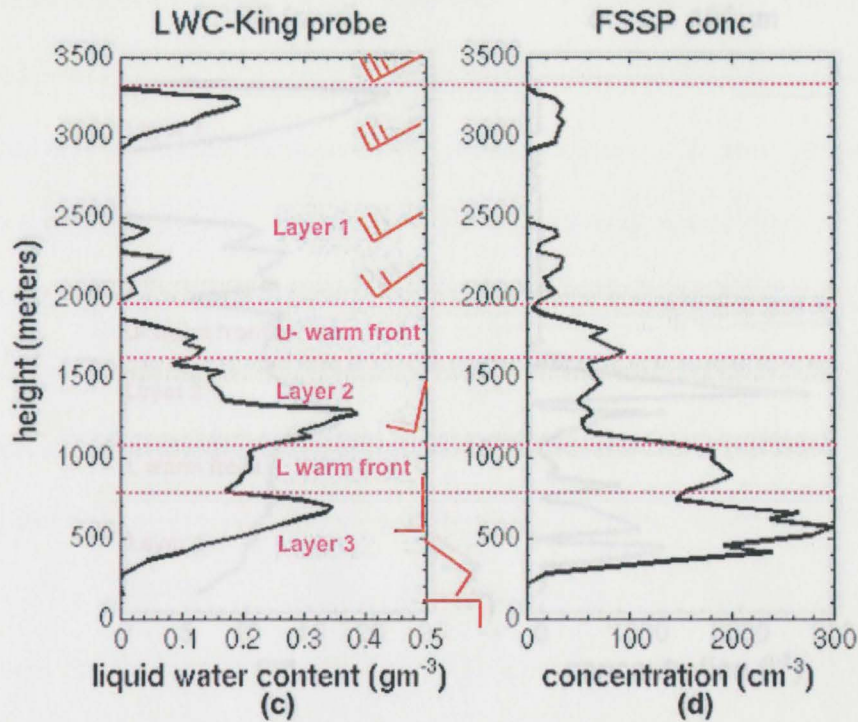


Figure 4.14 (cont). The King liquid water (c) and FSSP concentration (d) from the 1998 JAN 26 1900 UTC research aircraft sounding. Winds from the 1998 JAN 27 0000 UTC KGRB NWS sounding. Each of the layers and warm fronts are identified in violet-red.

Fig. 4.14a shows sub-freezing temperatures were present through the depth of the sounding suggesting that the liquid was formed through condensation and collision-coalescence, not melting ice. The three well-mixed layers and the three inversions, which bound the layers, are defined. The inversions are associated with the boundary between the dry air slab (Layer 0) and Layer 1 and the upper and lower warm fronts. This thermodynamic profile was very similar to the 0000 UTC JAN 27 KGRB sounding (Fig. 4.10). The research aircraft sounding was generally quite moist, but some drier air was observed within Layer 1 near 2600m.

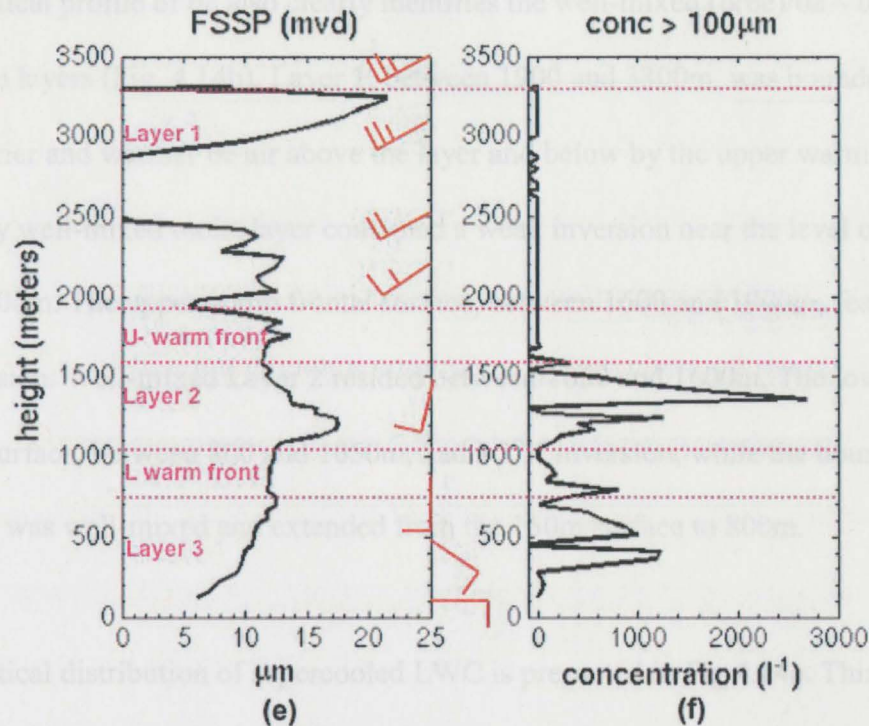


Figure 4.14 (cont). FSSP median volume diameter (e) and 2DC Gray concentration of particles  $> 100 \mu\text{m}$  (f). Negative values in (f) indicate data removed due to low  $< 0.5 \text{ l}^{-1}$  sample volumes for the 2DC Gray. The sounding is from the 1998 JAN 26 1900 UTC research aircraft sounding. Winds from the 1998 JAN 27 0000 UTC KGRB NWS sounding. Each of the layers and warm fronts are identified in violet-red.

Fig. 4.14a shows sub-freezing temperatures were present through the depth of the sounding suggesting that the liquid was formed through condensation and collision-coalescence, not melting ice. The three well-mixed layers and the three inversions, which bound the layers, are defined. The inversions are associated with the boundary between the dry air aloft (Layer 0) and Layer 1 and the upper and lower warm fronts. This thermodynamic profile was very similar to the 0000 UTC JAN 27 KGRB sounding (Fig. 4.10). The research aircraft sounding was generally quite moist, but some drier air was observed within Layer 1 near 2600m.

The vertical profile of  $\theta_e$  also clearly identifies the well-mixed ( $\delta(\theta_e)/\delta z \sim 0 \text{ K m}^{-1}$ ) and inversion layers (Fig. 4.14b). Layer 1, between 1900 and 3300m, was bounded on the top by the drier and warmer  $\theta_e$  air above the layer and below by the upper warm front. This generally well-mixed moist layer contained a weak inversion near the level of the drier air at 2600m. The upper warm frontal surface, between 1600 and 1900m, featured a  $6^\circ\text{K}$   $\theta_e$  inversion. Well-mixed Layer 2 resided between 1050 and 1600m. The lower warm frontal surface, between 800 and 1050m, had a  $3^\circ\text{K}$  inversion, while the boundary layer, Layer 3, was well-mixed and extended from the 150m surface to 800m.

The vertical distribution of supercooled LWC is presented in Fig 4.14c. This distribution agrees with the layer definitions presented earlier. LWCs exceeding  $0.1 \text{ g m}^{-3}$  were present in all three layers and within the two frontal inversions. Layer 1 had two thin low-LWC layers at the base of the layer, dry air in the mid-levels, and a 300m layer of LWC  $\sim 0.2 \text{ g m}^{-3}$  at the top of the layer. The upper warm front had low LWC which decreased to zero at the layer top. Layer 2 had the highest LWC within the entire cloud depth approaching  $0.4 \text{ g m}^{-3}$ , while the lower warm front had LWC  $> 0.2 \text{ g m}^{-3}$ . Layer 3 also had significant LWC, exceeding  $0.3 \text{ g m}^{-3}$  at the top.

The vertical profile of the cloud drop concentrations from the FSSP also shows the differences between the various layers and warm fronts (Fig. 4.14d). Each of the three cloudy layers within Layer 1 contained only  $30 \text{ drops cm}^{-3}$ . The cloud drop concentration of the upper warm front was  $80 \text{ cm}^{-3}$  while the high-LWC Layer 2 below had a lower concentration of  $60 \text{ cm}^{-3}$ . Near the surface the cloud drop concentrations increased

significantly. The lower warm front had a concentration of  $200 \text{ cm}^{-3}$ , while Layer 3 had a cloud drop concentration of more than  $300 \text{ cm}^{-3}$ .

Figs. 4.14 e and f show the profiles of the FSSP median volume diameter (MVD) for cloud drop sizes  $< 47 \mu\text{m}$ , and the concentration for large drops (FZDZ  $> 100\mu\text{m}$ ) from the 2DC Gray. The images of only two ice crystals were present in the 2DC Gray data for the entire thirteen minute vertical profile, so the particles were assumed to be liquid drops (this will be shown in more detail below). The cloud top layer contained large MVDs, exceeding  $21\mu\text{m}$ , while there are no large drops observed in the cloud sampled by the 2DC Gray. The MVD's were  $\sim 12\mu\text{m}$  at the bottom of Layer 1 and in the upper warm frontal cloud layer, and no FZDZ was present in either of those layers. Near the base of Layer 2, at the level of maximum LWC, there was a sharp increase in the MVD to  $18\mu\text{m}$ . Also within Layer 2 large drop concentrations  $> 2000 \text{ L}^{-1}$  were observed by the 2D probe. This is the highest level where large drops were found. Within the lower warm front and Layer 3 the MVD suggested small cloud drops dominated, although significant numbers of large drops were also present.

#### 4.5 Discussion

The large and small-scale structure of an SLD-producing warm frontal cloud was described above. In this section each of the cloud layers with  $\text{LWC} > 0.2 \text{ g m}^{-3}$  will be discussed in terms of possible forcing, aerosol population and the resulting microphysical properties.

Layer 1, between 1900 and 3300m, had three levels with supercooled cloud drop concentrations of  $30\text{cm}^{-3}$ . The LWC was  $< 0.1\text{ g m}^{-3}$  in the two lower layers while the cloud-top layer contained significantly more LWC. This layer was 400m thick, well-mixed, had a base temperature of  $-12.5^\circ\text{C}$ , a top temperature of  $-14.5^\circ\text{C}$ , and contained an adiabatic (well-mixed) LWC profile. Fig. 4.15 shows the particle images and drop size spectrum (bin counts) from the FSSP and 2DC Gray for the cloud top layer. Although the FSSP has an MVD of  $21\mu\text{m}$ , the maximum FSSP size is  $27.5\mu\text{m}$ . The particle images captured by the 2DC Gray probe suggests that drops as large as  $75\mu\text{m}$  may have been present, but the probe often contains significant sizing errors for drops  $< 100\mu\text{m}$  (Cober et. al. 1998).

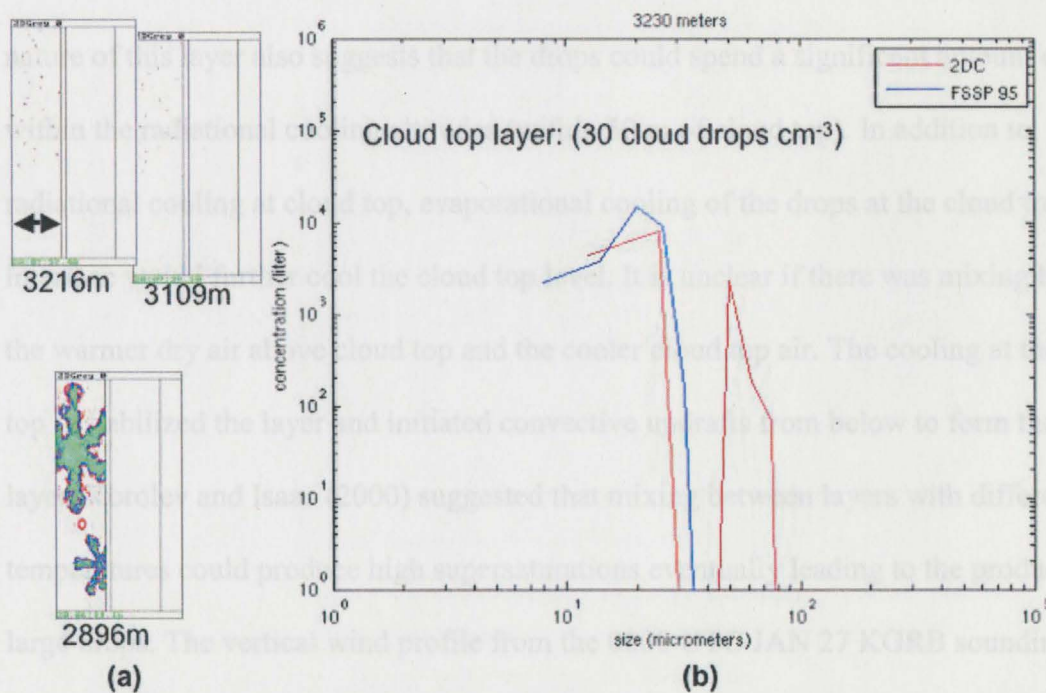


Figure 4.15. (a) Layer 1 imagery from the 2DC Gray, width of box (black double arrow line)  $960\mu\text{m}$ . (b) size distribution at 3230m FSSP (blue) 2DC Gray (red).

The ice phase was largely absent in this cloud top layer. Only two slightly decomposed plate ice crystals were observed in the 2DC imagery in the dry air just below the base of the layer. These were the only crystals captured in the entire sounding. Since the ice phase is often present within cloud layers with cloud top temperatures  $< -12^{\circ}\text{C}$ , the lack of observed ice crystals within this layer may suggest the air mass was somewhat depleted of ice forming nuclei.

The conceptual model of this layer begins with radiational cooling at cloud top. The modeling work of Hartman and Harrington (2005) suggest long-wave radiational cooling of the large cloud drops ( $> 20\mu\text{m}$ ) at cloud top would be present under the fairly weak solar radiation on Jan 26 at KGRB ( $45^{\circ}$  north latitude) at 1900 UTC. The relatively thin nature of this layer also suggests that the drops could spend a significant amount of time within the radiational cooling altitudes (within 50 m of cloud top). In addition to radiational cooling at cloud top, evaporational cooling of the drops at the cloud top interface would further cool the cloud top level. It is unclear if there was mixing between the warmer dry air above cloud top and the cooler cloud top air. The cooling at the cloud top destabilized the layer and initiated convective updrafts from below to form the cloud layer. Korolev and Isaac (2000) suggested that mixing between layers with different temperatures could produce high supersaturations eventually leading to the production of large drops. The vertical wind profile from the 0000 UTC JAN 27 KGRB sounding suggested that a shear layer at cloud top, which could mix down warmer sub-saturated air, was absent. Fig. 4.16 shows the Hysplit 80-km model back trajectory for the 3000m

level. This suggests that air entering the cloud top layer had been isolated from the boundary layer for many hours. Brownian motion, aggregation, coagulation, and nucleation scavenging will eventually reduce the cloud condensation nuclei (CCN) concentration once the air mass is isolated from the earth's surface, the source of new aerosols (Ludlam 1980). In addition snow had previously formed within and fallen through this layer, which further depleted both CCN and IN concentrations by scouring. The  $30 \text{ cm}^{-3}$  small drop concentration and lack of ice crystals lends additional support that this layer was very clean of both CCN and IN. FZDZ larger than  $100 \mu\text{m}$  did not form in this layer although small SLD ( $< 100 \mu\text{m}$ ) may have been present. These drops did not fall into the lower cloud layers due to the dry air below.

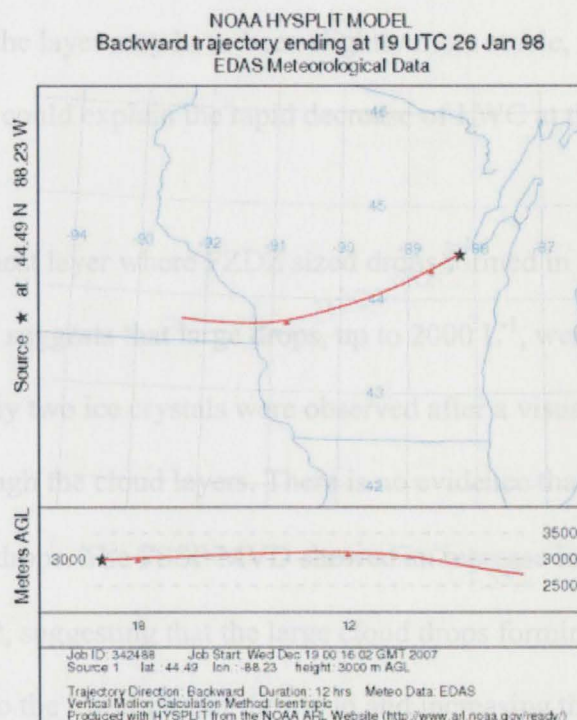


Figure 4.16. NOAA 80-km Hysplit back trajectory model for Layer 1. Upper red line shows the horizontal motion from 0700–1900 UTC JAN 26 1998 while the lower plot red line shows the vertical change using the model vertical velocity field

#### 4.5.1 Layer 2

The upper warm front had low LWC and no FZDZ formed there so the next layer of interest is Layer 2 between 1050 and 1600m. This 550m-thick layer was generally well-mixed, had a maximum LWC  $> 0.4 \text{ g m}^{-3}$ , and a  $60 \text{ cm}^{-3}$  drop concentration. The layer was bounded by the upper and lower warm fronts. This may have been a convective layer, based on the adiabatic (constant  $\theta_e$ ) profile, which formed within the larger warm frontal structure. The temperature at the base was  $-4^\circ\text{C}$  and the temperature at the top was  $-7^\circ\text{C}$ , optimal temperatures for supercooled liquid water production. The base of the layer had a LWC of  $0.2 \text{ g m}^{-3}$  which increased adiabatically to  $0.4 \text{ g m}^{-3}$  at the 1300m level. Above this level the LWC decreased, reaching  $\sim 0.1 \text{ g m}^{-3}$  at the top of Layer 2. The  $\theta_e$  profile suggests that the layer may have been slightly more stable, no longer convective, above 1300m, which could explain the rapid decrease of LWC at this level.

Layer 2 was the highest layer where FZDZ sized drops formed in significant numbers. The 2DC Gray probe suggests that large drops, up to  $2000 \text{ L}^{-1}$ , were present. As mentioned above, only two ice crystals were observed after a visual inspection of the aircraft's ascent through the cloud layers. There is no evidence that the layers above provided any seeder drops. The FSSP MVD showed an increase in the drop size to  $18\mu\text{m}$  at the base of Layer 2, suggesting that the large cloud drops forming within this cloud layer were falling into the lower part of the cloud and increasing the MVD at the layer base. Fig. 4.17 shows the particle images and drop size distribution (bin counts) at the level of maximum LWC (1243 m). Large drops were observed in the 2DC Gray imagery.

The size distribution also shows significant numbers of drops larger than  $100\ \mu\text{m}$  and some as large as  $200\ \mu\text{m}$  were present. High concentrations of small drops were present and their maximum sizes were also large ( $40\ \mu\text{m}$ ; from the FSSP).

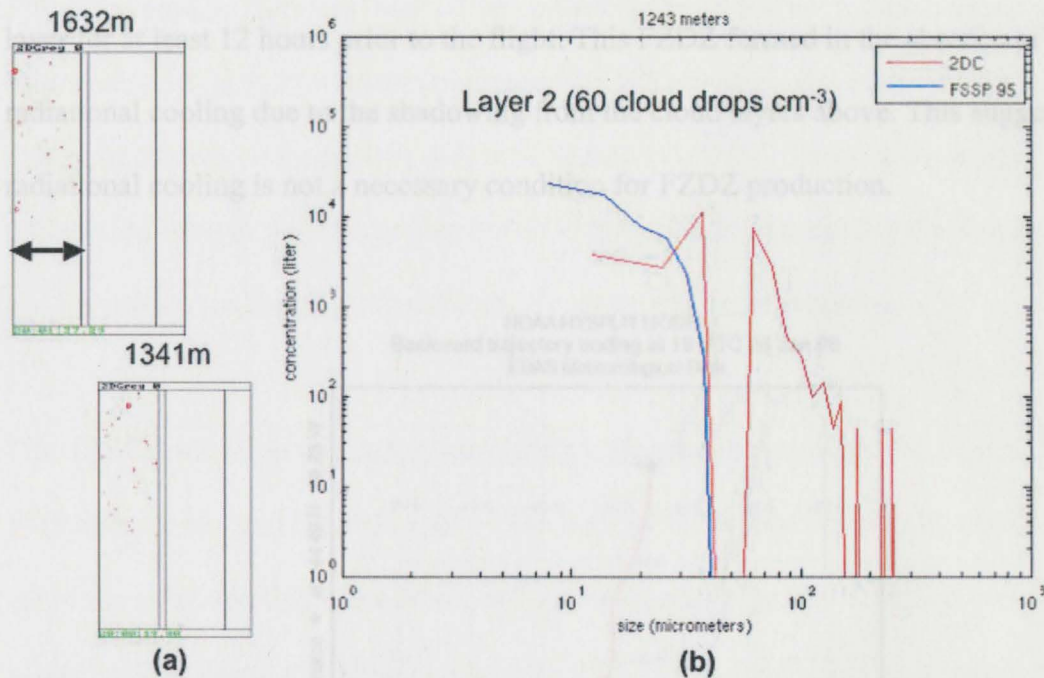


Figure 4.17. (a) Layer 2 imagery from the ZDC Gray, width of box (black double arrow line)  $960\ \mu\text{m}$ . (b) size distribution at 1243 m, FSSP (blue) ZDC Gray (red)

The conceptual model of this layer begins with the strong warm air advection at its base. This warm saturated air increased  $\theta_e$  at the base until the layer became convectively unstable. Since the LWC at the base was already  $0.2\ \text{g m}^{-3}$ , due to air rising along the slope of the lower warm front, the convective adiabatic ascent increased the LWC to  $0.4\ \text{g m}^{-3}$  over a thin 250m layer. The lift apparently began to decrease above 1300m, but supersaturated conditions were still present at the top of the layer. The high LWC, lack of

ice crystals falling from above, and low drop concentrations allowed significant production of SLD. These drops grew into drizzle drops by collision-coalescence then fell into the layers below. The low drop numbers were due to low CCN and IN concentrations within the Layer 2 air mass, which had been detached from the boundary layer for at least 12 hours (see Fig. 4.18). Also snow and FZDZ had fallen through the layer for at least 12 hours prior to the flight. This FZDZ formed in the absence of radiational cooling due to the shadowing from the cloud layers above. This suggests that radiational cooling is not a necessary condition for FZDZ production.

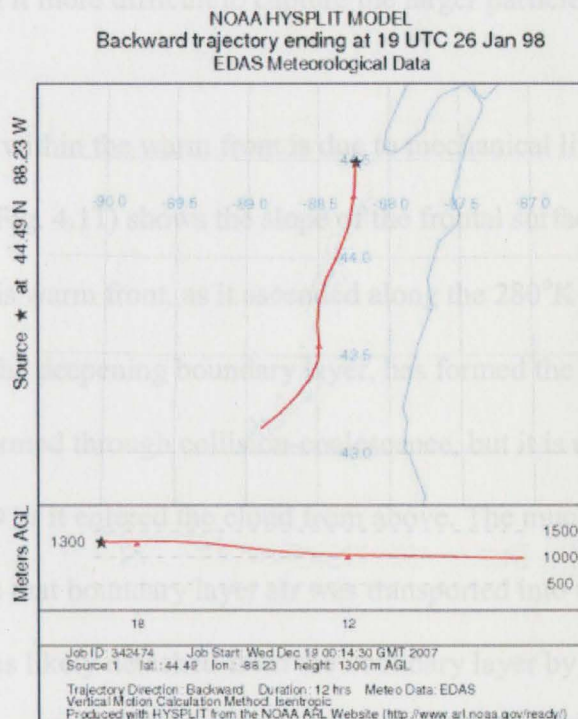


Figure 4.18. NOAA 80-km Hysplit back trajectory model for Layer 2. Upper red line shows the horizontal motion from 0700 – 1900 UTC JAN 26 1998 while the lower plot red line shows the vertical change using the model vertical velocity field

#### 4.5.2 Lower Warm Front

The lower warm front, between 800-1050m, contained LWC values  $\sim 0.2 \text{ g m}^{-3}$  within a highly stable layer. The temperatures at the layer base and top were both  $-4.5^\circ\text{C}$  with a  $3^\circ\text{K}$   $\theta_e$  inversion. The cloud had a drop concentration of  $200 \text{ cm}^{-3}$ , much higher than the layers above. The SLD concentration appeared to decrease in this layer but the much higher small drop concentration may have reduced the 2DC Gray sample volume (the probe stops sampling when the data buffer is filled and is transmitting the data to the storage media) making it more difficult to capture the larger particles.

The LWC production within the warm front is due to mechanical lifting. The KDVN-KGRB cross-section (Fig. 4.11) shows the slope of the frontal surface. The mechanical lift of the air within this warm front, as it ascended along the  $280^\circ\text{K}$   $\theta_e$  surface in southerly flow above the deepening boundary layer, has formed the cloud layer. SLD was present in the layer, formed through collision-coalescence, but it is uncertain if the layer itself formed new SLD or it entered the cloud from above. The much higher drop concentration suggests that boundary layer air was transported into this layer from below. Although this layer was likely detached from the boundary layer by the thermal inversion, strong updrafts from the cloudy boundary layer may have penetrated into the base of the lower warm front. This added CCN and increased the drop concentration, likely suppressing FZDZ. At the same time precipitation scouring from the FZDZ forming above likely removed some of the additional CCN, keeping the drop concentration below the boundary layer value.

#### 4.5.3 Layer 3

The Lake Effect boundary layer, between 150-800m, contained  $LWC > 0.3 \text{ g m}^{-3}$ . The layer had a small drop concentration of  $300 \text{ cm}^{-3}$  and FZDZ concentration  $> 1000 \text{ L}^{-1}$ . The FSSP MVD showed boundary layer cloud with very small drops at the cloud base increasing to  $12 \mu\text{m}$  at the layer top (Fig. 4.14e). The cloud base temperature was  $-1.5^\circ\text{C}$  and the layer top temperature was  $-4.5^\circ\text{C}$ . The lapse rate appeared to be convective (moist-adiabatic). No ice phase was observed within or below the cloud. Fig. 4.19 shows the images from the 2DC Gray and particle size distribution (bin counts) from both the FSSP and 2DC Gray within and below the cloud. Within the cloud, the small-drop concentration seen in the FSSP size distribution, showed high concentration of drops  $< 20 \mu\text{m}$  and no cloud drops in the  $30\text{-}47 \mu\text{m}$  range, or below the FSSP detection limit. The FZDZ is also clearly seen in both the 2DC Gray imagery and the size distribution. The largest FZDZ drops were  $\sim 200 \mu\text{m}$ .

The conceptual model of the boundary layer cloud is a capped, shallow, supercooled liquid Lake Effect cloud that is growing seeded from above by large drops. The Lake effect cloud serves as the feeder cloud in the feeder-feeder scenario. As the cold boundary layer air crossed Lake Michigan (Fig. 4.20) the temperature and moisture gradient between the lake and air invited fluxes of heat and moisture into the boundary layer. These fluxes warmed the lower boundary layer and eventually destabilized it. Convective updrafts rose until they encountered the inversion, the lower warm front. It was likely that the updrafts occasionally penetrated into the lower warm front providing additional CCN from the surface layer. These clouds typically don't form FZDZ unless the LWC is very high (Bernstein et. al 2006).

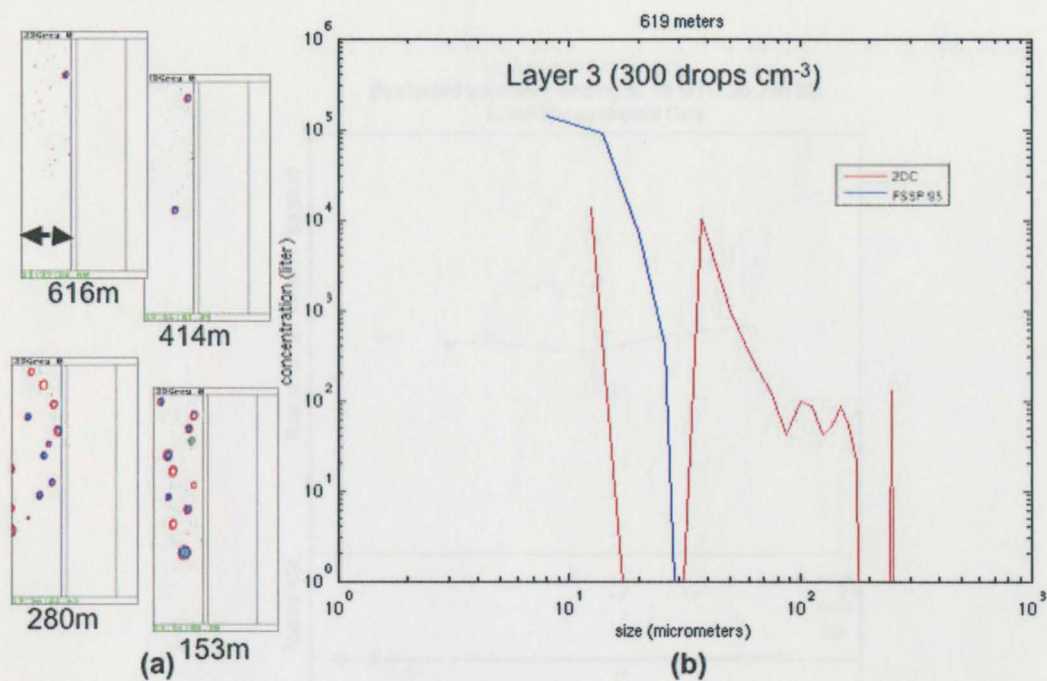


Figure 4.19. (a) Layer 3 imagery from the 2DC Gray, width of box (black double arrow line) 960 $\mu$ m. (b) size distribution at 619m, FSSP (blue) 2DC Gray (red)

The conceptual model of the boundary layer cloud is a capped, shallow, supercooled liquid Lake Effect cloud that is getting seeded from above by large drops. The Lake effect cloud serves as the feeder cloud in the seeder-feeder scenario. As the cold boundary layer air crossed Lake Michigan (Fig. 4.20) the temperature and moisture gradient between the lake and air invited fluxes of heat and moisture into the boundary layer. These fluxes warmed the lower boundary layer and eventually destabilized it. Convective updrafts rose until they encountered the inversion, the lower warm front. It was likely that the updrafts occasionally penetrated into the lower warm front providing additional CCN from the surface layer. These clouds typically don't form FZDZ unless the LWC is very high (Bernstein et. al 2006).

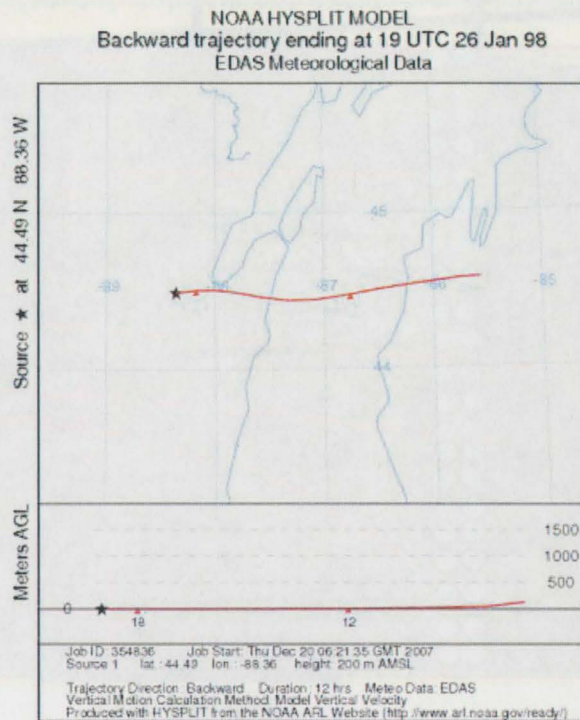


Figure 4.20. NOAA 80-km Hysplit back trajectory model for Layer 3. Upper red line shows the horizontal motion from 0700 – 1900 UTC JAN 26 1998 while the lower plot red line shows the vertical change using the model vertical velocity field

The conceptual model of the FZDZ producing cloud at KGRB is presented in Fig 4.21.

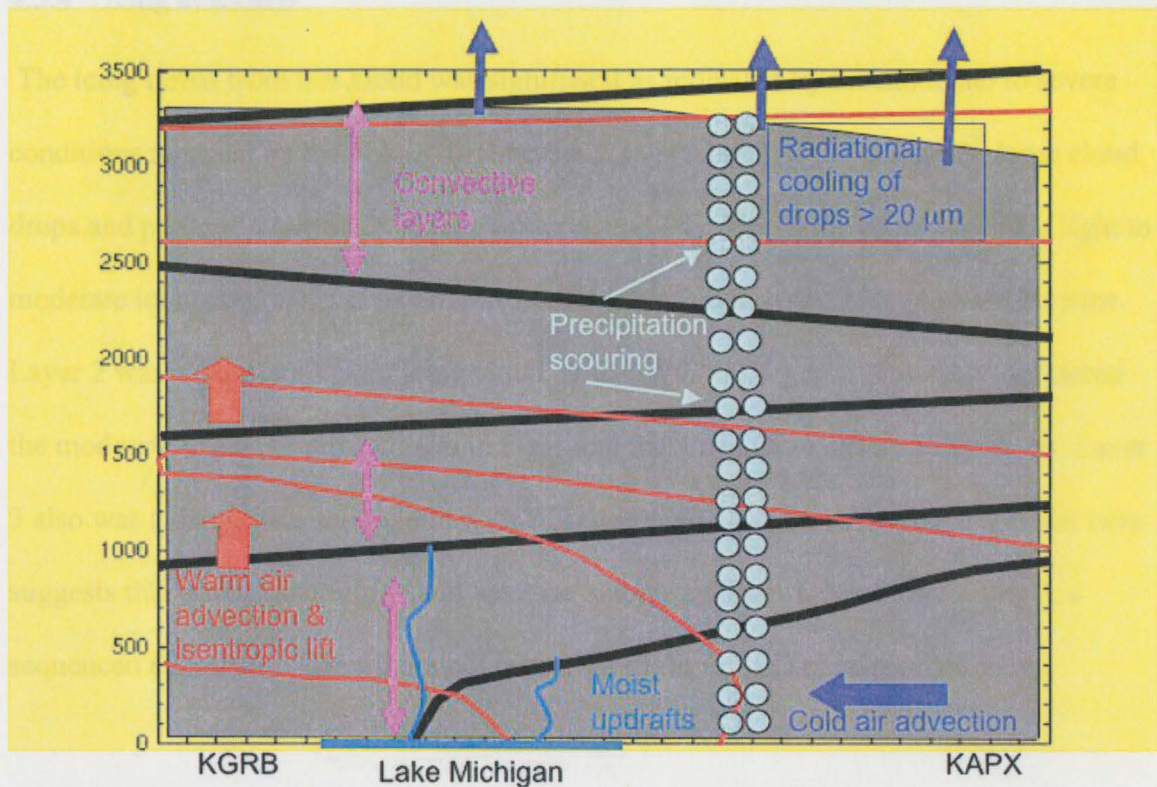


Fig. 4.21. The conceptual model of the cloud at KGRB is presented. The black lines identify the  $\theta_e$  inversions, the red lines identify the isotherms, and the gray shaded region identifies the cloud/moist layers. Radiational cooling (blue) and shallow convection (magenta) may have played a role in the large drop production at cloud top. Warm air advection produced significant FZDZ in the mid-layer due to isentropic lifting above a deepening Lake Effect cloud layer. The boundary layer cloud at KGRB was driven by moist updrafts from the open water of Lake Michigan into the cold air above the surface. Precipitation scouring (light blue) helped remove CCN from the cloud layers, which reduced the drop concentrations, and led to increased chances of FZDZ.

#### 4.5.4 Icing at KGRB

The icing threat from this cloud was significant as indicated by the moderate to severe conditions reported by the NASA flight crew. Layer 1 had LWC  $\sim 0.2 \text{ g m}^{-3}$ , large cloud drops and perhaps some SLD, at temperatures  $\sim -14^\circ\text{C}$ . This layer should produce light to moderate icing conditions if an aircraft remained within the cloud for an extended time.

Layer 2 was a dangerous SLD icing cloud, with LWC  $> 0.4 \text{ g m}^{-3}$ . This layer produced the moderate to severe icing shown in Fig 1 and the Twin Otter severe pilot report. Layer 3 also was a dangerous icing cloud with SLD and LWC  $> 0.3 \text{ g m}^{-3}$ . The low cloud base suggests that aircraft landing would have ice accretions from Layer 2 and Layer 3, a sequenced encounter. Aircraft are not tested for flight in SLD or sequenced icing.

- Descending motion aloft due to negative vorticity advection increasing with height will lower and warm the cloud top as well as form the cloud top inversion.

- An increased dew point temperature in the shear layer just above the cloud top may be present. This has been observed in other supercooled large drop case studies (Peters et al. 1993; Rasmussen et al. 1995).

- Discrete layers of warm air advection may be present within the larger overrunning layer forcing multiple thin convective cloud layers, each with a unique drop concentration and temperature.

- The identification of the well-mixed layers and the stable layers is useful and more LWC may be found in the well-mixed layers.

- SLD is more likely in well-mixed layers detached from the boundary layer.

- Both cases were associated with low ceilings.

## 5.0 Principal findings

### 5.1 Identification of weather features associated with SLD forming clouds

Identification of weather systems that produce overrunning cloud layers likely to produce freezing drizzle may exhibit the following characteristics.

- Overrunning clouds formed from warm  $\theta_e$  advection over an existing cold air mass should be present.
- Descending motion aloft due to negative vorticity advection increasing with height will lower and warm the cloud top as well as form the cloud top inversion.
- An increased dew point temperature in the shear layer just above the cloud top may be present. This has been observed in other supercooled large drop case studies (Pobanz et al. 1993; Rasmussen et. al. 1995).
- Discrete layers of warm air advection may be present within the larger overrunning layer forming multiple thin convective cloud layers, each with a unique drop concentration and temperatures.
- The identification of the well-mixed layers and the stable layers is useful and more LWC may be found in the well-mixed layers.
- SLD is more likely in well-mixed layers detached from the boundary layer.
- Both cases were associated with low ceilings.

## 5.2 Large drop formation

This study showed that freezing drizzle formed in the clean low cloud droplet concentration clouds with moderate LWC. Large drops were also found in thin layers at cloud top. SLD in this region of the cloud likely formed from radiational cooling (Juneau) and perhaps isobaric mixing.

## 5.3 Implications for models

Case studies such as presented in this paper are important for model verification. The large scale warm air advection created discrete thin convective cloud layers. High vertical resolution is needed to resolve these discrete layers. Drop concentrations within these layers at JNU ranged from  $300 \text{ cm}^{-3}$  in the boundary layer to  $5 \text{ cm}^{-3}$  in the upper cloud layers. These case studies suggest the need for models to have explicit CCN concentrations and model aerosol interactions such as Brownian motion, coagulation, aggregation, nucleation scavenging and precipitation scouring to accurately predict freezing drizzle. Radiational cooling and the subsequent broadening of the droplet population was important in these cases and needs to be included in the model.

## 5.4 Icing

The aircraft icing was highly variable in these clouds. At JNU the LWC remained mostly  $< 0.2 \text{ g m}^{-3}$  with SLD in all the layers. The pilots did not mention icing as a problem, which suggests that the SLD in a low LWC environment may not be a significant icing hazard. The LWC in these very low drop concentration, weakly forced, cloud layers may remain low since the drops quickly grow to sizes where their fall speeds exceed the

vertical velocity. Thus limiting the LWC and the icing threat. Cloud layers with similar vertical velocities and high drop concentrations can have much larger LWC but are less likely to contain SLD.

At GRB the icing also was highly variable although the icing at the high LWC and SLD levels was reported as moderate to severe, with heavy ice forming and ice accreted well aft of the deicing boots. Therefore SLD in a moderate or high LWC environment can be dangerous. Inversion layers within the warm frontal structure contained the lowest quantities of SLD and may provide an escape zone in an icing emergency. Pilots, forecasters, and automated icing detection algorithms such as the Current Icing Product (CIP, Bernstein et. al. 2005) should monitor the heights of these inversions. Small drop cloud layers that have been seeded by SLD from layers aloft can be especially hazardous for icing due to the higher LWC and presence of SLD. These layers are often found near the surface where aircraft operate closer to stall speeds.

Another possible dangerous icing threat is due to an aircraft encountering several different icing layers each with unique icing characteristics. This can lead to a 'sequenced' icing encounter where one ice accretion shape is put on top of a different ice accretion shape leading to unknown aircraft performance. Aircraft are not tested for flight in these types of icing encounters.

## 5.5 Future Work

Additional overrunning cases should be analyzed to see if the drop concentration is lower in the non-boundary layer clouds other cases. A climatological analysis of soundings and associated surface observations of FZDZ should be conducted to explore the vertical structure of clouds, which produce freezing drizzle. Layer analysis of the FZDZ soundings should be built and the role of elevated cloud layers and their temperature structure should be evaluated. This may lead to a forecast algorithm, which could identify SLD icing conditions aloft.

- Bernstein, B. C., F. McDonough, M. K. Politovich, B. G. Brown, T. P. Zatzvsky, D. H. Miller, C. A. Wolff, G. Cunniff 2005: Current Icing Potential: Algorithm description and comparison with aircraft observations. *J. Appl. Meteor.*, 44, 987-986.
- Bernstein, B. C., T. A. Omerci, F. McDonough, M. K. Politovich, 1997: The relationship between aircraft icing and synoptic-scale weather conditions. *Wet and Frost*, 15, 493-508.
- Cober, S.G., J.W. Strapp, G.A. Isaac, 1996: An example of supercooled drizzle drops formed through a collision-coalescence process. *J. Appl. Meteor.*, 35, 2250-2260.
- Cober, S. G., G. A. Isaac, A. V. Korolev, J. W. Strapp 2001: Assessing cloud-phase conditions. *J. Appl. Meteor.*, 40, 1984-2002.
- Hallet, J., and S. C. Mossop, 1994: Production of secondary ice particles during the riming process. *Nature*, 349, 26-28.
- Harrington, J. M., G. Felsgold, and W. R. Cotton, 2000: Radiative impacts on the growth of a population of drops within a simulated summertime Arctic stratus. *J. Atmos. Sci.*, 57, 766-785.
- Holton, J. R. 1992: An introduction to dynamic meteorology. Academic press. 166-167.
- Huffniss, G. J. 1938: The supercooled warm rain process and the specification of freezing precipitation. *Mon. Wea. Rev.*, 116, 2173-2182.

## 6.0 References

- Ashenden, R.A 1997: Turboprop aircraft performance response to various environmental conditions. Univ. of Wyoming PhD dissertation. 185 pages.
- Baumgardner, D. 1983: An analysis and comparison of five water droplet instruments. *J. Climate Appl. Meteor.*, **22**, 891-910.
- Bernstein, B. C., F. McDonough, C. A. Wolff 2005: An inferred climatology of icing conditions including supercooled large drops. Part 1: Canada and the continental U.S. In preparation for *J. Appl. Meteor.*
- Bernstein, B. C., F. McDonough, M. K. Politovich, B. G. Brown, T. P. Ratvasky, D. R. Miller, C. A. Wolff, G. Cunnig 2005: Current Icing Potential: Algorithm description and comparison with aircraft observations. *J. Appl. Meteor.*, **44**, 969-986.
- Bernstein, B. C., T. A. Omeron, F. McDonough, M. K. Politovich, 1997: The relationship between aircraft icing and synoptic-scale weather conditions. *Wea and Forcst.*, **15**, 485-508
- Cober, S.G., J.W.Strapp, G.A.Issac, 1996: An example of supercooled drizzle drops formed through a collision-coalescence process. *J. Appl. Meteor.*, **35**, 2250-2260.
- Cober, S. G., G. A. Isaac, A. V. Korolev, J. W. Strapp 2001: Assessing cloud-phase conditions. *J. Appl. Meteor.*, **40**, 1984-2002.
- Hallet, J., and S. C. Mossop, 1994: Production of secondary ice particles during the riming process. *Nature*, **249**, 26-28.
- Harrington, J. M., G. Feingold, and W. R. Cotton, 2000: Radiative impacts on the growth of a population of drops within a simulated summertime Arctic stratus. *J. Atmos. Sci.*, **57**, 766-785.
- Holton, J. R. 1992: An introduction to dynamic meteorology. Academic press. 166-167.
- Huffman, G. J. 1988: The supercooled warm rain process and the specification of freezing precipitation. *Mon. Wea. Rev.*, **116**, 2172-2182.

- Klett, J. D., and M. H. Davis, 1973: Theoretical collision efficiencies of cloud droplets at small Reynolds numbers. *J. Atmos. Sci.*, **30**, 107-117.
- Korolev, A. V. and G. A. Isaac 2000: Drop growth due to high supersaturation caused by isobaric mixing. *J. Atmo. Sci.*, **57**, 1675-1685.
- Levin, Z., and W.R. Cotton 2009: Aerosol Pollution Impact on Precipitation: A scientific review. Springer Science and Business.
- Ludlam, F. H. 1980: Clouds and storms. Pennsylvania State University Press. 64-79.
- Meyers, M. P., P. J. DeMott, W. R. Cotton 1992: New primary ice-nucleation parameterizations in an explicit cloud model. *J. Appl. Meteor.*, **31**, 708-721.
- Paulch, I. R. 1979: The entrainment mechanism in Colorado cumuli. *J. Atmo. Sci.*, **36**, 2467-2478.
- Politovich, M. K. 1989: Aircraft icing caused by large supercooled droplets. *J. Appl. Meteor.*, **28**, 856-868.
- Pobanz, B. M., J. D. Marwitz, M. K. Politovich 1994: Conditions associated with large drop regions. *J. Appl. Meteor.*, **33**, 1366-1372.
- Petty, K. R., C. D. J. Floyd 2004: A statistical review of aviation airframe icing accidents in the U.S. *11<sup>th</sup> Conf. on Aviation Range and Aerospace Meteorology*, 4-7 Oct., Hyannis, MA.
- Rogers, R. R., M. K. Floyd 1989: A short course on cloud physics. Pergamon Press, Oxford England.
- Rasmussen, R. M., B. C. Bernstein, M. Murakami, G. Stossmeister, and J. Reisner 1995: The 1990 Valentine's Day arctic outbreak . Part I: Mesoscale and microscale structure and evolution of a Colorado Front Range shallow upslope cloud. *J. Appl. Meteor.*, **34**, 1481-1511.
- Sand, W. R., W. A. Cooper, M. K. Politovich, and D. L. Veal, 1984: Icing conditions encountered by a research aircraft. *J. Climate Appl. Meteor.*, **23**, 1427-1440.
- Stephens, G. L., Tsay, S-C 1990: On the cloud absorption anomaly. *Q. R.J. Meteor.*, **116**, 671-704